Development and Application of Two-Dimensional Micro Gas Chromatography

by

Menglian Zhou

A dissertation submitted in partial fulfillment
of the requirements for the degree of
Doctor of Philosophy
(Biomedical Engineering)
in the University of Michigan
2019

Doctoral Committee:

Professor Xudong Fan, Chair
Professor Katsuo Kurabayashi
Professor Kevin Ward
Associate Professor Zhaohui Zhong

Menglian Zhou

sharonml@umich.edu

ORCID iD: 0000-0001-6644-8172

Dedication

To

My husband, Dr. Zeyu Li

And my entire family

Thank you for all your support along the way

Acknowledgements

First and foremost I would like to thank my advisor, Professor Xudong Fan, for his continuous support, guidance and patience throughout my graduate studies. The problem solving methodology and critical thinking skills that I learnt from him will be invaluable in my future life.

I want to present my gratitude to Prof. Kevin Ward, his insightful suggestions and clinical resources have provided great support on my current research project.

I would thank my committee members, Prof. Katsuo Kurabayashi and Prof. Zhaohui Zhong, for serving on my committee and the valuable feedback to my research work.

I want to give my special thanks to Prof. Zhen Xu, who introduced me to my current research group and being an excellent example to me as a female researcher.

My gratitude also goes to my awesome lab mates, Dr. Jiwon Lee, Dr. Hongbo Zhu, Dr. Ruchi Sharma, Shiyu Wang, Jiliang Li and Ziqi Li, your amazing work is indispensable to the completion of my Ph.D. I also would like to thank the help, advice and companion of all my previous and current group members, Maxwell Li, Dr. Qiushu Chen, Dr. Victoria Zhang, Dr. Malcolm Khaing Oo, Dr. Xiaoqin Wu, Dr. Yu-cheng Chen, Xiaotian Tan, Xuzhou Li and everyone else.

Last but not least, I would like to thank my husband, Dr. Zeyu Li and my whole family. Their unconditional trust, support and love have led me this far and will continue lead me to my next destination in life.

Table of Contents

List of Tables

List of Figures

Abstract

The increasing need for rapid and on-site analysis of environmental, pharmaceutical and petrochemical samples has driven the development of micro gas chromatographs (μGC) for the last few decades. To improve the μGC's ability to separate and analyze complex samples, we implemented multi-channel multi-dimensional μGC technology. This dissertation describes the design, assembly, characterization, operation and chromatogram reconstruction of a 1D & 2D μGC system as well as their applications on water contamination analysis and exhaled breath analysis.

The 1D μGC system has sub-parts-per-billion level sensitivity and can analyze a water sample in 15 minutes. This system was coupled with purge-and-trap sampling and provided sensitive and rapid field analysis of water contamination. Quantification results agreed well with those obtained by an analytical lab using standard analytical methods and benchtop instruments. This system offers a lab-on-a-chip solution for sensitive and rapid water analysis with EPA compliant sample collection methods.

The 2D μGC system has high peak capacity (>200 for 1-by-2 channel and >430 for 1-by-4 channel) and high sensitivity (sub-ppb). The 1-by-2 channel 2D μGC was used to analyze the exhaled breath of acute respiratory distress syndrome (ARDS) patients. ARDS is the most severe form of acute lung injury, responsible for high mortality and long-term morbidity, and is notably difficult to diagnosis. Breath samples were drawn from mechanical ventilators in the ICU and analyzed by the fully automated 2D μGC within about 30 minutes. A machine learning algorithm was developed to analyze the metabolic information within breath chromatograms and achieved an overall diagnostic accuracy of 87.1% with 94.1% positive predictive value and 82.4% negative predictive value when compared to adjudications performed by physicians based on the Berlin

criteria. The ability to continuously and non-invasively monitor exhaled breath for early diagnosis, disease trajectory tracking, and outcome prediction monitoring of ARDS may have a significant impact on changing medical practices and improving patient outcomes.

Chapter 1 Introduction

1.1 Introductory Remarks

This chapter presents introductory information about benchtop gas chromatography (GC), including working principles, applications, basic components and performance metrics in Section 1.2. Principles and advantages of multi-dimensional GC (MDGC) will be presented in Section 1.3. The last section will discuss recent development of micro-GC (μGC), including miniature components, μGC system performance compared to regular GC, and μGC applications.

1.2 Gas chromatography

1.2.1 Principles

Gas chromatography (GC) is a powerful separation technique for vapor mixtures[1]. The heart of the GC is the column, in which the components of a sample are partitioned between stationary phase and mobile phase. Based on their unique vapor pressures and affinities to the stationary phase, different components of the vapor mixture are separated and elute from the column at different times[2]. Figure 1.1 shows the essential components of a GC instrument: Gas cylinder (for providing carrier gas to push the sample through the column), two stage regulator (for reducing cylinder pressure), electronic pressure controller (for electrical pressure setting), injector (for sample injection), column (mixture separation), oven (for column heating), detector (for eluted vapor detection to generate a chromatogram), and GC software (for instrument control and data acquisition and processing). Additional details of these GC components are given in Section 1.2.2. Current benchtop GC technology provides sensitive detection (ppb to ppt level),

efficient separation (tens to hundreds peak capacity), high accuracy quantitative results (1-5% RSD), and has a significant role in numerous environmental[3], pharmaceutical[4] and clinical[5] applications.

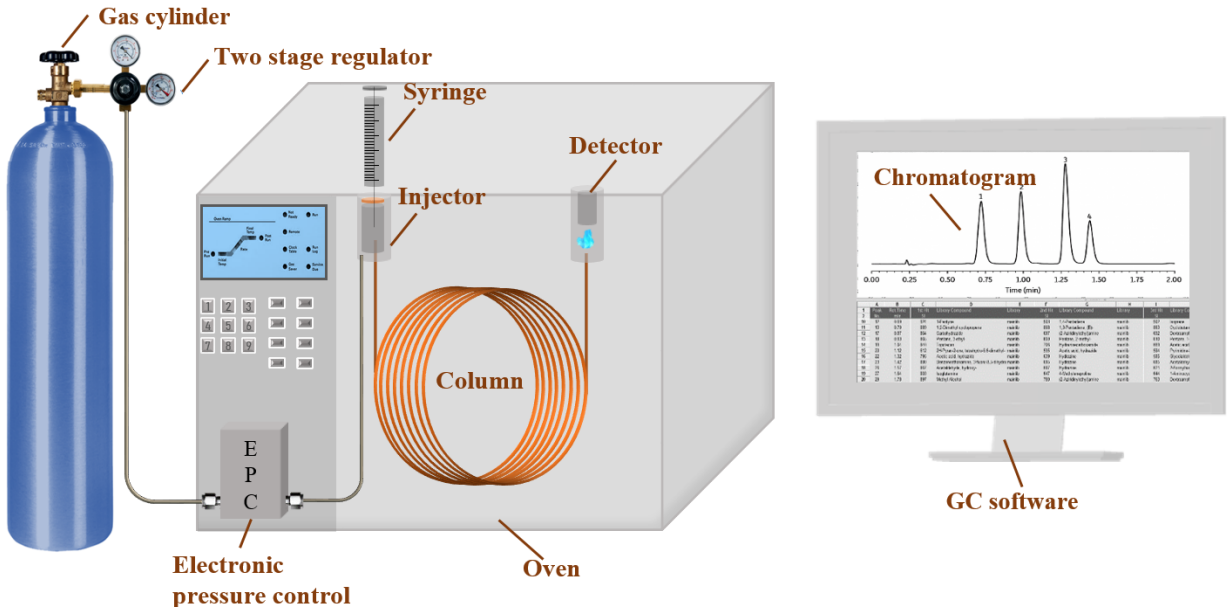

Figure 1.1 Schematic of a typical gas chromatography

1.2.2 Main GC components

Injectors

Samples are injected into the head of GC column from injectors, as shown in Figure 1.2 (a) A typical split/splitless GC injector. A typical GC injector consists of a septum, a glass liner, and a heating block. Because separation of compound mixtures in the column occurs while they are in gas state, solid and liquid samples must first be vaporized. The syringe needle pierces a rubber septum and inject samples into the glass liner, which is heated to 50°C above the sample boiling point to rapidly vaporize the sample. To achieve the best separation performance at given flow rate, a sharp injection peak is desired. Thus, a split mode injection is often used. In split mode,

only a small fraction of sample is injected into the column; the rest is washed out from split venting. Split ratios are controlled by adjusting the flow resistance of the split vent. For batch analysis, an auto sampler (normally placed on the top of the GC injector) can also be used to automatically inject samples.

Sometimes, manual syringe injection cannot handle samples directly or cannot achieve satisfactory GC performance. In this scenario, specific sample preparation techniques are required to introduce samples into the GC column, as shown in Figure 1.2 (b)-(e). A comprehensive review on sample preparation techniques for GC analysis can be found in Sjaak et al[6]. A brief summary of solid phase micro-extraction (SPME)[7], sampling loops[8], thermal desorption (TD)[9-10] and cold traps[11] are summarized in Table 1.1.

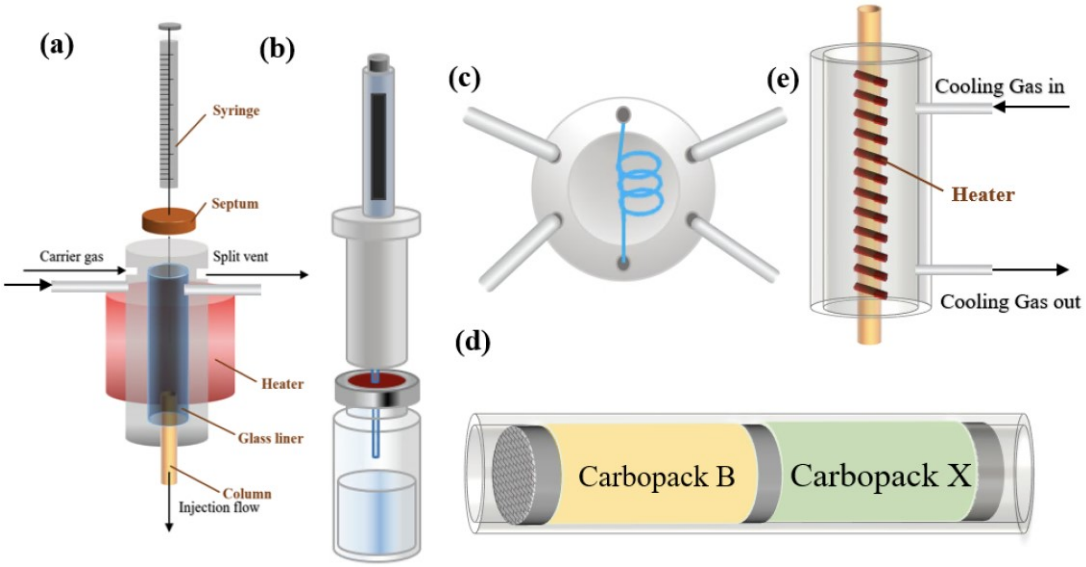

Figure 1.2 (a) A typical split/splitless GC injector (b) SPME (c) Sampling Loop (d) TD tube (e) cold trap

Table 1.1 Sample preparation techniques

	Sampling Method	Sampling Device	Sampling Procedure	Advantage	Disadvantage
Static headspace (HS) sampling (Direct sampling of liquid/solid sample HS)	SPME	Fused-silica fiber (with a stationary phase coated on surface) mounted on a modified GC syringe	Immerse SPME fiber into HS until reached equilibrium; Thermally desorb into GC injector;	Easiness of automation; Simultaneous sample introduction; Low cost	Low effectiveness due to small stationary phase coating area
	Sampling loop	Six port valve; Sampling loop	Fill the loop with HS gas; Switch the valve and sweep HS gas onto the column	Simultaneous sample introduction	Cannot concentrate trace level samples
Dynamic headspace sampling (Continuous flow of an inert gas either through or above a solid or liquid sample)	Thermal desorption (TD)	TD tube (cartridge packed with adsorbents)	Adsorption trap is swept with sample and carrier gas; Heat the trap to release the sample into injector/ focuser	Broad target compound range	Long desorption time; Broad injection band
	Cold trap (CT)	Cryogen (gas or liquid)	Trap sample via condensation at very low temperatures; Instantaneous evaporation for desorption	Peak focusing; Sharp injection band	High amount of accumulated water; cryogen handling difficulty

Columns

Currently, there are three main types of GC columns in common use: packed columns (stationary phase directly coated in the inert solid support material inside column), porous layer

open tubular (PLOT) columns (stationary phase coated on a porous layer of a solid adsorbent such as alumina, molecular sieves, and Porapak) and wall coated open tubular (WCOT) columns (stationary phase coated on the column inner wall)[12]. Figure 1.3 shows a typical diagram of WCOT capillary column. A fused silica tubing (0.1-5 µm i.d.) is coated with polyimide on its outer wall and with the stationary phase (sub-µm thin layer) on its inner wall. As aforementioned, different compounds are injected together into the head of the GC column. The compounds flow through the column (via inert carrier gas, normally helium, nitrogen, or hydrogen) partitioned between mobile and stationary phases, and finally elute at different times based on their volatility and polarity.

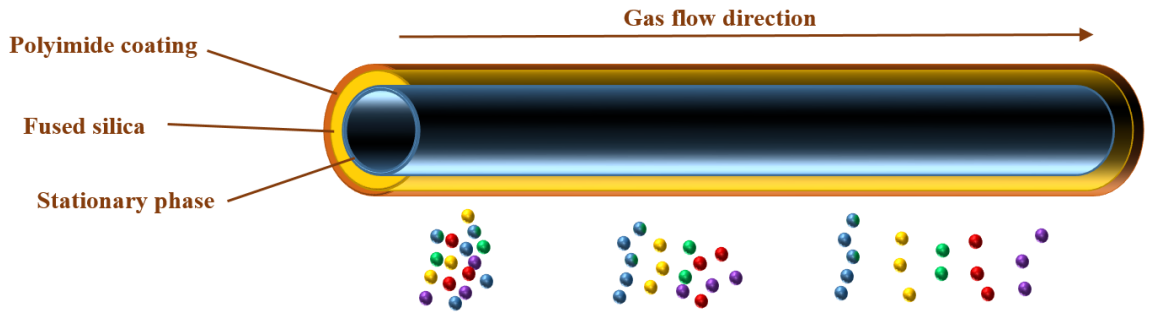

Figure 1.3 Representation of a WCOT capillary column

The stationary phase can be either liquid (gas-liquid chromatography) or solid (gas-solid chromatography). Solid stationary phases are normally used in packed columns, while liquid stationary phases can be coated on both packed column and OT column. Liquid phases are primarily silicone-based oils with high temperature stability and are available in a range of polarities.

Column parameters, including stationary phase, length, inner diameter, coating thickness, temperature profile, and flow rate, directly affect GC separation performance and should be decided carefully based on specific application requirements. In short, longer columns result in better separation, but longer analysis times; smaller inner diameters result in better resolution but

smaller sample loading capacity (smaller sample quantities can be accommodated); thinner film thickness results in faster separation but smaller sample loading capacity. Higher temperature ramping rates and carrier gas flow rates result in faster analysis but lower resolution.

Detectors

The chemicals eluted from GC columns require some form of detection in order to generate a chromatogram. Among the over 60 different detectors that have been used in GC instruments[2], the most widely used are flame-ionization detection (FID[13]), thermal conductivity detection (TCD[14]), electron-capture detection (ECD[15]), photoionization detector (PID[16-18]) and mass spectrometry (MS).

An FID collects ions that are generated while burning effluent with oxy-hydrogen flame, hence it responds to all organic compounds that can burn in the flame with signal proportional to carbon content[2]. FID has good sensitivity, high dynamic range, and short response time; however it consumes hydrogen and oxygen, which requires safety precautions.

Like FID, TCDs are also equipped in most commercial GC instruments. A TCD measures the thermal conductivity of analytes in carrier gas (helium or hydrogen) and compares this with the thermal conductivity of pure carrier gas. The thermal conductivity differences are measured with a Wheatstone bridge. Although the TCD detection limit (ng level) is not as good as the FID's (pg level), TCDs are responsive to all compounds, including CO, H_2, and other inorganic compounds.

ECDs are selective detectors for compounds that 'capture electrons', such as halogenated materials. Electronegative analytes capture the free electrons generated from radioactive ^{63}Ni and N_2 interactions and decrease the ionization level of the ECD. Although ECD are not universal detectors, their detection limit can be as low as fg level.

PIDs utilize high energy photons that are emitted from a UV lamp to ionize organic compounds. PIDs have excellent sensitivities and fast response times with no need for external gases. However, effluents whose photoionization energies are above the UV photon energy cannot be detected.

Helium discharged PID (HDPID[19]) emits photons from 13.5 to 17.5 eV, hence could be used as universal detector. HDPIDs have good detection limit (pg level) but their lifetime are usually short due to ion sputtering effect.

Mass spectrometer (MS) is the most information-rich detection method, capable of not only measuring compound abundance, but also analyzing and providing compound identity (i.e. molecular mass), which standalone GC cannot achieve. Effluents from GC are firstly passed into a heated ionization source at low vacuum. These ions are then repelled and focused by charged lenses into the mass analyzer (quadrupole, ion trap, or time of flight) whereupon they are separated by their mass to charge ratio (m/z).

Other than the aforementioned detector, surface acoustic waves (SAWs)[20-22], optical vapor sensors [23-30], chemicapacitors [31-32], chemiresistors [33], and nanoelectronic sensors [34-35] can also be used as GC detector.

1.3 GC performance metrics

When individual solute molecules pass through the column, the molecular distribution (or peak shape) is broadened and sometimes becomes asymmetric (fronting, tailing) due to diffusion and retention. However, in this section, Gaussian peak shape is assumed for discussion simplicity.

1.3.1 Plate number

Number of theoretical plates is a measurement of column efficiency and is defined as[2]:

$$N = (\frac{t_R}{\sigma})^2 = 16\left(\frac{t_R}{w_b}\right)^2 = 5.54(\frac{t_R}{w_h})^2. \quad (1.1)$$

where t_R is the retention time, σ is the standard deviation of the Gaussian peak, w_b is the bottom to bottom peak shape, and w_h is the full width half maximum (FWHM).

Columns with high plate numbers have higher column efficiency, since at a given retention time, the peak height is narrower.

1.3.2 Plate height

Column efficiency can also be expressed as plate height, which is also called the Height Equivalent to One Theoretical Plate (HETP):

$$H = \frac{L}{N} \quad \textbf{(1.2)}$$

where L is the column length and N is the plate number.

1.3.3 Golay equation

The plate height H of a capillary column is a function of average linear velocity $\overline{\mu}$:

$$H = \frac{B}{\overline{\mu}} + (C_s + C_M)\overline{\mu} = \frac{2D_G}{\overline{\mu}} + \frac{2kd_f{}^2}{3(1+k)^2 D_s}\overline{\mu} + \frac{(1+6k+11k^2)r_c{}^2}{24(1+k)^2 D_G}\overline{\mu} \quad \textbf{(1.3)}$$

where B accounts for molecular diffusion, C_s and C_M are mass transfer in stationary phase and mobile phase, k is the retention factor (the mass ratio of solute in stationary phase to mobile phase), D_G and D_S are the diffusion coefficients in carrier gas and in stationary gas, d_f is the film thickness, and r_c is the column radius. With this equation, the optimal linear velocity $\overline{\mu}$ is:

$$\overline{\mu}_{opt} = \sqrt{\frac{B}{C_s + C_M}} \quad \textbf{(1.4)}$$

1.3.4 Resolution

Resolution is used to evaluate the degree to which two adjacent peaks are separated. Its definition is

$$R_s = 2\frac{(t_R)_B - (t_R)_A}{(w_b)_B + (w_b)_A} = \frac{2d}{(w_b)_B + (w_b)_A} \quad \textbf{(1.5)}$$

where $(t_R)_B$ and $(t_R)_A$ are the retention times of adjacent peaks A and B, and $(w_b)_B$ and $(w_b)_A$ are the bottom to bottom peak widths of these two peaks. The chromatogram resolution can be defined as: [36]

$$R = 1/4\sqrt{N} \times (\alpha - 1) \times \frac{k}{1+k} \quad \textbf{(1.6)}$$

where N is plate number (a function of column length, inner diameter, carrier gas type, and linear velocity), α is separation factor (a function of stationary phase composition and temperature), and k is retention factor (a function of inner diameter, film thickness and composition, and temperature).

1.3.5 Analysis time

Analysis time is the time needed for all analytes from the sample to elute. Depending on application and sample complexity, this time can vary from several seconds to several hours. Analysis time can be reduced with faster flow rate, higher temperature, shorter column length, and smaller column diameter, at the cost of sacrificing system resolution. Decreasing injection peak

width, changing the carrier gas to hydrogen or using columns with smaller radii and proportionally thinner film thicknesses can reduce analysis time without compromising GC system resolution.

1.3.6 Detection limit

Detection limit is the lowest quantity or concentration of a component that can be detected reliably (usually with a sigma to noise ratio of 3). This is mainly dependent on the sampling method (whether or not it concentrates the sample) and the detectors' detection limit.

1.4 Multi-dimensional GC system

1.4.1 MDGC overview

Multidimensional gas chromatography (MDGC) is a powerful separation technique that provides high-resolution analysis of complex samples[37], and has been widely used for petrochemical, geochemical and environmental analysis. In classic heart cutting GC, one or more selected groups of compounds eluted from the primary column onto a second column, and then separated in the second column by another retention mechanism. In comprehensive GC x GC, a long 1st-dimensional (^{1}D) column, usually coated with a non-polar stationary phase, is connected to a short 2nd-dimensional (^{2}D) column that is usually coated with a polar stationary phase [38-42]. A modulator is placed between the two columns to cut the eluents from the ^{1}D column periodically (modulation period (P_M): ~1-10 s [43-44]) and re-inject each sliced segment into the ^{2}D column sequentially [45]. Consequently, each analyte is subject to two independent separation processes: first by vapor pressure in the ^{1}D column and then by polarity in the ^{2}D column. A 2-D chromatogram consisting of the ^{1}D and ^{2}D retention times can be reconstructed by analyzing the eluted peaks detected by a vapor detector installed at the end of the ^{2}D column. Ideally, the total

peak capacity of GC x GC is $n_{GCXGC}=n_1 x n_2$, where n_1 and n_2 are the peak capacities for ^1D and ^2D separation, respectively.

1.4.2 Column combinations

Phase selection: To achieve ideal GCxGC analysis, it is critical to maximize the "orthogonality" of the primary and secondary columns. **.** Clearly any GC column has a boiling point contribution to its retention property, but it will be subtle differences in the two columns' retention mechanisms (such as polarity or shape selectivity) that determine the ability to resolve components[46].

Length selection: Since GCxGC relies on fast analysis of accumulated ^1D elution to avoid wrap around (^1D separation order changing in ^2D column separation), ^2D columns are usually much shorter than ^1D, and sometimes have smaller column radii and thinner film thicknesses to ensure best separation efficiency. The ^1D column normally has a normal separation length (several meters to several tens of meters) while the ^2D column length is usually sub-meter or several meters long,

1.4.3 Modulation methods

The modulator transfers the peaks that elute from the ^1D column to be sampled into the ^2D column. There are multiple methods to achieve this modulation, as summarized in reference [47]. In GCxGC, a sharp transfer peak is normally desired, since board transfer peaks hinder the ^2D column separation performance. Hence modulators with peak focusing (cryo-trap or thermal focuser) are more popular.

Cryogenic modulator

The cryogenic modulator (with liquid N_2 or liquid CO_2 as cryogen) is the most common commercial modulator. As shown in Figure 1.4, the dual cryogenic jet modulator[48] switches on

and off periodically at different times to condense and then quick release the effluent from ^{1}D column.

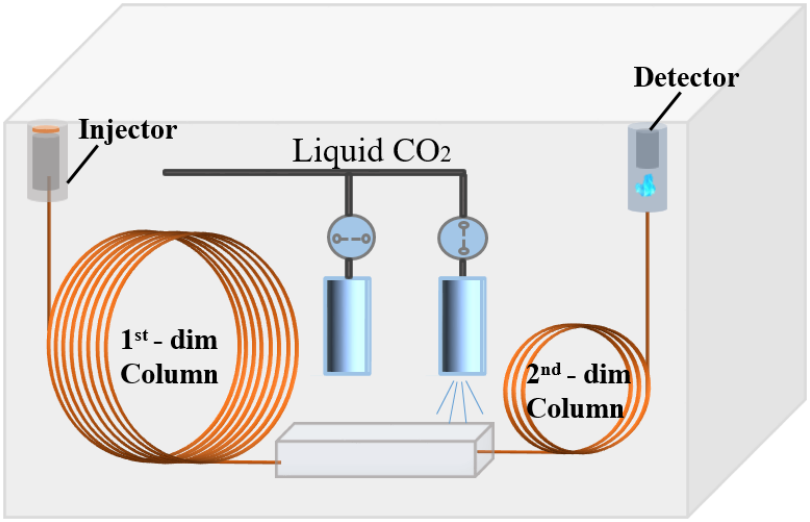

Figure 1.4 Schematic of the dual cryogenic jet modulator

Fluidic modulator

In addition to sample loop based fluidic modulators, another Deans switch setup[49] is designed as shown in Figure 1.5. By switching a 3 port value, the upstream flow (inert gas) can be modulated between the two downstream 2D columns. More details on Deans switch are provided in Section 3.2.1.4.

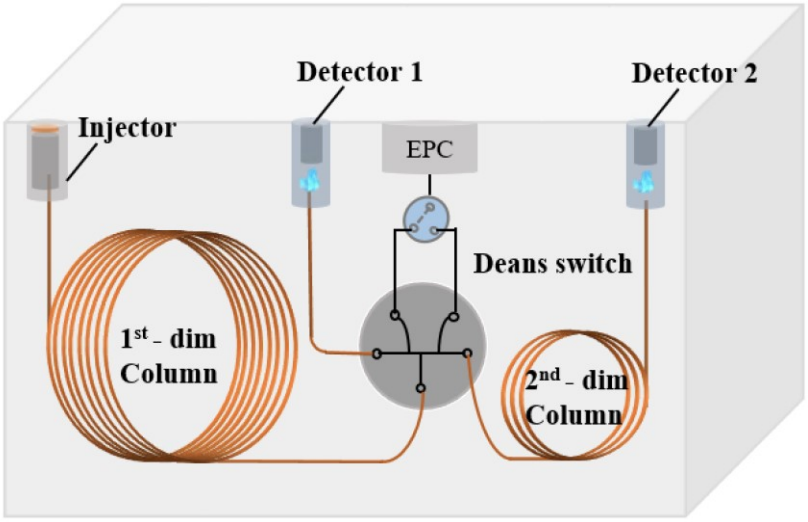

Figure 1.5 Schematic of deans switch modulator

1.5 µGC system

1.5.1 µGC overview

Throughout this article, we use the term "µGC" to refer any field portable versions of a GC comprising one or more microfabricated components[50]. A µGC comprises a number of components, including a source of carrier gas, preconcentratorinjector, separation column, detector, pump, valves, and software for instrument control, data acquisition, and analysis.

Since the pioneering work by Terry *et al.* [51], portable gas chromatography (GC) systems have been intensively investigated for a broad range of field applications such as environmental (air, water, and soil), chemical (explosive vapors, and chemical warfare agents), pharmaceutical and clinical (urine), and anthropogenic (indoor gas and operation) gas monitoring [23, 25, 52-65]. However, current portable GC systems, particularly commercialized ones such as Photovac Voyager GC (Photovac Inc.), Portable zNose (Electronic Sensor Techonology), SeaPORT Mini-GC (Seacoast Science Inc.), 490 Micro GC (Agilent Technologies), FROG-4000™ (Defiant Technologies), and 3000 Micro GC Gas Analyzer (Inficon) are simply miniaturized versions of

the one-dimensional (1-D) bench-top GC. While field-deployable and capable of rapid vapor analysis, they suffer severely from deteriorated separation capabilities or peak capacities due to short column lengths and wide peak widths resulting from miniaturization and requirements for short analysis times. Therefore, these portable GCs can usually separate only a small set or limited, well-defined class of vapors (such as gasoline, chlorinated alkenes, and diesel) [58] and often fail when complex sample matrices are present.

1.5.2 µGC components

To make the GC system portable while maintaining system performance (such as separation capability, detection limit and analysis time) comparable to benchtop GC, multiple micro-fabricated GC components have been integrated.

Micro pre-concentrator and injectors (µPCI)

Since portable GCs are normally designed for field analysis, sample collection and preparation is critical for these systems. Micro preconcentrators/thermal injectors (µPCI) are typical components used for sampling and injection in µGCs and are similar to the aforementioned TD/CT used in benchtop GC systems. µPCI integrates chemical trapping and injection together in the same device. In sampling mode, the µPCI is connected to a pump, whereupon chemicals will be sucked into the µPCI and trapped by adsorption materials such as activated charcoal and porous polymers. In injection mode, µPCI is connected to a carrier gas flow source and heated rapidly. Trapped chemicals are released from the adsorption material quickly, resulting in a sharp injection to the separation column. µPCI can be used to concentrate chemicals from large volumes of sample gas while injecting with small volumes in order to increase the low detection limit without any detector improvements. A typical µPCI has a shallow chamber area etched on a silicon wafer for

adsorption material loading. The heater deposited on the bottom side of the silicon rapidly introduces thermal energy into the sorption bed via resistive heating.

Micro column

Traditional columns require long columns (up to 30 to 60 m) to ensure high enough total column efficiencies. This requires large column thermostat ovens and high-pressure gas control systems, which are the main reasons for high power consumption and bulky size. With MEMS technology, miniaturized columns integrate heaters and micro fluidic channels on chip[66-70]. Micro columns are convenient for direct heating and temperature control, which can greatly reduce power consumption and volume. Micro column design involves tuning channel layouts[71], cross section[72] shapes, in-column (fluid channel) structures[66, 70, 73], column materials[66, 68, 74], coating materials, and coating methods[75-77].

In general, the stationary phase can be coated with either dynamic or static coating. In dynamic coating, the coating solution is slowly passed through the column by controlling the purging gas pressure. In order to coat the stationary phase film uniformly throughout the column, a dummy column with the same cross-sectional dimensions is connected at the end of the column. The coating solution is then purged out with a purging gas supplied continuously for several hours to ensure that the solvent is completely evaporated. The film thickness of the stationary phase is determined by tuning the coating speed and the concentration of the stationary phase in the solvent. Crosslinking and deactivation are required after coating to increase thermal stability and reduce tailing for polar compounds.

Micro detector

Many types of micro detectors have been developed with MEMS technology with various detection mechanisms, including thermal ductility, ionization, and interface material property

changes by vapor adsorption. Micro thermal conductivity detectors (μTCD) are flow-through, nondestructive detectors which generate signals by detecting thermal conductivity differences between analyte flows and reference gases[78-79]. Due to the small differences in thermal conductivities of the gases, the low detection limit of μTCD is typically on the order of a few nano-grams. Micro flame ionization detectors (μFID) generate signals by collecting ion charges from analytes that are ionized by hydrogen flame[80]. The low detection limit is similar to the μTCD's because the ionization efficiency is impaired by flame size reduction. For cantilever bridges[81], surface acoustic waves[82-83], and quartz crystal microbalance transducers[84-85], the signal is generated by resonance frequency changes caused by interface material mass changes after vapor adsorption. Charge density changes of graphene[86] and nanowires[87] can generate current changes in transistor type transducers. Polymer resistance, dielectric constant, and refractive index changes after vapor adsorption have been applied in chemresistors[88-90], chemcapacitors[91-93], and optical sensors[94-96], respectively. Multiple nondestructive detectors can be integrated to make sensor arrays providing chemical identification through multivariate analysis.

Photoionization detectors (PID) are one of the most widely used gas detectors and are applicable to a variety of organic and inorganic compounds [97]. The non-destructive nature of the PID enables the use of multiple PIDs for *in-situ* vapor detection in multi-dimensional GC. Recently, μPIDs have been developed with on-chip designs, miniaturized dimensions, and small ionization chambers [16-18]. They have fast response times (<0.1 s) and significantly improved sensitivities (picogram or ppt level), and can readily be integrated with micro-GC (μGC) for field applications.

1.6 References

1. Guiochon, G.; Guillemin, C. L., Gas chromatography. *Review of Scientific Instruments* **1990,** *61* (11), 3317-3339.
2. McNair, H. M.; Miller, J. M.; Snow, N. H., *Basic gas chromatography*. John Wiley & Sons: 2019.
3. Camino-Sánchez, F. J.; Zafra-Gómez, A.; Pérez-Trujillo, J. P.; Conde-González, J. E.; Marques, J. C.; Vílchez, J. L., Validation of a GC–MS/MS method for simultaneous determination of 86 persistent organic pollutants in marine sediments by pressurized liquid extraction followed by stir bar sorptive extraction. *Chemosphere* **2011,** *84* (7), 869-881.
4. Bristow, T.; Harrison, M.; Sims, M., The application of gas chromatography/atmospheric pressure chemical ionisation time-of-flight mass spectrometry to impurity identification in Pharmaceutical Development. *Rapid Communications in Mass Spectrometry* **2010,** *24* (11), 1673-1681.
5. Wolthers, B. G.; Kraan, G. P. B., Clinical applications of gas chromatography and gas chromatography–mass spectrometry of steroids. *Journal of Chromatography A* **1999,** *843* (1), 247-274.
6. de Koning, S.; Janssen, H.-G.; Brinkman, U. A. T., Modern Methods of Sample Preparation for GC Analysis. *Chromatographia* **2009,** *69* (1), 33.
7. Lara-Gonzalo, A.; Sánchez-Uría, J. E.; Segovia-García, E.; Sanz-Medel, A., Critical comparison of automated purge and trap and solid-phase microextraction for routine determination of volatile organic compounds in drinking waters by GC–MS. *Talanta* **2008,** *74* (5), 1455-1462.
8. Vreuls, J. J.; de Jong, G. J.; Brinkman, U. A. T., On-line coupling of liquid chromatography, capillary gas chromatography and mass spectrometry for the determination and identification of polycyclic aromatic hydrocarbons in vegetable oils. *Chromatographia* **1991,** *31* (3), 113-118.
9. Aragón, M.; Borrull, F.; Marcé, R. M., Thermal desorption-gas chromatography–mass spectrometry method to determine phthalate and organophosphate esters from air samples. *Journal of Chromatography A* **2013,** *1303*, 76-82.
10. Marcillo, A.; Jakimovska, V.; Widdig, A.; Birkemeyer, C., Comparison of two common adsorption materials for thermal desorption gas chromatography – mass spectrometry of biogenic volatile organic compounds. *Journal of Chromatography A* **2017,** *1514*, 16-28.
11. Jaillais, B.; Bertrand, V.; Auger, J., Cryo-trapping/SPME/GC analysis of cheese aroma. *Talanta* **1999,** *48* (4), 747-753.
12. Basic Overview on Gas Chromatography Columns. In *Analytical Separation Science*, pp 823-834.
13. McWilliam, I. G.; Dewar, R. A., Flame Ionization Detector for Gas Chromatography. *Nature* **1958,** *181* (4611), 760-760.
14. Camin, D. L.; King, R. W.; Shawhan, S. D., Capillary Gas Chromatography Using Micro-Volume Thermal Conductivity Detectors. *Anal. Chem.* **1964,** *36* (7), 1175-1178.
15. Klee, M. S., Chapter 12: Detectors. In *Gas Chromatography*, Poole, C. F., Ed. Elsevier: New York, 2012.
16. Narayanan, S.; Rice, G.; Agah, M., A micro-discharge photoionization detector for micro-gas chromatography. *Microchim. Acta* **2014,** *181*, 493-499.
17. Cai, Q. Y.; Zellers, E. T., Dual-chemiresistor GC detector employing layer-protected metal nanocluster interfaces. *Anal. Chem.* **2002,** *74* (14), 3533-3539.
18. Lin, H. B.; Shih, J. S., Fullerene C60-cryptand coated surface acoustic wave quartz crystal sensor for organic vapors. *Sens. Actuators B: Chemical* **2003,** *92* (3), 243-254.
19. Lewis, P. R.; Manginell, R. P.; Adkins, D. R.; Kottenstette, R. J.; Wheeler, D. R.; Sokolowski, S. S.; Trudell, D. E.; Byrnes, J. E.; Okandan, M.; Bauer, J. M.; Manley, R. G.; Frye-Mason, G. C., Recent advancements in the gas-phase MicroChemLab. *IEEE Sens. J.* **2006,** *6* (3), 784-795.
20. Shopova, S. I.; White, I. M.; Sun, Y.; Zhu, H.; Fan, X.; Frye-Mason, G.; Thompson, A.; Ja, S.-j., On-Column Micro Gas Chromatography Detection with Capillary-Based Optical Ring Resonators. *Anal. Chem.* **2008,** *80*, 2232-2238.

21. Liu, J.; Sun, Y.; Fan, X., Highly versatile fiber-based optical Fabry-Pérot gas sensor. *Opt. Express* **2009,** *17* (4), 2731-2738.
22. Liu, J.; Sun, Y.; Howard, D. J.; Frye-Mason, G.; Thompson, A. K.; Ja, S.-j.; Wang, S.-K.; Mengjun Bai; Taub, H.; Almasri, M.; Fan, X., Fabry-Perot Cavity Sensors for Multipoint On-Column Micro Gas Chromatography Detection. *Anal. Chem.* **2010,** *82*, 4370–4375.
23. Sun, Y.; Liu, J.; Howard, D. J.; Fan, X.; Frye-Mason, G.; Ja, S.-j.; Thompson, A. K., Rapid tandem-column micro-gas chromatography based on optofluidic ring resonators with multi-point on-column detection. *Analyst* **2010,** *135*, 165-171.
24. Reddy, K.; Guo, Y.; Liu, J.; Lee, W.; Khaing Oo, M. K.; Fan, X., Rapid, sensitive, and multiplexed on-chip optical sensors for micro-gas chromatography. *Lab Chip* **2012,** *12*, 901-905.
25. Reddy, K.; Liu, J.; Khaing Oo, M. K.; Fan, X., Integrated Separation Columns and Fabry-Perot Sensors for Microgas Chromatography Systems. *IEEE JMEMS* **2013,** *22*, 1174-1179.
26. Scholten, K.; Fan, X.; Zellers, E. T., Microfabricated optofluidic ring resonator structures. *Appl. Phys. Lett.* **2011,** *99* (14), -.
27. Scholten, K.; Fan, X.; Zeller, E. T., A microfabricated optofluidic ring resonator for sensitive, high-speed detection of volatile organic compounds. *Lab Chip* **2014,** *14*, 3873-3880.
28. McCorkle, D. L.; Warmack, R. J.; Patel, S. V.; Mlsna, T.; Hunter, S. R.; Ferrell, T. L., Ethanol vapor detection in aqueous environments using micro-capacitors and dielectric polymers. *Sens. Actuators B: Chemical* **2005,** *107* (2), 892-903.
29. Patel, S. V.; Hobson, S. T.; Cemalovic, S.; Mlsna, T. E., Detection of methyl salicylate using polymer-filled chemicapacitors. *Talanta* **2008,** *76* (4), 872-877.
30. Wright, L. K.; Zellers, E. T., A nanoparticle-coated chemiresistor array as a microscale gas chromatograph detector for explosive marker compounds: flow rate and temperature effects. *Analyst* **2013,** *138* (22), 6860-6868.
31. Lee, C. Y.; Sharma, R.; Radadia, A. D.; Masel, R. I.; Strano, M. S., On-Chip Micro Gas Chromatograph Enabled by a Noncovalently Functionalized Single-Walled Carbon Nanotube Sensor Array. *Angew. Chem. Int. Ed.* **2008,** *47*, 5018-5021.
32. Kulkarni, G. S.; Reddy, K.; Zhong, Z.; Fan, X., Graphene nanoelectronic heterodyne sensor for rapid and sensitive vapour detection. *Nature Commun.* **2014,** *5*, 4376.
33. Grob, R. L.; Barry, E. F., *Modern practice of gas chromatography*. John Wiley & Sons: 2004.
34. Kulsing, C.; Nolvachai, Y.; Rawson, P.; Evans, D. J.; Marriott, P. J., Continuum in MDGC Technology: From Classical Multidimensional to Comprehensive Two-Dimensional Gas Chromatography. *Anal Chem* **2016,** *88* (7), 3529-3538.
35. Dallüge, J.; Beens, J.; Brinkman, U. A. T., Comprehensive two-dimensional gas chromatography: a powerful and versatile analytical tool. *J. Chromatogr. A* **2003,** *1000* (1–2), 69-108.
36. Marriott, P. J.; Chin, S.-T.; Maikhunthod, B.; Schmarr, H.-G.; Bieri, S., Multidimensional gas chromatography. *TrAC* **2012,** *34*, 1-21.
37. Seeley, J. V.; Seeley, S. K., Multidimensional Gas Chromatography: Fundamental Advances and New Applications. *Anal. Chem.* **2012,** *85* (2), 557-578.
38. Seeley, J. V.; Seeley, S. K., Multidimensional Gas Chromatography: Fundamental Advances and New Applications. *Anal. Chem.* **2013,** *85* (2), 557-578.
39. Chin, S.-T.; Marriott, P. J., Multidimensional gas chromatography beyond simple volatiles separation. *Chem. Comm.* **2014,** *50* (64), 8819-8833.
40. Edwards, M.; Mostafa, A.; Górecki, T., Modulation in comprehensive two-dimensional gas chromatography: 20 years of innovation. *Anal. Bioanal. Chem.* **2011,** *401* (8), 2335-2349.
41. Pursch, M.; Sun, K.; Winniford, B.; Cortes, H.; Weber, A.; McCabe, T.; Luong, J., Modulation techniques and applications in comprehensive two-dimensional gas chromatography (GC×GC). *Anal. Bioanal. Chem.* **2002,** *373* (6), 356-367.
42. Dallüge, J.; Beens, J.; Brinkman, U. A. T., Comprehensive two-dimensional gas chromatography: a powerful and versatile analytical tool. *J. Chromatogr. A* **2003,** *1000*, 69-108.

43. Marriott, P. J.; Kinghorn, R. M., New operational modes for multidimensional and comprehensive gas chromatography by using cryogenic modulation. *Journal of Chromatography A* **2000,** *866* (2), 203-212.
44. Ong, R. C.; Marriott, P. J., A review of basic concepts in comprehensive two-dimensional gas chromatography. *Journal of chromatographic science* **2002,** *40* (5), 276-291.
45. Peter Baugh, J., Advances and Changes in the Techniques of Multi-Dimensional and Comprehensive Chromatography and When Coupled with Mass Spectrometry. *J Anal Bioanal Tech* **2016,** *7* (323), 2.
46. Legrum, C.; Gracia-Moreno, E.; Lopez, R.; Potouridis, T.; Langen, J.; Slabizki, P.; Weiand, J.; Schmarr, H.-G., Quantitative analysis of 3-alkyl-2-methoxypyrazines in German Sauvignon blanc wines by MDGC–MS or MDGC–MS/MS for viticultural and enological studies. *European Food Research and Technology* **2014,** *239* (4), 549-558.
47. Jerman, J. H.; Terry, S. C., A miniature gas chromatograph for atmospheric monitoring. *Environ. Int.* **1981,** *5* (2), 77-83.
48. Bond, E. J.; Dumas, T., A portable gas chromatograph for macro- and microdetermination of fumigants in the field. *J. Agric. Food Chem.* **1982,** *30* (5), 986-988.
49. Lorenzelli, L.; Benvenuto, A.; Adami, A.; Guarnieri, V.; Margesin, B.; Mulloni, V.; Vincenzi, D., Development of a gas chromatography silicon-based microsystem in clinical diagnostics. *Biosens. Bioelectron.* **2005,** *20* (10), 1968-1976.
50. Thompson, C. V.; Goedert, M. G., Field-Portable Instrumentation for Gas and Vapor Samples. In *Encyclopedia of Analytical Chemistry*, John Wiley & Sons, Ltd: 2006.
51. Ohira, S.-I.; Toda, K., Micro gas analyzers for environmental and medical applications. *Anal. Chim. Acta.* **2008,** *619* (2), 143-156.
52. Liu, X.; Pawliszyn, J., On-site environmental analysis by membrane extraction with a sorbent interface combined with a portable gas chromatograph system. *Int. J. Environ. Anal. Chem.* **2005,** *85* (15), 1189-1200.
53. Mohsen, Y.; Lahlou, H.; Sanchez, J.-B.; Berger, F.; Bezverkhyy, I.; Weber, G.; Bellat, J.-P., Development of a micro-analytical prototype for selective trace detection of orthonitrotoluene. *Microchem. J.* **2014,** *114*, 48-52.
54. Jian, R.-S.; Wang, T.-Y.; Song, L.-Y.; Kuo, C.-Y.; Tian, W.-C.; Lo, E.-W.; Lu, C.-J., Field investigations and dynamic measurements of process activity induced VOCs inside a semiconductor cleanroom. *Build. Environ.* **2015,** *94*, 287-295.
55. Akbar, M.; Shakeel, H.; Agah, M., GC-on-Chip: Integrated Column and Photo Ionization Detector. *Lab Chip* **2015,** *15*, 1748-1758.
56. Akbar, M.; Restaino, M.; Agah, M., Chip-scale gas chromatography: From injection through detection. *Microsyst. Nanoeng.* **2015,** *1*, 15039.
57. Yutao, Q.; Yogesh, B. G., iGC2 : an architecture for micro gas chromatographs utilizing integrated bi-directional pumps and multi-stage preconcentrators. *J. Micromech. Microeng.* **2014,** *24* (6), 065011.
58. Qin, Y.; Gianchandani, Y. B., iGC1: An Integrated Fluidic System for Gas Chromatography Including Knudsen Pump, Preconcentrator, Column, and Detector Microfabricated by a Three-Mask Process. *J. Microelectromech. Syst.* **2014,** *23* (4), 980-990.
59. Bulbul, A.; Kim, H., A bubble-based microfluidic gas sensor for gas chromatographs. *Lab Chip* **2015,** *15* (1), 94-104.
60. Hsieh, H.-C.; Kim, H., A miniature closed-loop gas chromatography system. *Lab Chip* **2016,** *16* (6), 1002-1012.
61. Jian, R.-S.; Huang, Y.-S.; Lai, S.-L.; Sung, L.-Y.; Lu, C.-J., Compact instrumentation of a μ-GC for real time analysis of sub-ppb VOC mixtures. *Microchem. J.* **2013,** *108*, 161–167.
62. Ali, S.; Ashraf-Khorassani, M.; Taylor, L. T.; Agah, M., MEMS-based semi-packed gas chromatography columns. *Sensors and Actuators B: Chemical* **2009,** *141* (1), 309-315.

63. Sun, J.; Cui, D.; Li, Y.; Zhang, L.; Chen, J.; Li, H.; Chen, X., A high resolution MEMS based gas chromatography column for the analysis of benzene and toluene gaseous mixtures. *Sensors and Actuators B: Chemical* **2009,** *141* (2), 431-435.
64. Agah, M.; Lambertus, G. R.; Sacks, R.; Wise, K., High-speed MEMS-based gas chromatography. *Journal of microelectromechanical systems* **2006,** *15* (5), 1371-1378.
65. Navaei, M.; Mahdavifar, A.; Dimandja, J.-M. D.; McMurray, G.; Hesketh, P. J., All silicon micro-GC column temperature programming using axial heating. *Micromachines* **2015,** *6* (7), 865-878.
66. Li, Y.; Du, X.; Wang, Y.; Tai, H.; Qiu, D.; Lin, Q.; Jiang, Y., Improvement of column efficiency in MEMS-Based gas chromatography column. *RSC Advances* **2014,** *4* (8), 3742-3747.
67. Radadia, A.; Salehi-Khojin, A.; Masel, R.; Shannon, M., The effect of microcolumn geometry on the performance of micro-gas chromatography columns for chip scale gas analyzers. *Sensors and Actuators B: Chemical* **2010,** *150* (1), 456-464.
68. Radadia, A. D.; Morgan, R. D.; Masel, R. I.; Shannon, M. A., Partially Buried Microcolumns for Micro Gas Analyzers. *Analytical Chemistry* **2009,** *81* (9), 3471-3477.
69. Nakai, T.; Nishiyama, S.; Shuzo, M.; Delaunay, J.; Yamada, I., Micro-fabricated semi-packed column for gas chromatography by using functionalized parylene as a stationary phase. *Journal of Micromechanics and Microengineering* **2009,** *19* (6), 065032.
70. MacNaughton, S. I.; Sonkusale, S., Gas Analysis System on Chip With Integrated Diverse Nanomaterial Sensor Array. *IEEE Sensors Journal* **2015,** *15* (6), 3500-3506.
71. Reidy, S.; Lambertus, G.; Reece, J.; Sacks, R., High-performance, static-coated silicon microfabricated columns for gas chromatography. *Analytical Chemistry* **2006,** *78* (8), 2623-2630.
72. Lambertus, G.; Elstro, A.; Sensenig, K.; Potkay, J.; Agah, M.; Scheuering, S.; Wise, K.; Dorman, F.; Sacks, R., Design, Fabrication, and Evaluation of Microfabricated Columns for Gas Chromatography. *Analytical Chemistry* **2004,** *76* (9), 2629-2637.
73. Terry, S. C.; Jerman, J. H.; Angell, J. B., A gas chromatographic air analyzer fabricated on a silicon wafer. *IEEE Transactions on Electron Devices* **1979,** *26* (12), 1880-1886.
74. Narayanan, S.; Alfeeli, B.; Agah, M., A micro gas chromatography chip with an embedded non-cascaded thermal conductivity detector. *Procedia Engineering* **2010,** *5*, 29-32.
75. Narayanan, S.; Agah, M., Fabrication and characterization of a suspended TCD integrated with a gas separation column. *Journal of Microelectromechanical Systems* **2013,** *22* (5), 1166-1173.
76. Deng, C.; Yang, X.; Li, N.; Huang, Y.; Zhang, X., A novel miniaturized flame ionization detector for portable gas chromatography. *Journal of chromatographic science* **2005,** *43* (7), 355-357.
77. Xu, P.; Li, X.; Yu, H.; Xu, T., Advanced nanoporous materials for micro-gravimetric sensing to trace-level bio/chemical molecules. *Sensors* **2014,** *14* (10), 19023-19056.
78. Yeo, L. Y.; Friend, J. R., Ultrafast microfluidics using surface acoustic waves. *Biomicrofluidics* **2009,** *3* (1), 012002.
79. Ballantine Jr, D. S.; Wohltjen, H., Surface acoustic wave devices for chemical analysis. *Analytical Chemistry* **1989,** *61* (11), 704A-715A.
80. Cheng, C.-S.; Chen, Y.-Q.; Lu, C.-J., Organic vapour sensing using localized surface plasmon resonance spectrum of metallic nanoparticles self assemble monolayer. *Talanta* **2007,** *73* (2), 358-365.
81. Chen, Y.-Q.; Lu, C.-J., Surface modification on silver nanoparticles for enhancing vapor selectivity of localized surface plasmon resonance sensors. *Sensors and Actuators B: Chemical* **2009,** *135* (2), 492-498.
82. Kulkarni, G. S.; Reddy, K.; Zhong, Z.; Fan, X., Graphene nanoelectronic heterodyne sensor for rapid and sensitive vapour detection. *Nature communications* **2014,** *5*, 4376.
83. Lee, C. Y.; Sharma, R.; Radadia, A. D.; Masel, R. I.; Strano, M. S., On-Chip Micro Gas Chromatograph Enabled by a Noncovalently Functionalized Single-Walled Carbon Nanotube Sensor Array. *Angewandte Chemie International Edition* **2008,** *47* (27), 5018-5021.
84. Steinecker, W. H.; Rowe, M.; Matzger, A.; Zellers, E. In *Chemiresistor array with nanocluster interfaces as a micro-GC detector*, TRANSDUCERS, Solid-State Sensors, Actuators and Microsystems, 12th International Conference on, 2003, IEEE: 2003; pp 1343-1346.

85. Zhong, Q.; Steinecker, W. H.; Zellers, E. T., Characterization of a high-performance portable GC with a chemiresistor array detector. *Analyst* **2009,** *134* (2), 283-293.
86. Kim, S. K.; Chang, H.; Zellers, E. T. In *Prototype micro gas chromatograph for breath biomarkers of respiratory disease*, TRANSDUCERS 2009 - 2009 International Solid-State Sensors, Actuators and Microsystems Conference, 21-25 June 2009; 2009; pp 128-131.
87. Qin, Y.; Gianchandani, Y. B., A fully electronic microfabricated gas chromatograph with complementary capacitive detectors for indoor pollutants. *Microsystems &Amp; Nanoengineering* **2016,** *2*, 15049.
88. Patel, S.; Mlsna, T.; Fruhberger, B.; Klaassen, E.; Cemalovic, S.; Baselt, D., Chemicapacitive microsensors for volatile organic compound detection. *Sensors and Actuators B: Chemical* **2003,** *96* (3), 541-553.
89. Mlsna, T. E.; Cemalovic, S.; Warburton, M.; Hobson, S. T.; Mlsna, D. A.; Patel, S. V., Chemicapacitive microsensors for chemical warfare agent and toxic industrial chemical detection. *Sensors and Actuators B: Chemical* **2006,** *116* (1-2), 192-201.
90. Sun, Y.; Fan, X., Optical ring resonators for biochemical and chemical sensing. *Analytical and bioanalytical chemistry* **2011,** *399* (1), 205-211.
91. Reddy, K.; Guo, Y.; Liu, J.; Lee, W.; Oo, M. K. K.; Fan, X., On-chip Fabry–Pérot interferometric sensors for micro-gas chromatography detection. *Sensors and Actuators B: Chemical* **2011,** *159* (1), 60-65.
92. Scholten, K.; Reddy, K.; Fan, X.; Zellers, E. T., Vapor discrimination by dual-laser reflectance sensing of a single functionalized nanoparticle film. *Analytical Methods* **2013,** *5* (16), 4268-4272.
93. Verner, P., Photoionization detection and its applications in gas chromatography. *J. Chromatogr.* **1984,** *300*, 249-264.
94. Sun, J.; Guan, F.; Cui, D.; Chen, X.; Zhang, L.; Chen, J., An improved photoionization detector with a micro gas chromatography column for portable rapid gas chromatography system. *Sens. Actuators B.* **2013,** *188*, 513– 518.
95. Akbar, M.; Restaino, M.; Agah, M., Chip-scale gas chromatography: From injection through detection. *Nat. Microsys. Nanoeng.* **2015,** *1*.
96. Zhu, H.; Nidetz, R.; Zhou, M.; Lee, J.; Buggaveeti, S.; Kurabayashi, K.; Fan, X., Flow-through microfluidic photoionization detectors for rapid and highly sensitive vapor detection. *Lab Chip* **2015,** *15* (14), 3021-3029.

Chapter 2 Portable GC for Water Contamination Analysis

Reproduced from Ref. 129 with permission from the Royal Society of Chemistry.

2.1 Introduction

Volatile organic compounds (VOCs) contamination in natural water is a major environmental issue due to their toxicity and various adverse effects on human health [98-99]. Sources of these compounds include industrial effluents, waste disposals, solvents, gasoline or oil spills on the ground surface, agricultural pesticides and herbicides, and disinfection processes [100]. To protect the public from contaminated water, the Environmental Protection Agency (EPA) has established maximum contaminant levels (MCLs), the highest concentration of a contaminant allowed in drinking water. Since the MCLs for many VOC contaminants are very low (μg L^{-1} or parts-per-billion in terms of mass), sensitive and quantitative analytical methods are greatly needed for long-term monitoring and remediation applications.

In recent years, sensor arrays or electronic noses have made significant progress in VOC mixture analysis, including surface acoustic wave (SAW) [101], quartz crystal microbalance (QCM) [102], metal-oxide-semiconductor field-effect transistor (MOSFET) [103] and colorimetric sensor [104]. These sensor arrays are cost effective and compact in size, some of which have also achieved low detection limits; however, with the increased number of compounds, the complexity of multivariate analysis or pattern recognition for reading sensor array's response patterns increases. On the other hand, gas chromatography (GC) coupled with spectrometers (such as mass spectrum (MS) [105-109], and ion mobility spectroscopy (IMS) [110-111]) or other vapor detectors (such as flame

ionization detector (FID) [112], photoionization detector (PID) [113], thermal conductivity detector (TCD) [114], and electron capture detector (ECD) [115]) are more suitable for the complex analysis, where VOC mixtures are separated and subsequently detected and quantified individually. Nowadays the well-established analytical method for VOCs quantification is EPA Method 5030/8260B [116-117], by which samples are first collected to canisters and then taken to a well-equipped analytical chemistry laboratory for GC–MS analysis. This process is time consuming (from a few days to over a week) and costly. Additionally, volatilization losses and contaminations of samples may occur during shipment and storage.

Field-portable GCs [58, 89, 112, 118-123] and MEMS-based micro scale gas chromatography (μGC) systems [17, 124-126] have been developed for analyzing VOCs on-site. Most portable GC/μGC systems consist of a preconcentrator/injector or an injection port, a separation column, a detector, and a pump or a carrier gas cartridge, all of which are fluidically interconnected. Various detectors have been integrated in these systems, such as chemiresistor [89, 118], ion trap mass spectrometer [118, 120-121], SAW microsenesor [121, 127], micro-FID [112] and bubble based microfluidic sensor [128]. However, most of these portable GC and μGC systems are focused on air sampling and only a few systems can be used to analyze VOCs in water sample such as the portable GC/SAW system with liquid extraction [120] or static headspace sampling [121], the portable GC-μFID systems coupled with headspace solid-phase extraction (HS-SPME) [112], the μPE (micro purge extraction) -μGC-μTCD system [126] and static headspace sampling with micro-helium discharge photoionization detector [17]. While those systems have all achieved compact size and fast analysis (a few seconds to several minutes, including sampling and analyzing time), they have either limited sensitivity (hundreds of $\mu g\ L^{-1}$) or insufficient separation capability for complex samples (usually fewer than 10 VOCs are analyzed).

To address this issue, we built a fully automated, portable gas chromatography system[129] integrated with a purge and trap water sampling system and flow-through PID (portable P&T-GC-PID) for sensitive and rapid VOC quantification in water. This system achieved a detection limit of sub μg L^{-1} (or sub-ppb in terms of mass) and short analysis time (~10 minutes, depending on the target VOCs, which can be further shortened) with light weight (less than 4 kg) and compact size (40 cm × 30 cm × 10 cm). Field studies using groundwater samples from a recovery well showed that VOC results obtained with our portable GC quantitatively match those generated with EPA standard procedures and benchtop instruments from an analytical lab.

2.2 Theoretical analysis to define purge and trap sampling parameters

For determination of VOC concentrations in water samples, several sample preparation techniques have been developed, such as membrane extraction [124, 130], static headspace techniques [17, 120], purge and trap (P&T) methods [108, 126, 131-132], and solid-phase microextraction (SPME) [106, 112, 133]. Compared to static headspace and SPME, P&T is capable of transferring more VOCs to the cryo- or sorbent- trap and thus has a better detection limit. In addition, P&T is in compliance with EPA Method 8260B, which is commonly used by analytical labs in water sample analysis. Therefore, we adopted P&T for our portable GC system.

2.2.1 Henry's law

Henry's law[134] states that at equilibrium conditions, the amount of dissolved gas in water is proportional to its partial pressure in gas phase under a given temperature. In essence, Henry's law expresses the distribution of a certain gas in water and headspace air. Notably, there are two common types of Henry's law constants due to historical reasons: the first is the aqueous phase concentration divided by the gas phase concentration, the second is the gas phase concentration divided by the aqueous phase concentration. Here, we use the first definition.

Assuming that the analyte is under partition equilibrium during the purging process, the concentration ratio between gas phase and liquid phase is constant and is given by the Henry's constant [134]:

$$K_H = \frac{c_r}{p_g}, \tag{2.1}$$

where c_r (mol L^{-1}) refers to analyte concentrations in water, K_H (mol L^{-1} atm^{-1}) is the Henry's law solubility constant for an analyte, and p_g (atm) is the partial pressure of the analyte in headspace. The temperature dependence of K_H can be expressed as:

$$K_H = K_H^0 \exp\left[\varepsilon\left(\frac{1}{T} - \frac{1}{T^0}\right)\right], \tag{2.2}$$

where K_H^0 is the Henry's constant under standard conditions (T^0=298.15 K) and ε (K) is the temperature dependent constant acquired experimentally.

2.2.2 Purge Efficiency

The process of purging organics out of water can be approximated as partitioning between the water and the purge gas. Purge efficiency (η) is defined as

$$\eta(\%) = \frac{c_0 - c_r}{c_0} \times 100, \tag{2.3}$$

where c_0 (mol L^{-1}) and c_r (mol L^{-1}) are the analyte concentrations of the water sample before and after purging, respectively.

Since c_r continuously decreases during the purging process, a differential model can be established. Assuming that the analyte concentration in the water sample decreases by Δc_r after a purge gas (*e.g.*, helium) volume ΔV_g passes through, and according to ideal gas law and mass conservation, we have:

$$p_g \cdot \Delta V_g = RT \cdot \Delta n_g, \tag{2.4}$$

$$\Delta n_g = -V_l \cdot \Delta c_r, \tag{2.5}$$

where R (L atm mol^{-1} K^{-1}) is the ideal gas constant, T (K) is the purging temperature, V_l (L) is the water sample volume, and Δn_g (mol) is the mole number of the analyte that shifts from liquid phase to gas phase. Solving Equations (2.4) and (2.5) with the initial condition of $c_r = c_0$ when $V_g = 0$, we have:

$$c_r = c_0 \exp(-\frac{V_g}{RTK_H V_l}). \tag{2.6}$$

Thus, the purge efficiency is:

$$\eta(\%) = \left[1 - \exp(-\frac{V_g}{RTK_H V_l})\right] \times 100 \tag{2.7}$$

Using Equations (2.2) and (2.7) and constants K_H^0 and ε listed in Table 2.1, the theoretical purge efficiency for benzene, cis-1,2-dichloroethylene (cis-1,2-DCE), p-xylene, trichloroethene (TCE), tetrachloroethylene (PCE), and toluene under different purging conditions are presented in Figure 2.1. For a water sample volume of V_l=10 mL, a purge gas volume of 500 mL results in V_g/V_l=50, which, according to Figure 2.1 (B), corresponds to a purge efficiency in excess of 99%, even at a temperature of 15 °C.

Table 2.1 Physical properties and calibration data summary of the six VOCs.

Compound name	Solubility in water (g L^{-1}) at 25 °C	K_H^0 (mol L^{-1} atm^{-1}) [134]	ε (K) [134]	R^2	Detection limit at 3σ (μg L^{-1} or ppb)	MCL* (μg L^{-1} or ppb)	Potential health effects
cis-1,2-dichloroethylene (cis-1,2-DCE)	3.5	0.27	4200	0.9997	0.11	70	Liver problems

benzene	1.8	0.18	3200	0.9999	0.28	5	Anemia; decrease in blood platelets; increased risk of cancer
trichloroethene (TCE)	1.1	0.11	4800	0.9997	0.31	5	Liver problems; increased risk of cancer
toluene	0.52	0.15	3400	0.9962	0.13	1000	Nervous system, kidney, or liver problems
tetrachloroethylene (PCE)	0.15	0.057	5100	0.9994	0.13	5	Liver problems; increased risk of cancer
p-xylene	0.20	0.17	4500	0.9991	0.15	10000 (xylenes total)	Nervous system damage

*Maximum contamination level. The highest level of a contaminant that is allowed in drinking water as defined by the United States Environmental Protection Agency.

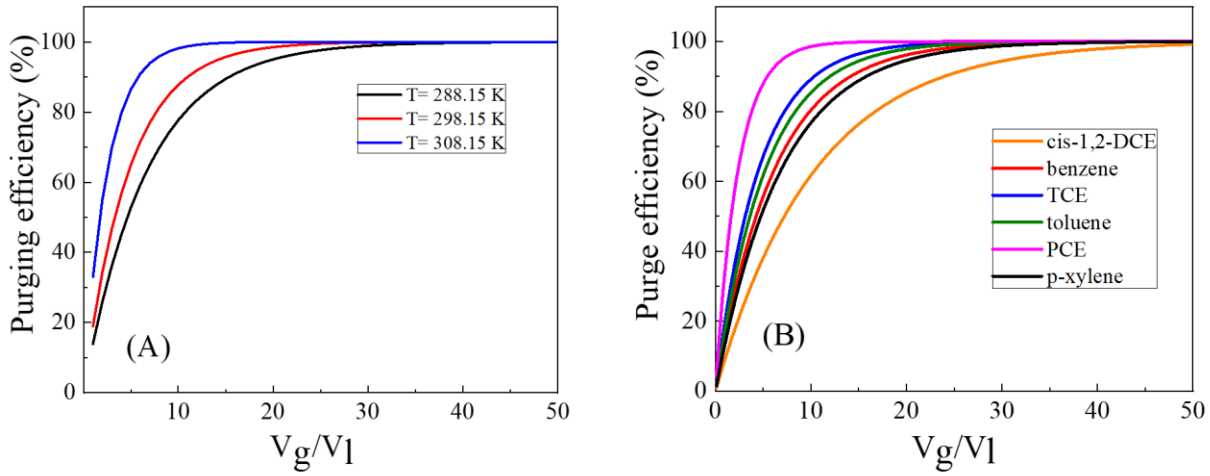

Figure 2.1 (A) Purge efficiency for p-xylene under different purge temperatures. For all VOCs with ε>0, purge efficiency increases with temperature. (B) Purge efficiency at 288.15 K for 6 VOCs with K_H^0 ranging from 0.05 to 0.27 mol L^{-1} atm^{-1} (see Table 2.1). A theoretical purge efficiency of over 99% can be achieved when V_g/V_l is 50 at 288.15K

2.3 Portable GC device assembly and characterization

2.3.1 Materials

All analytes used in the experiment were purchased from Sigma Aldrich (St. Louis, MO) or Fisher Scientific (Pittsburgh, PA) and had purity greater than 97%. Carbopack™ X, adsorbent material for the microfabricated preconcentrator/injector (μPCI), was purchased from Supelco (Bellefonte, PA). Universal quick seal connectors, universal "Y" connectors, 20 mL vials, and Rtx-VMS capillary columns (10 m × 0.25 mm i.d., 1.4 μm film thickness) were purchased from Restek (Bellefonte, PA). Two-port and three-port solenoid valves were purchased from Lee Company (Westbrook, CT). A mini-diaphragm pump was purchased from Gast Manufacturing (Benton Harbor, MI). Nickel wire (0.32 mm diameter, 1.24 Ohms/m), used as heating wire for the capillary column, was purchased from Lightning Vapes (Bradenton, FL). Disposable helium cartridges (95 cm^3, 2500 psig) were purchased from Leland (South Plainfield, NJ). Commercial PIDs with built-in lamp drive circuits and amplifiers were purchased from Baseline-Mocon (Lyons, CO). Type K thermocouples were purchased from Omega Engineering (Stamford, CT). A data acquisition card, USB-6003 (16 bits) and a USB-TC01 (for thermocouple measurement) were purchased from National Instruments (Austin, TX).

2.3.2 Device setup and operation

Figure 2.2 presents a photograph of the portable GC. The system is housed in an approximately 40 cm (L) × 30 cm (W) × 10 cm (H) plastic case and weighs less than 4 kg. It operates on 110V AC power with an average power consumption of 25 W. Operation using batteries is also possible for field applications. The disposable helium cartridge provides purging gas during sampling and carrier gas during analyzing. Each cartridge provides enough helium for

more than 25 analyses. A LabView™ control program developed in-house is used for automated system.

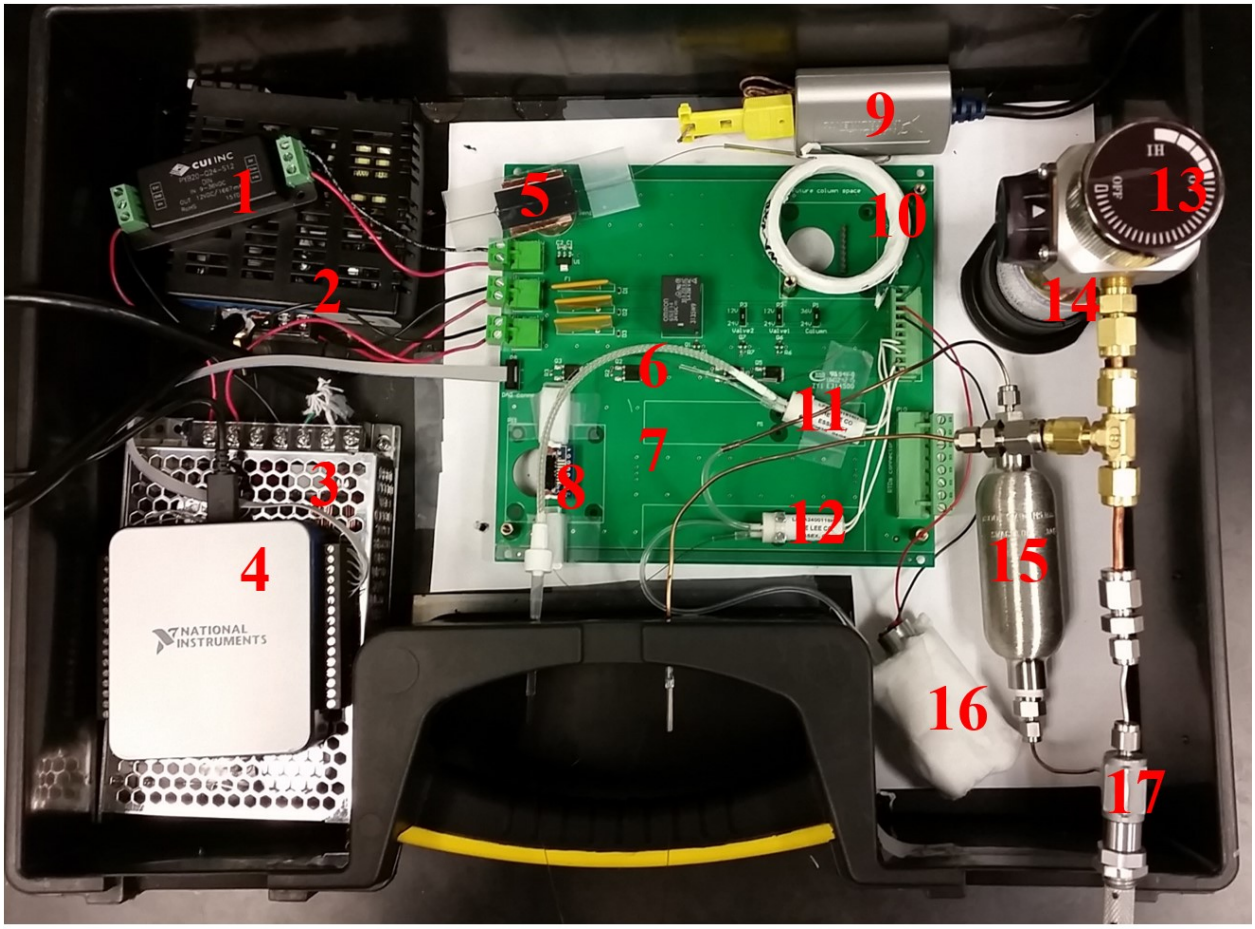

Figure 2.2 Photo of a portable GC system. Components are numbered on the diagram. 1. 12V DC-DC converter; 2. 24V power supply; 3. 36V power supply; 4. data acquisition card; 5. home-made photoionization detector; 6. moisture filter; 7. printed circuit board; 8. µ-preconcentrator/injector; 9. thermocouple data acquisition card; 10. GC column with thermocouple; 11. 3-port solenoid valve; 12. 2-port solenoid valve; 13. regulating valve; 14. helium cartridge; 15. flow buffer; 16. diaphragm pump; and 17. needle valve.

The µPCI was used to trap and accumulate low-concentration VOCs followed by sharp injection into the downstream separation column by thermal desorption. A channel with tapered inlet and outlet ports was etched on a Si wafer by deep-reactive-ion-etching (DRIE), then anodically bonded to a Pyrex Borofloat 33 glass wafer. A platinum microheater and a resistance

temperature detector (RTD) were evaporated onto the backside. Carbopack™ X granules were loaded into the cavity between the etched channel and Pyrex wafer through a third port, which was sealed after loading. For fluidic connections, guard columns were inserted into each port and secured with silicone adhesive. For electrical connections, the microheater and RTD were wire-bonded to a printed circuit board (custom designed and manufactured by M.A.K.S., Inc.). The μPCI was preconditioned at 300 ˚C for 12 hours under helium flow.

The Rtx-VMS capillary column and nickel wire (both 10 meters long) were placed in parallel and wrapped by Teflon tape [135], and then coiled into a helix of 10 cm in diameter and 1 cm in height. A type K thermocouple was inserted into the coil to measure the column temperature via USB-TC01. To achieve a programmed temperature ramping profile, a pulse-width-modulated signal (4.0-Hz square wave) was generated via the USB-6003 and applied to the heater power relay on the printed circuit board. The duty cycle of the square wave was calculated by a proportional-integral-derivative controller in the Labview™ program and updated every 0.4 s based on the set-point temperature and currently measured actual temperature [136].

A PID module was assembled using the commercial PID (which contains a built-in lamp drive circuit and amplifier) and a home-made flow-through ionization chamber. The small dead volume of the ionization chamber allows for rapid response time and sharp chromatographic peaks in comparison with regular ionization chambers [113]. As shown in Figure 2.3, a 2 cm long straight microfluidic channel was created by a 380 μm gap etched onto a conductive silicon wafer with a resistivity of 0.001-0.005 Ω cm and a thickness of 380 μm. The bottom and top of the microfluidic channel was covered by a Krypton UV lamp and a glass slide, respectively, which were then glued to the conductive silicon electrodes with an optical epoxy. Two guard columns (250 μm i.d. and 380 μm o.d.) were inserted into the inlet and outlet of the PID and sealed with optical epoxy. The

output signal of PID was sampled at a rate of 40 KHz and averaged every 0.25 s to yield data points for the chromatogram. Further details of the PID assembly and characterization can be found in reference .

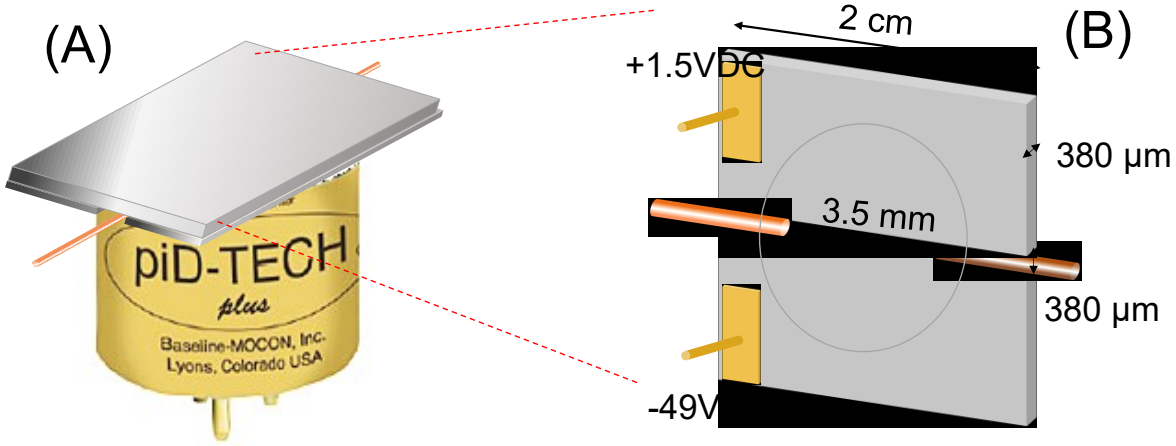

Figure 2.3 Schematic of a home-made PID module with built-in lamp drive circuit and amplifier from a commercial PID. (B) Dimensions and electrical connections of the PID module. A 380 µm wide, 380 µm tall and 2 cm long microfluidic channel was created by a gap between two conductive silicon wafers. A small segment of a guard column was inserted into the channel inlet/outlet for fluidic connection. The bottom and top of the microfluidic channel were covered by a Krypton UV lamp and a glass slide, respectively, which were then glued to the conductive silicon wafers with an optical epoxy. The UV illumination length was about 3.5 mm, as defined by the Krypton window diameter. Two copper wires with copper tape were bonded to the wafers and connected to the amplifier. Reproduced from Ref. 16 with permission from the Royal Society of Chemistry

The instrument operates in two modes as illustrated in Figure 2.4.

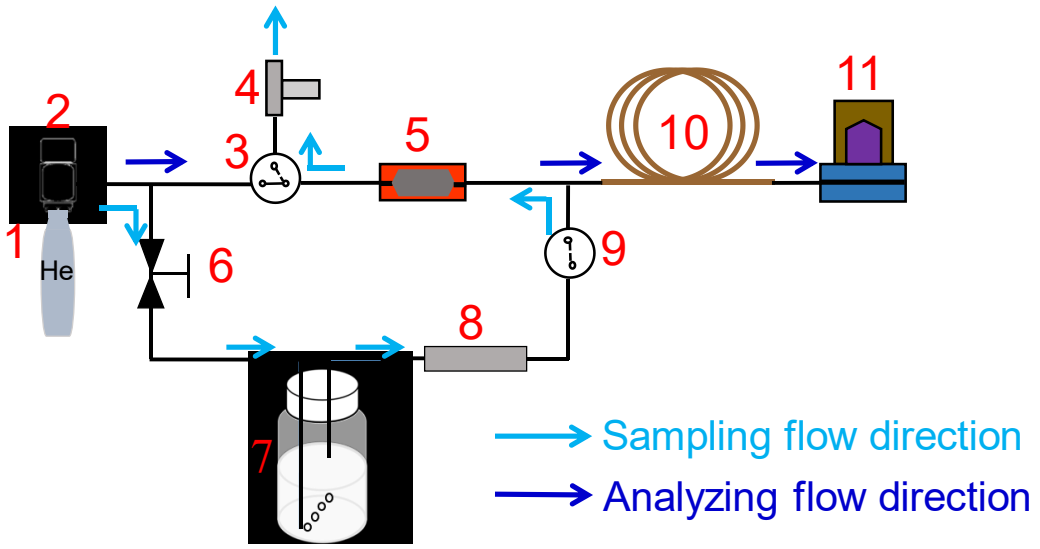

Figure 2.4 Schematic of the portable GC. Flow directions for sampling and analyzing are marked on the figure. Components on the diagram: 1. helium cartridge; 2. regulating valve; 3. 3-port solenoid valve; 4. diaphragm pump; 5. µPCI; 6. needle valve; 7. purging vial; 8. moisture filter; 9. 2-port solenoid valve; 10. GC column with thermocouple; and 11. PID module.

In sampling mode, the two solenoid valves were actuated. Helium gas was bubbled from a 250 µm i.d. fused silica tubing into the water sample, which was held in a purging vial at ambient temperature. Head space vapor was simultaneously drawn by a diaphragm pump through a moisture filter and then a µPCI at a flow rate of 100 mL min^{-1}. The vapors were adsorbed to Carbopack X inside the µPCI during sampling mode. Sampling was performed for 5 minutes, but can be further shortened.

In analyzing mode, the diaphragm pump and solenoid valves were closed. Helium gas was directed through the µPCI and then the column and PID module at a flow rate of 1 mL min^{-1}. After 60 seconds of pressure stabilization and PID baseline recovery period, the µPCI was heated to 270 ˚C in 0.6 s and then kept at 250 ˚C for 5 s for thermal desorption. The column was first heated to and kept at 40 ˚C for 1 min, then ramped to 120 ˚C at a rate of 5 ˚C min^{-1}.

2.3.3 Device characterization

We characterized our device with water samples containing six analytes (benzene, cis-1,2-dichloroethylene (cis-1,2-DCE), p-xylene, trichloroethene (TCE), tetrachloroethylene (PCE), and toluene) at various concentration levels (from 1 μg L^{-1} to 500 μg L^{-1}). These samples were prepared by serial dilution with ultrapure water obtained from a Milli-Q water purification system (Thermo Fisher Scientific, Wayne, MI). All solutions were stored in 20-mL vials, each of which contained 10 mL of water samples and 10 mL of air-filled headspace. All water samples were stored in a 4 ˚C refrigerator, then restored to room temperature before use.

We first characterized the purge efficiency of our system using p-xylene as a model. During the experiment, 10 mL of p-xylene solution with concentrations of 5 μg L^{-1}, 5 μg L^{-1}, 50 μg L^{-1} and 500 μg L^{-1} were placed in four 20-mL purging vials. The helium purging rate and pumping rate were adjusted to 40 mL min^{-1} for the first vial (Column (A) in Figure 2.5) and 100 mL min^{-1} for the other three vials (Columns B-D in Figure 2.5). The time for each purge was set to 5 minutes, resulting in $V_g/V_l = 20$ for the first vial and $V_g/V_l = 50$ for the other three vials. All purge efficiency experiments were performed in a controlled lab environment (temperature 21 ºC). Other experimental conditions are described in section 2.3.3.

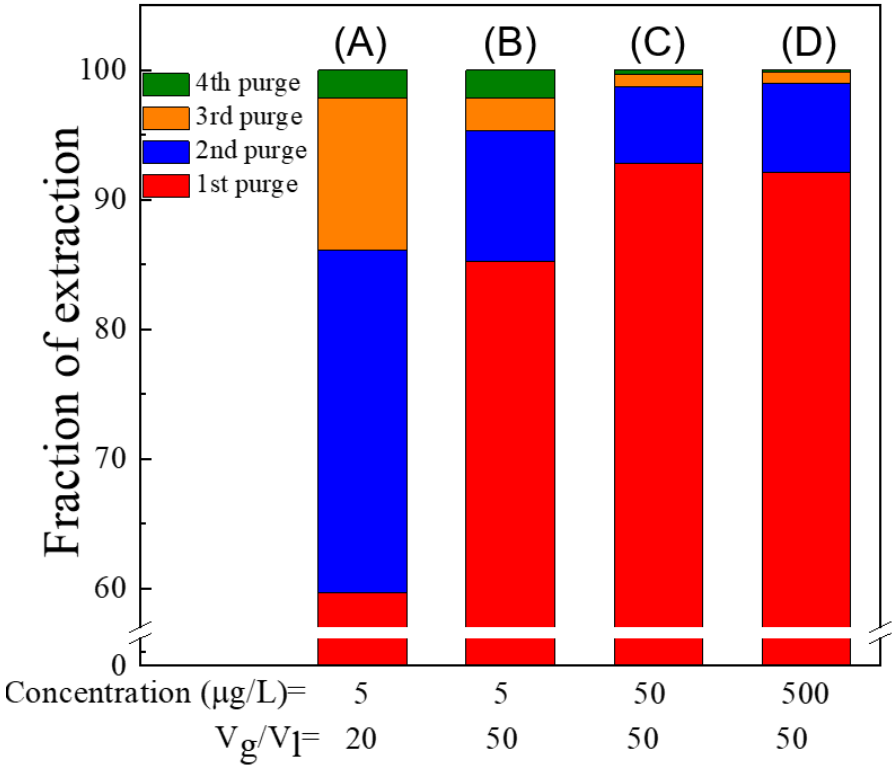

Figure 2.5 Comparison of extraction profiles for various concentrations of p-xylene in water with different helium purging volumes. Under each purging condition, the water sample was purged consecutively four times. The time for each purge was 5 minutes. The helium flow rate was 40 mL min^{-1} for Column (A) and 100 mL min^{-1} for Columns (B)-(D). V_g/V_l for each purge was 20 for Column A and 50 for Columns (B)-(D). Details of p-xylene detection can be found in Figure 2.6.

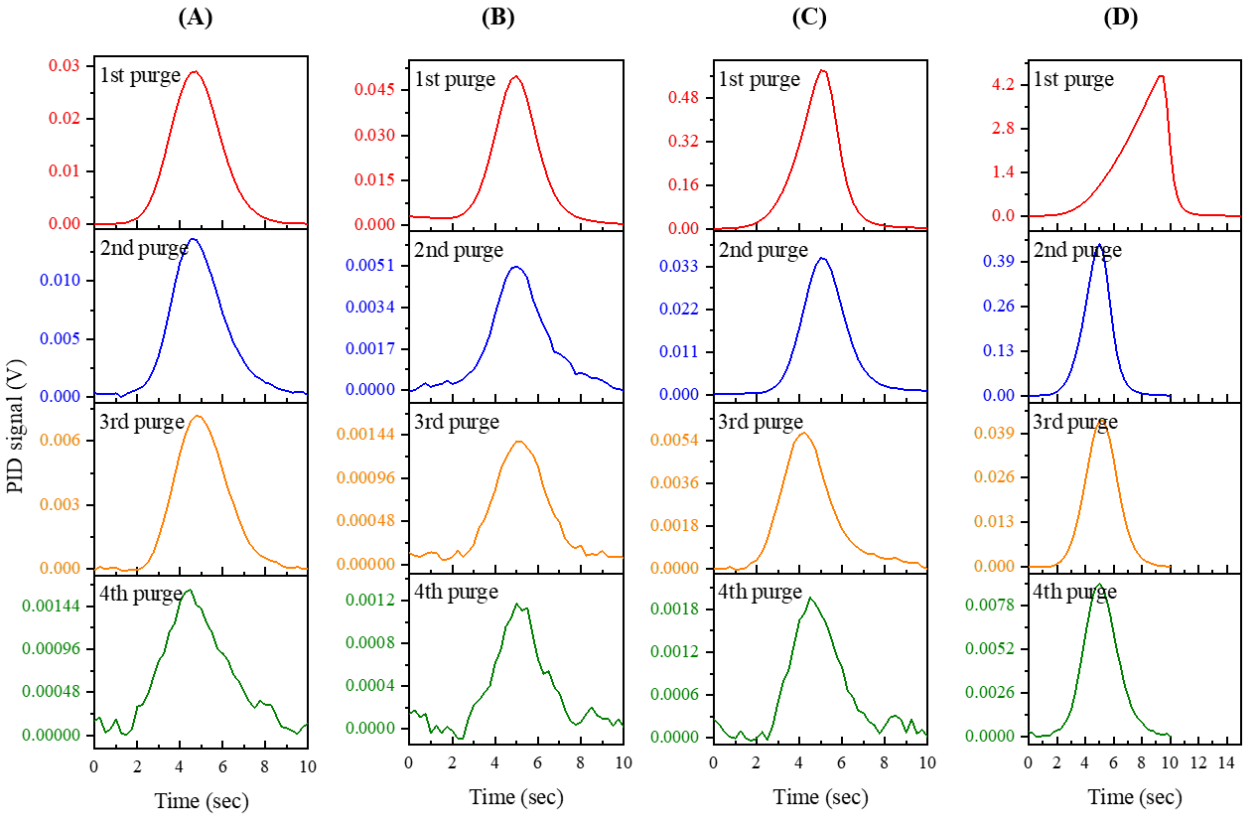

Figure 2.6 System responses of 4 times of consecutive extraction of p-xylene in water. Each extraction time was 5 minutes. (A) V_g/V_l=20, p-xylene concentration: 5 µgL^{-1}. (B) V_g/V_l=50, p-xylene concentration 5 µg L^{-1}. (C) V_g/V_l=50, p-xylene concentration 50 µg L^{-1}. (D) V_g/V_l=50, p-xylene concentration 500 µg L^{-1}.

Each vial was purged and analyzed four times consecutively without changing any solutions. Due to the fact that the concentration of the solution decreased after each purge, the system actually measured analytes from high to low concentrations during the four purges. To avoid possible memory effects between two adjacent purges, the system was cleaned by trigging µPCI injection (heated to 270 ˚C in 0.6 s then kept at 250 ˚C for 5 s at 1 mL mn^{-1} helium flow) three times.

The experimental fraction of extraction for each purge presented in Figure 2.5 is defined as:

$$\eta_e^i = \frac{A_i}{\sum_{n=1}^{4} A_n} \times 100, \tag{2.8}$$

where n is the number of consecutive purges and A_i is the peak area for the i^{th} purge. Column (A) in Figure 2.5 shows that with V_g/V_l=20, a purge efficiency of only 59.6% was obtained from the first purge. With an increased purge flow rate such that V_g/V_l=50, significant improvement in purge efficiency (85.2%) was observed. Although the experimental purge efficiency at V_g/V_l=50 (85.2%, 92.8%, and 92.1% for the first purge in Columns (B), (C), and (D), respectively) is slightly lower than the corresponding theoretical efficiency (all 99.9%), it is adequate for the system to extract and analyze VOCs in water. Therefore, in following experiments, we used V_g/V_l=50 with a purge flow rate of 100 mL min^{-1} and purge time of 5 minutes. One explanation for the discrepancy between the experimental and theoretical purge efficiency is that the equilibrium partitioning between the water sample and the helium bubbles was not fully reached [137-138].

Linear range, detection limit, and precision

The linearity, detection limit, and detection precision of the portable GCwere characterized using the six VOCs listed in Table 2.1 at ambient temperature (21 ºC). The corresponding chromatographic peak (raw response data) of the six VOCs in water with concentrations of 1 µg L^{-1} and 20 µg L^{-1} are presented in Figure 2.7(A) and (B), respectively. The full-widths-at-half-maximum ($fwhm$) of these VOCs at 1 µg L^{-1} vary from 2.25 s to 3 s.

The detection limit (LOD) for the six compounds are calculated based on Equation (2.9):

$$LOD = \frac{3\sigma}{Ph}, \tag{2.9}$$

where σ is the standard deviation of the baseline noise and Ph is the peak height at 1 µg L^{-1} in Figure 2.7(A). Since the LODs (sub-µg L^{-1} level) of these VOCs are at least one order of magnitude lower than the MCLs listed in Table 2.1, the sensitivity of our portable GC is sufficient

for field analysis of water samples. Figure 2.7(C) presents a set of calibration curves for the six VOCs with water sample concentrations ranging from 1 μg L^{-1} to 500 μg L^{-1}. The peak area in Figure 2.8 shows excellent linear response with $R^2 > 0.99$ from linear regression analysis (forced zero Y-intercept on the linear-linear scale). Precisions were calculated using three measurements.

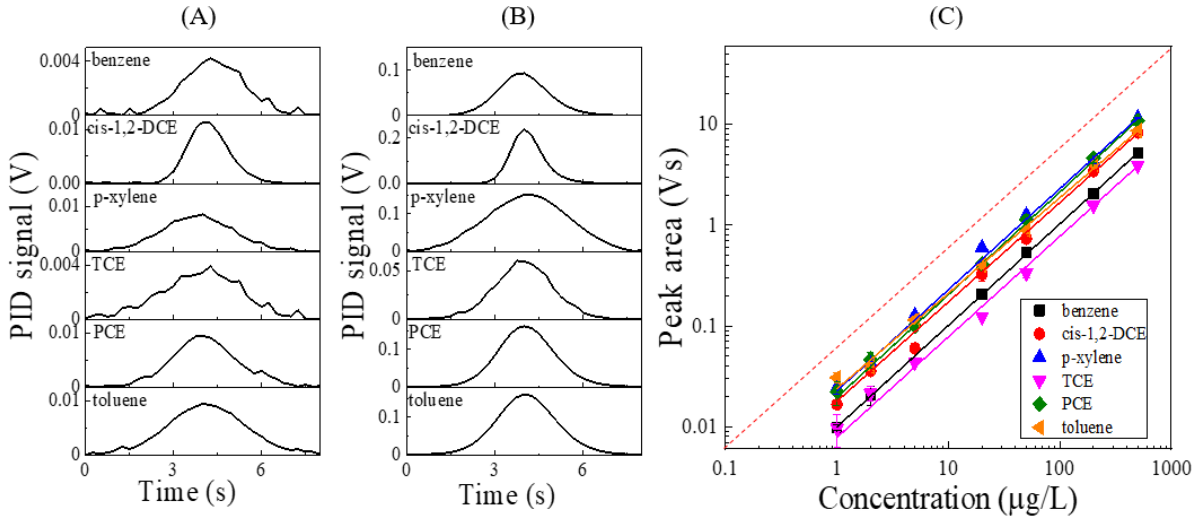

Figure 2.7 Representative chromatograms for the six different compounds at concentrations of (A) 1 μg L^{-1} and (B) 20 μg L^{-1}. Each chromatographic peak is horizontally shifted to be aligned and centered around 4 seconds. (C) Linearity test for the six compounds in (A) and (B). Peak areas as a function of concentrations are plotted on a log–log scale. Error bars are obtained from three measurements. Solid lines are linear fits in log-log scale. The slopes are 1.008, 0.986, 1.003, 0.998, 1.019, and 0.948 for benzene, cis-1,2-DCE, p-xylene, TCE, PCE and toluene, respectively. The dashed line is a curve with slope unity for reference. Details of the linearity, detection limit, and detection precision for these compounds are given in Table 2.1 and Figure 2.8.

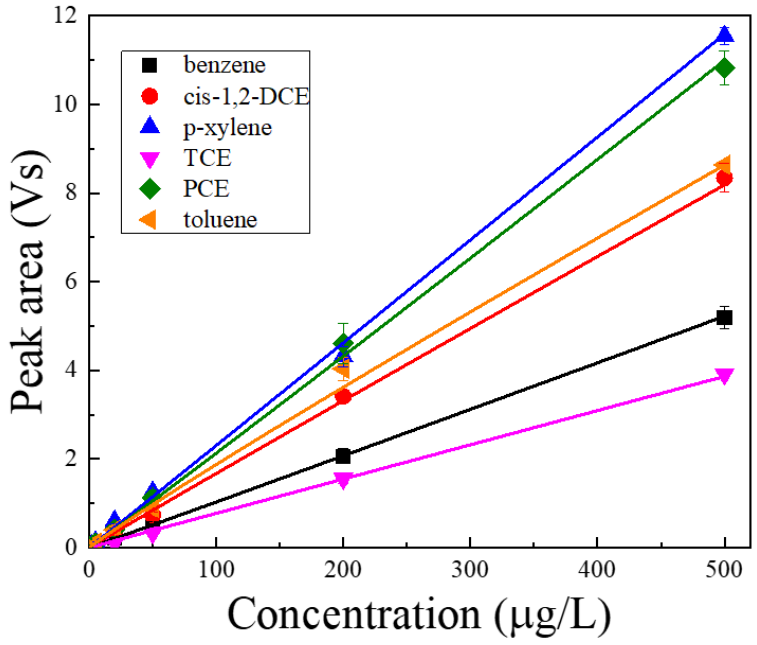

Figure 2.8 Peak areas as a function of analyte concentrations in water are plotted on a linear–linear scale. Error bars are obtained with three measurements. Solid lines are linears fit in linear–linear scales. The R-squared values are 0.999, 0.991, 0.996, 0.990, 0.997 and 0.996 for benzene, cis-1,2-DCE, p-xylene, TCE, PCE, and toluene, respectively. The corresponding log-log scale plot is shown in Figure 2.7(C).

2.4 Portable GC application

2.4.1 Analysis of a complex VOC mixture

In most applications, water samples are complex mixtures of target VOCs and many unrelated VOCs. Thus, a system with strong separation capabilities is desired. To test the separation performance of the portable GC, a water sample containing 26 organic compounds (selected from the EPA Method 8260B [116] analyte list, vapor pressures ranging from 0.087 Torr to 180 Torr), was analyzed. The concentration for each compound was 5 µg L^{-1} in water. A representative chromatogram is presented in Figure 2.9, which provides a retention time reference library for identification of VOCs. The six VOCs previously used to characterize the system were

eluted in less than 6 minutes, and the whole mixture was eluted in 15 minutes. Better separations can be achieved by optimizing the column temperature ramping profile and the analyzing flow rate; shorter analysis times can be achieved by increase the temperature ramping rate, though loss of resolution may occur.

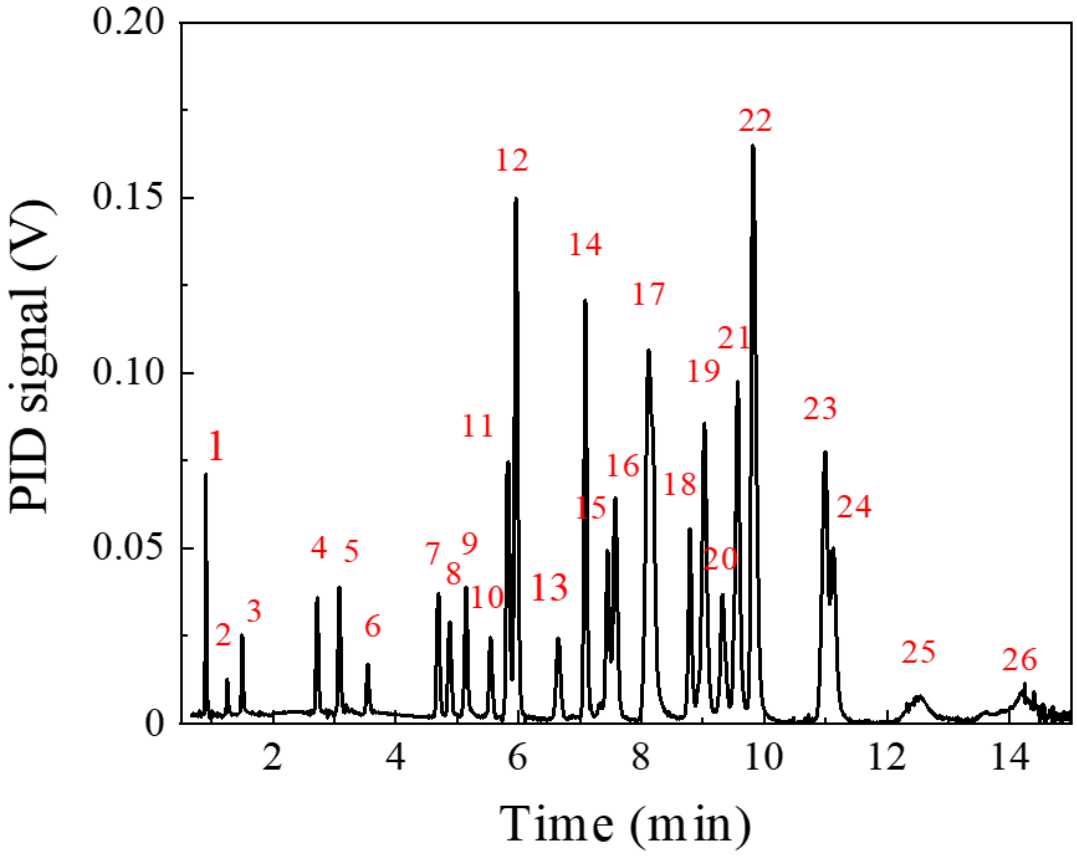

Figure 2.9 Chromatogram of a mixture of 26 VOCs in water at a concentration of 5 µg L^{-1} for each analyte. 1. cis-1,2-dichloroethylene; 2. benzene; 3. trichloroethene; 4. toluene; 5. tetrachloroethylene; 6. 1,2-dibromoethane; 7. chlorobenzene; 8. ethylbenzene; 9. p-xylene; 10. styrene; 11. bromobenzene; 12. propylbenzene; 13. 2-chlorotoluene; 14. mesitylene; 15. 4-chlorotoluene; 16. tert-butylbenzene; 17. 1,2,4-trimethylbenzene; 18. sec-butylbenzene; 19. 1,3-dichlorobenzene; 20. 1,4-dichlorobenzene; 21. butylbenzene; 22. 1,2-dichlorobenzene; 23. nitrobenzene; 24. hexachlorobutadiene; 25. 1,2,3-trichlorobenzene; and 26. naphthalene.

2.4.2 Quantification of VOC concentration in groundwater samples

To test the practical utility of our portable GC, a groundwater sample obtained from a recovery well located in Pinckney, MI was field analyzed by our portable GC system with assistance from local environmental service company (Quantum Environmental, Ann Arbor, MI). The recovery well is a groundwater remediation system, by which groundwater is pumped through one or more vessels containing activated carbon to adsorb organic contaminants in groundwater. Field technicians collect water samples monthly from the outlets of the vessel and send them to an analytical chemistry lab (Brighton Analytical, Brighton, MI) for water VOCs determination based on EPA Method 5030/8260B. The results determine whether vessels can still effectively adsorb pollutants from groundwater or need to be replaced. The whole procedure (sample collection, transportation, and analysis) normally takes about two weeks.

In our experiment, as shown in Figure 2.10, a 10 mL of groundwater sample collected from the outlet of the vessels (inset of Figure 2.10) was placed in the purging vials and analyzed by our portable GC. Cis-1,2-DCE, TCE, and PCE were identified based on their respective retention times provided in Figure 2.9 and their concentrations were calculated using the calibration curves in Figure 2.7(C). The whole procedure took 11 minutes (5 minutes of sampling, 1 minute of holding and 5 minutes of analysis). Table 2 presents the quantitative results, precisions, and LODs of these three VOCs by both our portable GC and the benchtop GC from the analytical chemistry lab. A performance comparison shows that our portable GC provides faster and more sensitive VOC quantification of water samples.

Table 2.2 Performance comparison of portable GC and benchtop GC from a local analytical chemistry lab.

Compound name	Qualification result (µg L^{-1})		Precision at 50 µgL^{-1}(%)		LOD (µgL^{-1})	
	P*	A**	P***	A	P	A
cis-1,2-dichloroethylene	7.2	7	8.4	2.9	0.11	1
trichloroethene	2.6	3	9.2	4.0	0.31	1
tetrachloroethylene	1.7	2	5.8	2.1	0.13	1

*Portable GC results.
**Analytical chemistry lab results.
***Based on Figure 2.7(C) and Figure 2.8.

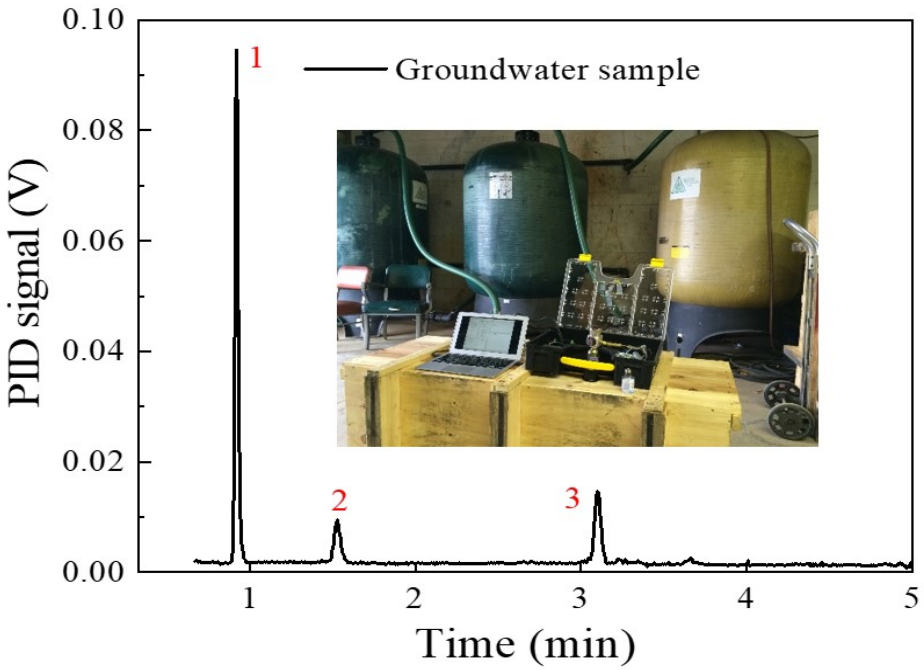

Figure 2.10 Chromatogram of a groundwater sample collected from a recovery well. Comparison between concentration results obtained with our portable GC and by an analytical lab is given in Table 2.2. Inset shows that our portable GC system was used to test water samples on site. The three vessels presented in the photo contain liquid phase carbon. The three organic compounds shown in the chromatogram are: 1. cis-1,2-dichloroethylene; 2. trichloroethene; and 3. tetrachloroethylene, which can be identified by their respective retention time in Figure 2.9.

2.5 Conclusions

We have developed and characterized the performance of a portable GC system for highly sensitive, rapid, and *in-situ* VOC quantification in water. Our results show that our portable GC is able to complete analytical testing in less than 20 minutes with a sub-μg L^{-1} level detection limit. Quantitative comparison with results obtained by analytical lab under standard procedures and benchtop instruments further validated the field-applicability of the portable GC system. Further development includes integration of a PID detector with higher sensitivity [113] to achieve a lower VOC detection limit down to ng L^{-1} in water samples. Multiple stages of μPCIs loaded with different adsorbents can also be implemented to trap VOCs of a wider range of volatilities [139-140]. Shorter purge times (< 1 minute) will be explored to further shorten the overall analysis time. Finally, multi-dimensional portable GC will be pursued in order to handle more complex mixtures. Our target is analyzing and quantifying all VOCs (>100) listed in EPA Method 8260B [116] *in-situ* in less than 20 minutes.

2.6 References

1. Rowe, B. L.; Toccalino, P. L.; Moran, M. J.; Zogorski, J. S.; Price, C. V., Occurrence and potential human-health relevance of volatile organic compounds in drinking water from domestic wells in the United States. *Environmental Health Perspectives* **2007,** *115* (11), 1539.
2. Kampa, M.; Castanas, E., Human health effects of air pollution. *Environ. Pollut.* **2008,** *151* (2), 362-367.
3. Risticevic, S.; Niri, V. H.; Vuckovic, D.; Pawliszyn, J., Recent developments in solid-phase microextraction. *Anal. Bioanal. Chem.* **2009,** *393* (3), 781-795.
4. Penza, M.; Cassano, G., Application of principal component analysis and artificial neural networks to recognize the individual VOCs of methanol/2-propanol in a binary mixture by SAW multi-sensor array. *Sens. Actuators, B* **2003,** *89* (3), 269-284.
5. Si, P.; Mortensen, J.; Komolov, A.; Denborg, J.; Møller, P. J., Polymer coated quartz crystal microbalance sensors for detection of volatile organic compounds in gas mixtures. *Anal. Chim. Acta* **2007,** *597* (2), 223-230.
6. Sundgren, H.; Lundström, I.; Winquist, F.; Lukkari, I.; Carlsson, R.; Wold, S., Evaluation of a multiple gas mixture with a simple MOSFET gas sensor array and pattern recognition. *Sens. Actuators, B* **1990,** *2* (2), 115-123.
7. Feng, L.; Musto, C. J.; Kemling, J. W.; Lim, S. H.; Suslick, K. S., A colorimetric sensor array for identification of toxic gases below permissible exposure limits. *Chem. Commun.* **2010,** *46* (12), 2037-2039.
8. Smith, P. A.; Koch, D.; Hook, G. L.; Erickson, R. P.; Lepage, C. R. J.; Wyatt, H. D.; Betsinger, G.; Eckenrode, B. A., Detection of gas-phase chemical warfare agents using field-portable gas chromatography–mass spectrometry systems: instrument and sampling strategy considerations. *TrAC, Trends Anal. Chem.* **2004,** *23* (4), 296-306.
9. Lee, M.-R.; Chang, C.-M.; Dou, J., Determination of benzene, toluene, ethylbenzene, xylenes in water at sub-ng l^{-1} levels by solid-phase microextraction coupled to cryo-trap gas chromatography–mass spectrometry. *Chemosphere* **2007,** *69* (9), 1381-1387.
10. Mahmoud, M. E.; AlBishri, H. M., Identification of dissolved organic species in non-drinking tap water by solid-phase extraction and gas chromatography–mass spectrometry. *J. Saudi Chem. Soc.* **2010,** *14* (1), 105-115.
11. Zoccolillo, L.; Amendola, L.; Cafaro, C.; Insogna, S., Improved analysis of volatile halogenated hydrocarbons in water by purge-and-trap with gas chromatography and mass spectrometric detection. *J. Chromatogr. A* **2005,** *1077* (2), 181-187.
12. Santos, F.; Galceran, M., Modern developments in gas chromatography–mass spectrometry-based environmental analysis. *J. Chromatogr. A* **2003,** *1000* (1), 125-151.
13. Aragon, P.; Atienza, J.; Climent, M., Analysis of organic compounds in air: a review. *Crit. Rev. Anal. Chem* **2000,** *30* (2-3), 121-151.
14. Dewulf, J.; Van Langenhove, H., Anthropogenic volatile organic compounds in ambient air and natural waters: a review on recent developments of analytical methodology, performance and interpretation of field measurements. *J. Chromatogr. A* **1999,** *843* (1), 163-177.
15. Ji, J.; Deng, C.; Shen, W.; Zhang, X., Field analysis of benzene, toluene, ethylbenzene and xylene in water by portable gas chromatography–microflame ionization detector combined with headspace solid-phase microextraction. *Talanta* **2006,** *69* (4), 894-899.
16. Zhu, H.; Nidetz, R.; Zhou, M.; Lee, J.; Buggaveeti, S.; Kurabayashi, K.; Fan, X., Flow-through microfluidic photoionization detectors for rapid and highly sensitive vapor detection. *Lab Chip* **2015,** *15* (14), 3021-9.
17. Garg, A.; Akbar, M.; Vejerano, E.; Narayanan, S.; Nazhandali, L.; Marr, L. C.; Agah, M., Zebra GC: A mini gas chromatography system for trace-level determination of hazardous air pollutants. *Sens. Actuators, B* **2015,** *212*, 145-154.

18. Antoniou, C. V.; Koukouraki, E. E.; Diamadopoulos, E., Determination of chlorinated volatile organic compounds in water and municipal wastewater using headspace–solid phase microextraction–gas chromatography. *J. Chromatogr. A* **2006,** *1132* (1), 310-314.
19. Techniquea, A. P., METHOD 8260B VOLATILE ORGANIC COMPOUNDS BY GAS CHROMATOGRAPHY/MASS SPECTROMETRY (GC/MS). **1996**.
20. No, C. C., METHOD 5030C PURGE-AND-TRAP FOR AQUEOUS SAMPLES. **2003**.
21. Zhong, Q.; Steinecker, W. H.; Zellers, E. T., Characterization of a high-performance portable GC with a chemiresistor array detector. *Analyst* **2009,** *134* (2), 283-293.
22. Jian, R.-S.; Wang, T.-Y.; Song, L.-Y.; Kuo, C.-Y.; Tian, W.-C.; Lo, E.-W.; Lu, C.-J., Field investigations and dynamic measurements of process activity induced VOCs inside a semiconductor cleanroom. *Build. Environ.* **2015,** *94*, 287-295.
23. Contreras, J. A.; Murray, J. A.; Tolley, S. E.; Oliphant, J. L.; Tolley, H. D.; Lammert, S. A.; Lee, E. D.; Later, D. W.; Lee, M. L., Hand-portable gas chromatograph-toroidal ion trap mass spectrometer (GC-TMS) for detection of hazardous compounds. *J. Am. Soc. Mass. Spectrom.* **2008,** *19* (10), 1425-1434.
24. Thompson, C. V.; Goedert, M. G., Field-Portable Instrumentation for Gas and Vapor Samples. *Encycl. Anal. Chem.* **2009**.
25. Staples, E. J.; Matsuda, T.; Viswanathan, S. In *Real time environmental screening of air, water and soil matrices using a novel field portable GC/SAW system*, Environmental Strategies for the 21st Century, Asia Pacific Conference, 1998; pp 8-10.
26. Watson, G. W.; Staples, E. J.; Viswanathan, S., Performance evaluation of a surface acoustic wave analyzer to measure VOCs in air and water. *Environmental progress* **2003,** *22* (3), 215-226.
27. Kim, S. K.; Chang, H.; Zellers, E. T., Microfabricated gas chromatograph for the selective determination of trichloroethylene vapor at sub-parts-per-billion concentrations in complex mixtures. *Anal. Chem.* **2011,** *83* (18), 7198-7206.
28. Haghighi, F.; Talebpour, Z.; Sanati-Nezhad, A., Through the years with on-a-chip gas chromatography: a review. *Lab Chip* **2015,** *15*, 2559-2575.
29. Akbar, M.; Restaino, M.; Agah, M., Chip-scale gas chromatography: From injection through detection. *Nat. Microsys. Nanoeng.* **2015,** *1*.
30. Segal, A.; Górecki, T.; Mussche, P.; Lips, J.; Pawliszyn, J., Development of membrane extraction with a sorbent interface–micro gas chromatography system for field analysis. *J. Chromatogr. A* **2000,** *873* (1), 13-27.
31. Qin, Y.; Gianchandani, Y. B., iGC1: An Integrated Fluidic System for Gas Chromatography Including Knudsen Pump, Preconcentrator, Column, and Detector Microfabricated by a Three-Mask Process. *J. Microelectromech. Syst.* **2014,** *23* (4), 980-990.
32. Akbar, M.; Narayanan, S.; Restaino, M.; Agah, M., A purge and trap integrated microGC platform for chemical identification in aqueous samples. *Analyst* **2014,** *139* (13), 3384-3392.
33. Groves, W.; Grey, A.; O'shaughnessy, P., Surface acoustic wave (SAW) microsensor array for measuring VOCs in drinking water. *J. Environ. Monit.* **2006,** *8* (9), 932-941.
34. Bulbul, A.; Kim, H., A bubble-based microfluidic gas sensor for gas chromatographs. *Lab Chip* **2015,** *15*, 94-104.
35. MING, H. T. Novel microextraction techniques for aqueous environmental analysis. 2012.
36. Allonier, A.-S.; Khalanski, M.; Bermond, A.; Camel, V., Determination of trihalomethanes in chlorinated sea water samples using a purge-and-trap system coupled to gas chromatography. *Talanta* **2000,** *51* (3), 467-477.
37. Saridara, C.; Brukh, R.; Mitra, S., Development of continuous on-line purge and trap analysis. *J. Sep. Sci.* **2006,** *29* (3), 446-452.
38. Menéndez, J. F.; Sánchez, M. F.; Uría, J. S.; Martínez, E. F.; Sanz-Medel, A., Static headspace, solid-phase microextraction and headspace solid-phase microextraction for BTEX determination in aqueous samples by gas chromatography. *Anal. Chim. Acta.* **2000,** *415* (1), 9-20.
39. Sander, R., Compilation of Henry's law constants (version 4.0) for water as solvent. *Atmos. Chem. Phys.* **2015,** *15* (8), 4399-4981.

40. Ehrmann, E.; Dharmasena, H.; Carney, K.; Overton, E., Novel column heater for fast capillary gas chromatography. *J. Chromatogr. Sci.* **1996,** *34* (12), 533-539.
41. Reidy, S.; George, D.; Agah, M.; Sacks, R., Temperature-programmed GC using silicon microfabricated columns with integrated heaters and temperature sensors. *Anal. Chem.* **2007,** *79* (7), 2911-2917.
42. Gvirtzman, H.; Gorelick, S. M., The concept of in-situ vapor stripping for removing VOCs from groundwater. *Transp. Porous Media* **1992,** *8* (1), 71-92.
43. Driss, M.; Bouguerra, M., Analysis of volatile organic compounds in water by purge-and-trap and gas chromatography techniques: operational parameters optimization of the purge step. *Int. J. Environ. Anal. Chem.* **1991,** *45* (3), 193-204.
44. Tian, W.-C.; Pang, S. W.; Lu, C.-J.; Zellers, E. T., Microfabricated preconcentrator-focuser for a microscale gas chromatograph. *J. Microelectromech. Syst.* **2003,** *12* (3), 264-272.
45. Tian, W.-C.; Chan, H. K.; Lu, C.-J.; Pang, S. W.; Zellers, E. T., Multiple-stage microfabricated preconcentrator-focuser for micro gas chromatography system. *J. Microelectromech. Syst.* **2005,** *14* (3), 498-507.

Chapter 3 Two Dimensional Micro GC

3.1 Introduction

Comprehensive GC x GC is widely used for analyzing complex samples due to its high peak capacity. However, the predominant effects in GC x GC have been dedicated to developing bench-top systems. Research related to portable GC x GC has been focused mainly on developing miniaturized components (in particular miniaturized modulators), but design and assembly of full portable 2DGC systems is still ongoing. No actual portable or miniaturized GC x GC instrument has yet been reported. In 2009, Whiting *et al.* demonstrated a miniaturized pneumatic modulator based on micro-valves [141]. While simple and responsive, the pneumatic modulator lacks the re-focusing capability of thermal modulators, thus resulting in peak broadening in ^{2}D separation and decreased detection sensitivity. Using the pneumatic modulator, a crude 2-D separation of 5 analytes was achieved using a conventional bench-top GC system. More recently, a micro-scale thermal modulator incorporating two series-coupled Pyrex-on-Si micro-channels coated with a thin layer (0.3 μm) polydimethylsiloxane (PDMS) was reported [142-145]. It employs a thermoelectric cooler (TEC) to cryogenically trap the analytes eluted from the ^{1}D column and re-focuses and thermally injects them into the ^{2}D column [142]. The thermal modulator can be heated from -30 ^{o}C

to ~210 ºC at a rate of 2400 ºC/s, thus generating a peak as narrow as ~100 ms (full-width-at-half-maximum, FWHM) [145]. A hybrid GC x GC system was constructed using this micro-scale thermal modulator and columns microfabricated on silicon wafers (6 m and 0.5 m long for the ^{1}D and ^{2}D, respectively). A macroscopic injector, flame ionization detector, and GC oven on a conventional bench-top GC were used, yielding 2-D separation of 36 analytes in 22 minutes. However, this type of thermal modulator faces several challenges, such as thermal crosstalk (which may affect trapping efficiency), coating material bleeding (currently PDMS) at high temperatures (currently, the highest temperature is 210 ºC), and breakthrough of highly volatile compounds (such as benzene) [145]. Furthermore, constant cooling of the thermal modulator using a TEC requires a power of 20-40 W. Finally, the GC x GC architecture is still the same as regular bench-top GC x GC, thus inhering the same limitations common to all existing GC x GC systems, *e.g.*, degraded ^{1}D peak capacity due to peak broadening caused by modulation, and insufficient ^{2}D separation capabilities arising from short maximally-allowed ^{2}D separation times imposed by the modulation period (*e.g.*, 6 s in Ref. [145]) [146-147].

This chapter reports both hardware (system design, integration and characterization) and software (algorithms on chromatogram reconstruction) development of a portable 2DGC. Section 3.2 demonstrates for the first time a fully automated, portable, comprehensive 2-D GC device. The system weighs less than 5 kg with dimensions of 60 cm × 50 cm × 10 cm. Multiple channels are employed in ^{2}D to increase the ^{2}D separation time (up to 32 s) and hence the ^{2}D peak capacity. A ^{1}D PID is installed at the end of the ^{1}D column to monitor the ^{1}D separation and assist in reconstructing ^{1}D elution peaks. The entire device consists of a micro-preconcentrator/injector (μPCI), commercial column, micro-Deans switch (μDS), micro-thermal injector (μTI), and photoionization detector (PID), as well as miniaturized valve, pump, helium cartridge, and power

supply. A Labview™ based user interface and operation control are also implemented for automation. This section also describes the details of system operating principles and discusses its advantages over the conventional GC x GC arrangement (*i.e.*, 1x1-channel with a vapor detector installed only at the end of the ^{2}D column).

Section 3.3 details sub-system calibration (mainly PID calibration). Due to its non-destructive nature, PIDs are used in both the ^{1}D and ^{2}D sub-systems of our 2DGC. These sub-system PIDs require uniform responses given any concentration of any chemical compounds. However, in practice, different PIDs have different responsivities towards the same chemical compound (even at the same concentration or mass) due to different aging conditions of the PID lamps and windows. As a result, response factors for all PIDs must be determined, and then PID signals of different channels can be normalized by their response factors. By using our 1x4-channel 2-dimensional μGC system to study the responses of 5 Krypton PIDs to 7 different volatile organic compounds (VOCs) with ionization potentials ranging from 8.45 eV to 10.08 eV and concentrations ranging from ~1 ng to ~2000 ng , we validated that the PID responses were highly uniform regardless of analyte, concentration, or chromatographic peak width. Based on this observation, we used the ^{1}D PID as a reference detector and calculated calibration factors for each one of the ^{2}D PIDs against the ^{1}D PID. With these calibration factors, we are then capable of quantitatively reconstructing coeluted ^{1}D peaks using signals obtained with the ^{2}D PID array.

Section 3.4 describes the approach and algorithm for reconstructing ^{1}D elution peaks using the information obtained jointly by the ^{1}D and ^{2}D detectors. We further experimentally validate the 1D reconstruction algorithm. Finally, we demonstrate 2-D separation of 50 analytes in 14 minutes with our 1x4-channel 2DGC system. The system peak capacity was also evaluated using three representative analytes.

3.2 Comprehensive 2D μGC system

3.2.1 Fabrication and characterization of individual components

Materials

All the analytes were purchased from Sigma-Aldrich (St. Louis, MO) and Fisher Scientific (Pittsburgh, PA) and were used as received (purity > 97%). Carbopack^{TM} B (60-80 mesh) was purchased from Supelco (Bellefonte, PA). Compressed helium gas (99.998%) was purchased from Cryogenic gases (Detroit, MI). GC guard columns (250 μm i.d. and 380 μm o.d.), Rtx-5ms (10 m × 250 μm i.d., 0.25 μm coating thickness), RTX-200 (12 m × 250 μm i.d., 0.25 μm coating thickness), universal press-tight glass capillary column connectors, and angled Y connectors were purchased from Restek (Belafonte, PA). 2-port and 3-port solenoid valves were purchased from Lee Company (Westbrook, CT). A diaphragm pump was purchased from Gast Manufacturing (Benton Harbor, MI). Nickel wire (0.32 mm diameter, 1.24 Ohms/m) was purchased from Lightning Vapes (Bradenton, FL). A type K thermocouple was purchased from Omega Engineering (Stamford, CT). Silicon wafers were purchased from University Wafer (Boston, MA). The UV lamps and amplifiers for PIDs were purchased from Baseline-Mocon (Lyons, CO). A 36V AC/DC converter was purchased from TDK-Lambda Americas Inc. (National City, CA). 24V and 12V AC/DC converters and axial fans were purchased from Delta Electronics (Taipei, Taiwan). Data acquisition cards (DAQ cards), USB-6212 (16 bits), and USB-TC01 (for thermocouple measurement), were purchased from National Instruments (Austin, TX). A customized printed circuit board (PCB) was designed and manufactured by M.A.K.S., Inc. (Troy, MI).

μPCI and μTI fabrication and characterization

The μPCI and μTI were based on the same design. Both of them consisted of a deep-reactive-ion-etched (DRIE) silicon cavity with tapered inlet/outlet ports, an integrated platinum

heater, a temperature sensor, and microfluidic channels. The μPCI had a cavity size of 8.15 mm x 2.9 mm x 0.25 mm, whereas the μTI's cavity was slightly smaller (4.1 mm x 1.6 mm x 0.25 mm). Carbopack^{TM} B granules were loaded into the cavity through a third port using a diaphragm pump, which was sealed with a silicone adhesive after loading. A small segment of guard column was inserted into the inlet and outlet fluidic ports, and secured with an epoxy adhesive. For electrical connections, the heater and resistive temperature detector (RTD) were wire-bonded to a PCB. The RTD on the backside was pre-calibrated in a conventional GC oven at temperatures of 50, 100, 150, and 200 ˚C to obtain the temperature calibration curve (*i.e.*, temperature response versus resistance). The μPCI and μTI were pre-conditioned at 300 ˚C for 12 hours under helium flow before use.

The insets of Figure 3.1(a) show the front and back side of the μPI. The front side photograph shows the well-packed Carbopack^{TM} B in the cavity. The volume of the cavity was 5.9 mm^3 and the mass of Carbopack^{TM} B was 1.135 mg. During operation, the μPCI was heated by applying 36 VDC for 0.6 s and subsequently 12 VDC for 10 s for complete desorption. To maintain a constant temperature for 10 s, a pulse-width-modulated signal (4.0-Hz square wave still at 12 VDC) was applied to the heater power relay via the USB-6212. Figure 3.1(a) shows that the μPCI reached 270 ˚C in 0.6 s at a ramping rate of 314 ˚C/s and then kept at 250 ˚C for 10 s. The normalized toluene peak injected under this condition is given in Figure 3.1(b), showing a FWHM of 700 ms.

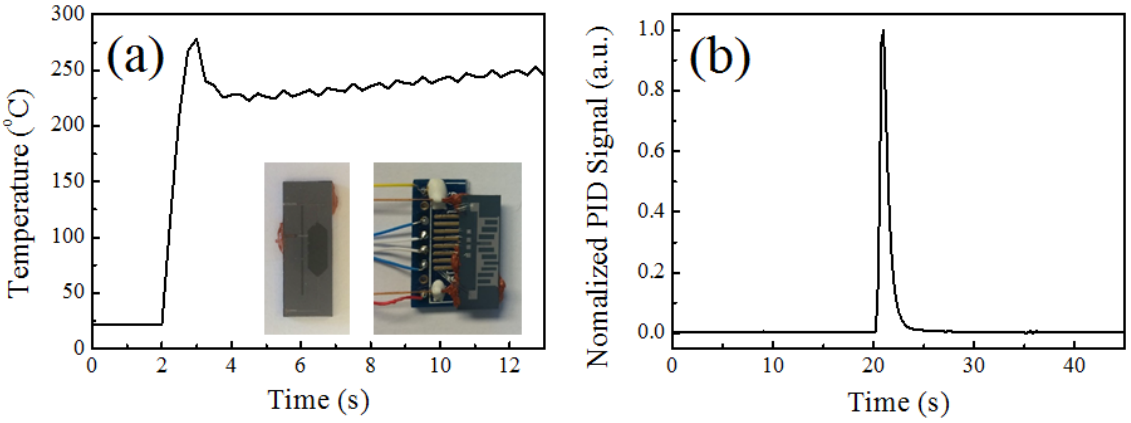

Figure 3.1 (a) The temperature response of the µPI. The µPCI reached 270 ˚C in 0.6 s and then was kept at 250 ˚C for 10 s. Inset shows the front and back side of the µPCI packed with Carbopack™ B. On the back side, the heater and resistive temperature detector (RTD) were wire-bonded to a printed circuit board. (b) Normalized toluene peak obtained with µPID 1 under the injection conditions given in (a). The helium flow rate was 2 mL/min. FWHM=700 ms.

Since the µTIs need to be heated periodically with short cycling times, we applied coaxial fans on all µTIs for rapid cooling, ensuring that µTIs were ready for the next sampling cycle. As shown in Figure 3.2, the µTI can be cooled down to room temperature in 16 s with the fan comparing to 205 s without the fan.

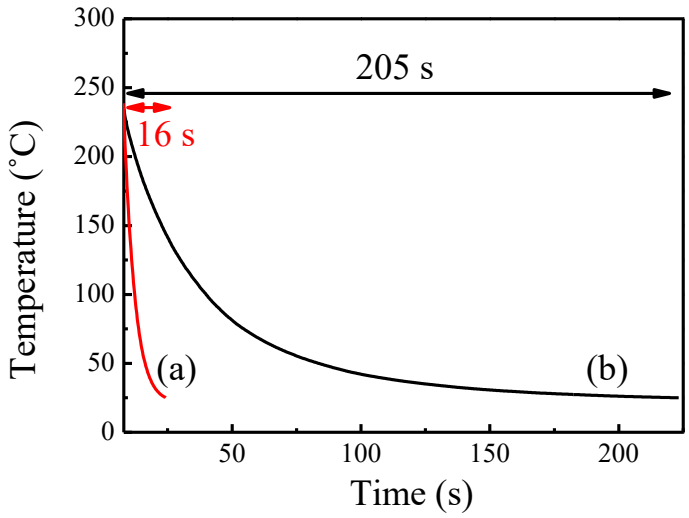

Figure 3.2 Cooling profile of the µTI with (a) and without (b) a coaxial fan. With the

fan, it takes 16 second for the μTI to cool from 240 ˚C to 25 ˚C.

Column assembly and temperature ramping

The 10 m long RTX-5ms column for the ^{1}D (or the 3 m long RTX-200 column for the ^{2}D) and nickel wire were placed in parallel, wrapped by Teflon tape, then coiled into a helix of 10 cm (or 5 cm for the RTX-200 column) in diameter and 1 cm in height. A type K thermocouple was inserted into the gap between the coiled column to monitor the column temperature in real time via USB-TC01. To achieve a programmable temperature ramping profile, a pulse-width-modulated signal (4.0-Hz square wave) was applied to the heater power relay via USB-6212. The duty cycle of the square wave was calculated by a proportional-integral-derivative controller in the LabView^{TM} program and updated every 0.4 s based on the set and actual measured temperatures. Figure 3.3(a) shows an example of the ^{1}D column temperature ramping profile. 2D columns are set to isothermal temperatures, which are tuned by different PWMs. Figure 3.3(b) shows the 2D column isothermal temperature at different PWMs, with minimal variation between the four ^{2}D columns.

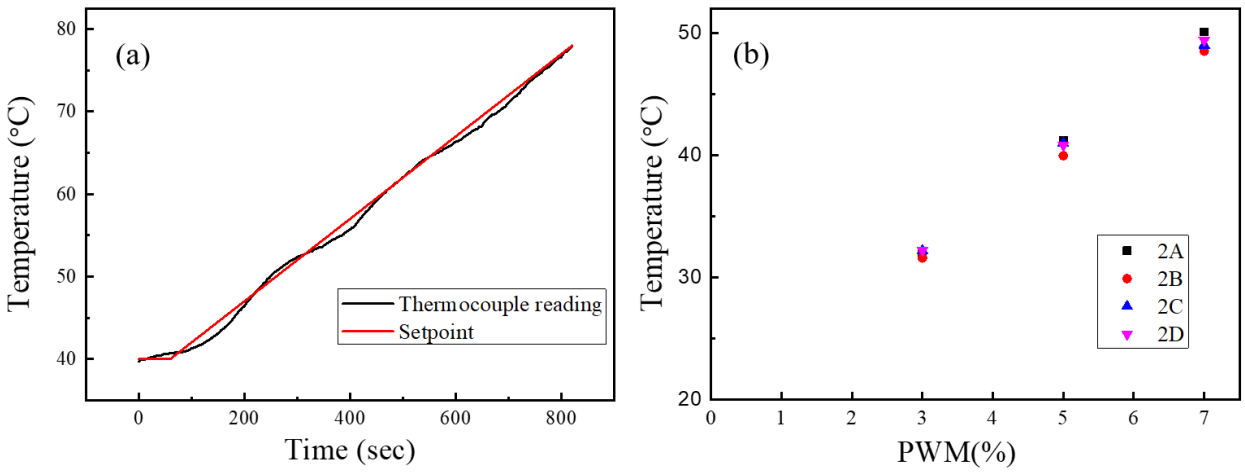

Figure 3.3 (a) ^{1}D column temperature ramping profile with proportional-integral-derivative control. (b) Column temperature of the four ^{2}D columns at a given PWM.

μDS fabrication and operation

A switching system was used to achieve routing of eluents from an upstream column to one of the four downstream columns (1 x 4 switching). It consisted of three μDSs and two 3-port valves that were connected to a helium source as shown in Figure 3.4. The μDS had a deep-reactive-ion-etched (DRIE) microfluidic channel with three inlets (on the left) and two outlets (on the right), an integrated platinum heater, and a temperature sensor. A small segment of capillary column was inserted into the inlet and outlet fluidic ports, and secured with an epoxy adhesive. The middle inlet of the μDS was connected to the upstream column, whereas the other two inlets were connected to a 3-port valve (N.O. and N.C. port) for control helium gas to enter. The two outlets of μDS 1 were connected to the middle inlet of μDS 2 and μDS 3, respectively, through the universal connectors. The details of routing the analytes to other ^{2}D 2B and 2C columns are given in Figure 3.5. By operating two 3-port valves ("on" while applying voltage and "off" while applying no voltage), the helium control flow is routed differently (to "N.O." port while valve is "off" or to "NC" port while valve is "on"). Thus, the eluent from the ^{1}D route can be sliced into one of the four columns in ^{2}D. During the operation, the flow rate was 2 mL/min for all ^{2}D channels.

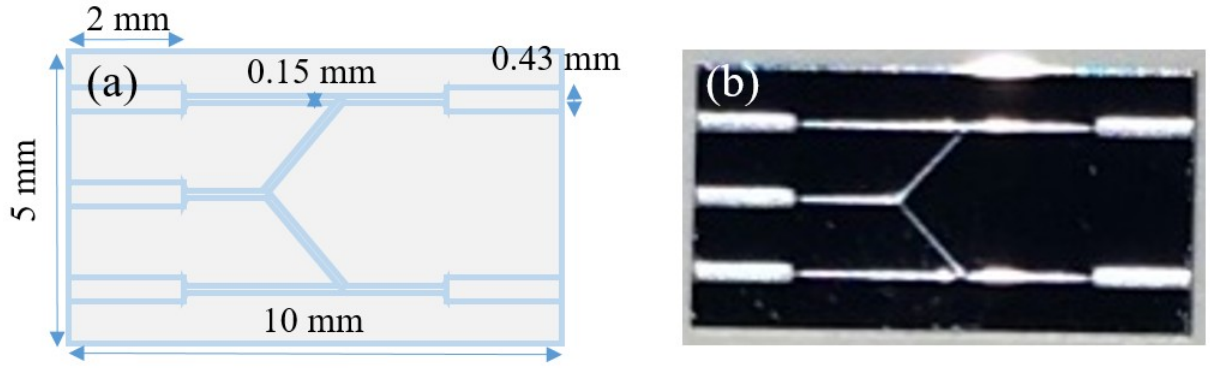

Figure 3.4 (a) Dimensions of the micro-fluidic channels of the µDS. (b) Front side of the µDS.

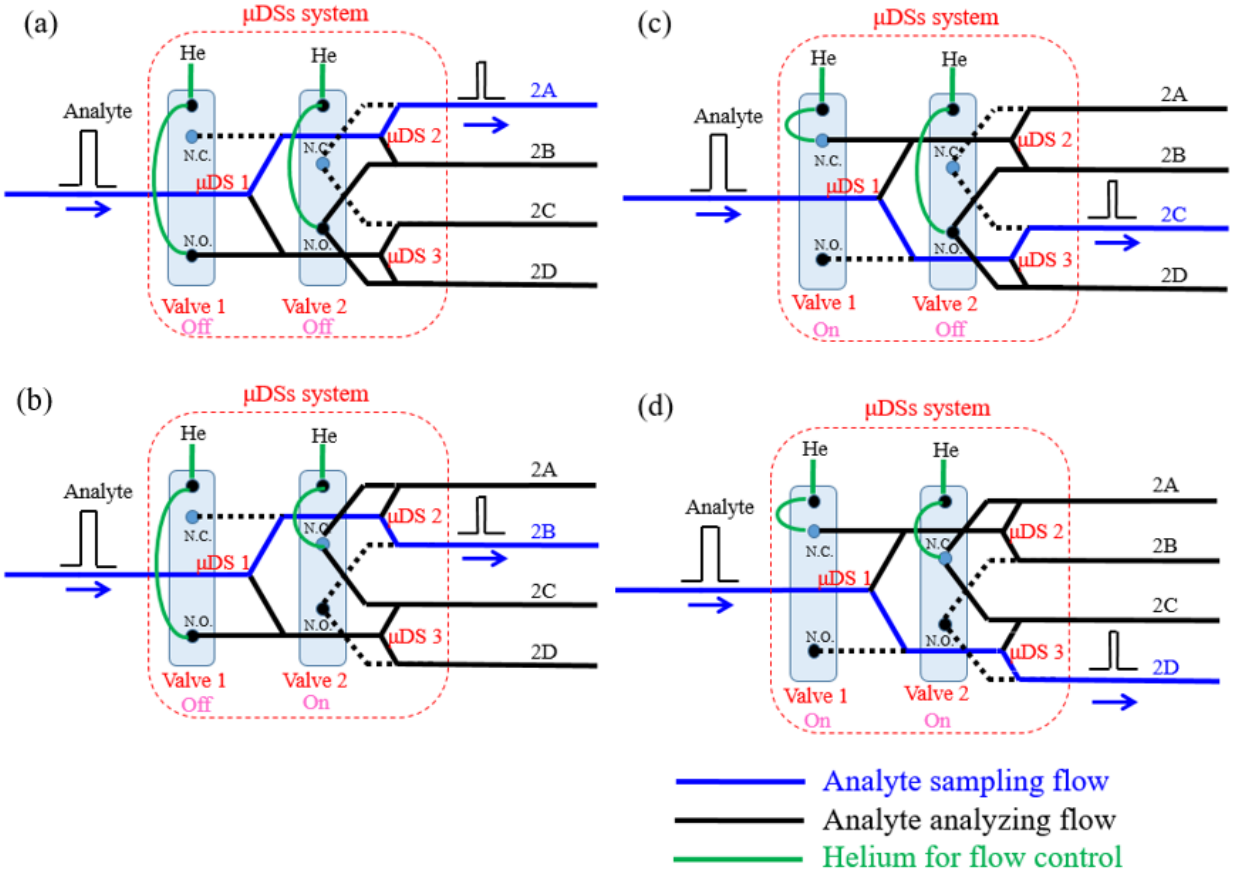

Figure 3.5 Schematic of the 1x4 flow switching module that consists of three µDSs (see the µDS picture in the inset) and two 3-port valves. Schematic diagram showing how the flow routing system consisting of three µDSs and two 3-port valves works to send analytes to (a) 2A, (b) 2B, (c) 2C and (d) 2D.

PID fabrication and assembly

The PID module used in this work was assembled with the Krypton UV lamp and the built-in lamp drive circuit and amplifier from Baseline-Mocon (Lyons, CO, P/N #043-234) as well as a home-made flow-through ionization chamber. Rather than using a serpentine microfluidic channel, which we reported previously [18], the current simplified PID shown in Figure 3.6(a) employed a 2-cm long straight microfluidic channel created by a 380 μm gap etched into a p-type <100> conductive silicon wafer with a resistivity of 0.001-0.005 Ω cm and a thickness of 380 μm. The bottom and top of the microfluidic channel were covered by a Krypton UV lamp and a glass slide, respectively, which were then glued to the conductive silicon wafer with an optical epoxy. The effective UV illumination length in the channel was about 3.5 mm (*i.e.*, the diameter of the Krypton lamp window). Since the side of the microfluidic channel was made of conductive silicon, it served as a signal collection electrode in this configuration. Two copper wires were bonded to the wafers and connected to the amplifier on the commercial PID. Finally, two guard columns (250 μm i.d. and 380 μm o.d.) were inserted into the inlet and outlet of the microfluidic channel and sealed with optical epoxy. The detailed dimensions and electrical connections of the home-made PID are shown in Figure 3.6(b). Before analysis, the four PIDs in ^{2}D were calibrated with toluene using PID 1 as the reference detector. Calibration details and results are described in Section 3.3.

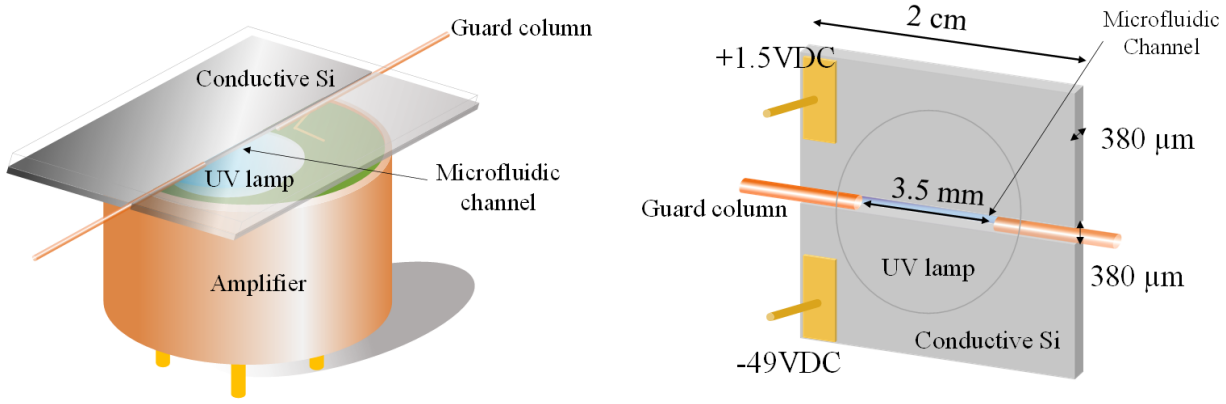

Figure 3.6 (a) Schematic of a home-made PID with built-in lamp drive circuit and amplifier from a commercial PID. A 380 µm wide, 380 µm tall and 2 cm long flow-through microfluidic channel was created using two conductive silicon wafers. (b)Dimensions and electrical connections of the home-made PID module. A 380 µm wide, 380 µm tall and 2 cm long microfluidic channel was created by a gap between two conductive silicon wafers. A small segment of a guard column was inserted to the channel inlet/outlet for fluidic connection. The bottom and top of the microfluidic channel were covered by a Krypton UV lamp and a glass slide, respectively, which were then glued to the conductive silicon wafers with an optical epoxy. The UV illumination length was about 3.5 mm as defined by the Krypton window diameter. Two copper wires with copper tape were bonded to the wafers and connected to the amplifier.

3.2.2 Device assembly and automation

Figure 3.7 shows a photograph of the portable GC x GC device. The system was housed in a custom 60 cm (L) × 50 cm (W) × 10 cm (H) plastic case and weighed less than 5 kg. It consisted of AC/DC converters, DAQ cards, a diaphragm pump, and a helium cartridge in the back row, and one ^{1}D and four ^{2}D separation modules and the µDSs system in the front row. As shown in Figure 3.8, the ^{1}D separation module was located in the middle of the front row, and µDSs system was placed under the ^{1}D separation module. The ^{2}D separation modules of 2A/2B and 2C/2D were stacked with the board spacers and were located to the left and right side of ^{1}D separation module, respectively. All components, µPCI, µTI, heater wrapped columns, and PIDs, were mounted on a custom printed circuit board. The guard column affixed to each component was connected by

universal press-tight glass capillary column connectors or angled Y connectors. A home-made LabView™ program was developed for automated control and operation of the system as well as PID signal readout.

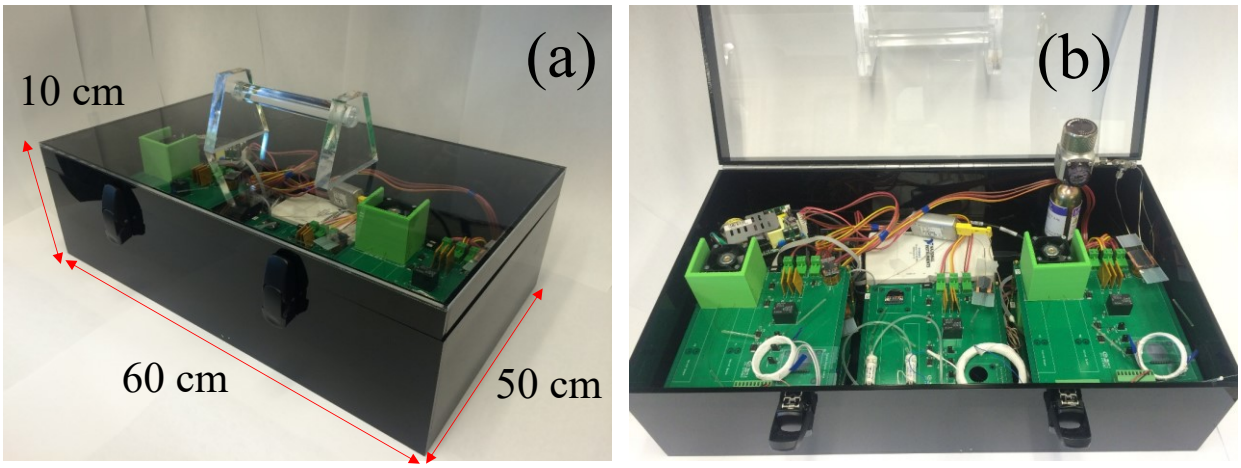

Figure 3.7 Photo of external (a) and internal (b) views of the automated portable 1x4-channel GC x GC device. Weight: <5 kg. The detailed layout of the device is shown in Figure 3.8.

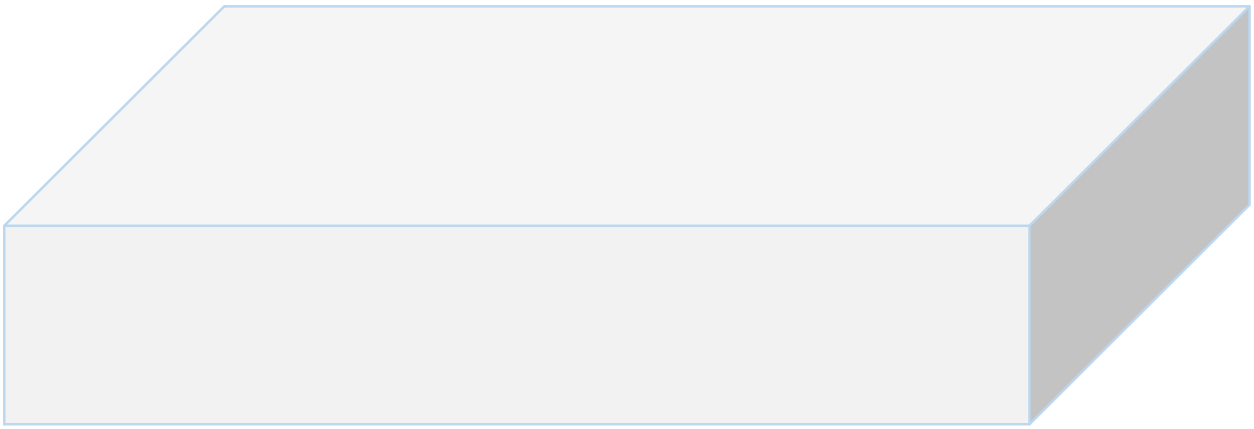

Figure 3.8 Layout of the portable 1x4-channel GC x GC device.

3.2.3 Operation of the multi-channel GC x GC

The general operation of the 1x4-channel GC x GC is illustrated in Figure 3.9. The analytes are first separated by the ^{1}D column and elution is monitored by a non-destructive detector installed

at the end of the ^{1}D column without interrupting the flow. A switching module is used to periodically send slices of eluents from the ^{1}D column to the multiple ^{2}D columns sequentially. The eluents from the ^{2}D columns are detected at the end of the columns. The ^{1}D elution peaks can be reconstructed from the information obtained jointly by the detectors in ^{1}D and ^{2}D (see details in Section 3.4).

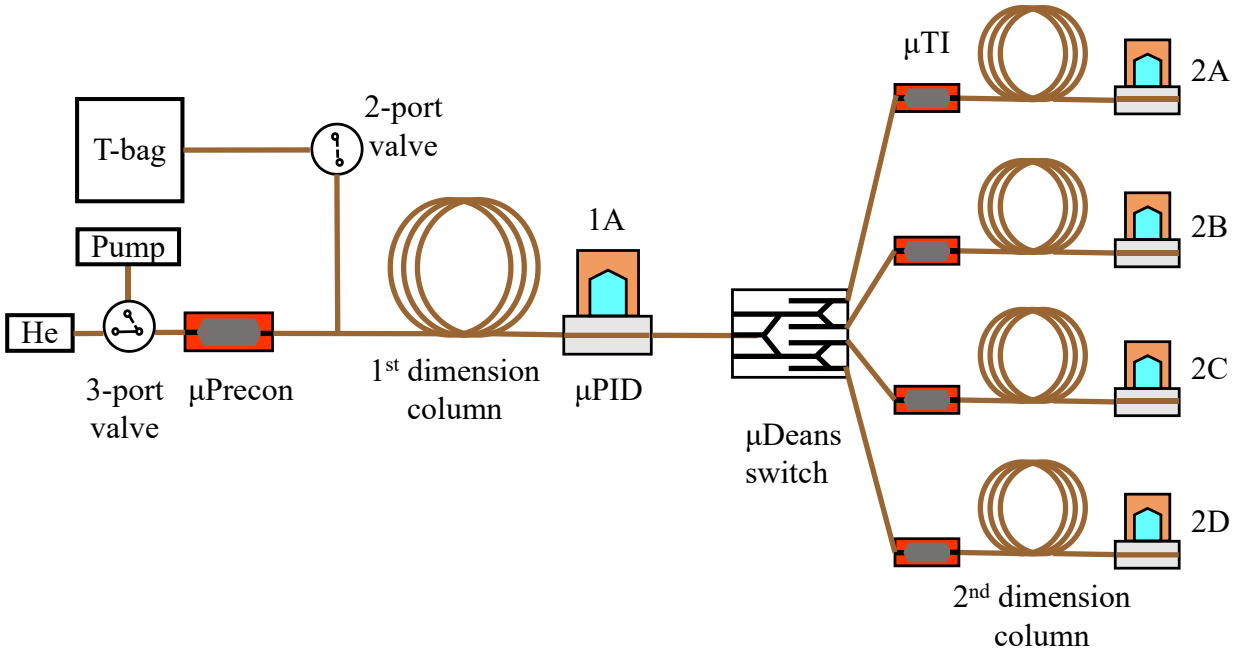

Figure 3.9 Schematic of the 1x4-channel experimental setup to characterize and calibrate the response of 5 PIDs (1A and 2A-D). Analytes are first injected to the 1st dimensional column and detected by PID 1A. After the analytes pass through PID 1A, they are routed to one of the 2nd dimensional columns via micro-Deans switches and a micro-thermal injector (μTI), and finally detected by the corresponding PID.

Modules for the 1x4-channel GC x GC

(1) Sampling and injection module, consisting of a Tedlar bag, μPCI, pump, 2-port valve, and 3-port valve. The gas analytes from the Tedlar bag were first drawn by the pump through the 2-port valve into the μPI. Then, the μPCI was heated to inject the analytes into the ^{1}D column.

(2) ^{1}D separation and detection module, consisting of a home-made temperature programmable separation column and a vapor detector (PID 1).

(3) Modulation and switching module, consisting of 3 μDSs to sequentially send the eluent from the ^{1}D column into one of the 4 ^{2}D columns, *i.e.*, Column 2A, 2B, 2C, 2D, then back to 2A, and so forth.

(4) Four identical ^{2}D separation and detection modules, each of which consists of a μTI, temperature programmable separation column, and vapor detector (PID 2A, 2B, 2C, and 2D). During operation, a slice of the ^{1}D eluent routed by the μDS was trapped by the μTI, then the μTI was heated to inject the analyte into the ^{2}D column for separation. Meanwhile, additional slices from the ^{1}D eluent were routed to the remaining three ^{2}D columns for separation. Therefore, the total separation time on each ^{2}D column was 4 times as long as the modulation period.

Operation procedures and parameters

(1) The VOC samples placed in the Tedlar bag were drawn by the diaphragm pump through the 2-port valve and adsorbed by the CarbopackTM B granules inside the μPCI (flow rate: 25 mL/min, sampling time: 2 minutes). After sampling, the 2-port valve was closed and the helium gas was flowed through the 3-port valve for 60 s to stabilize the flow. Finally, the μPCI was heated to 270 ˚C in 0.6 s and then kept at 250 ˚C for 10 s for complete thermal desorption.

(2) The analyte was separated by the 10 m long RTX-5ms column, then detected by μPID 1. During the separation, the column was heated and kept at 50 ˚C for 1 min, then ramped at a rate of 5˚C min^{-1} to 120 ºC and held for 4 min. μPID 1 was kept at room temperature (25 ˚C). The flow rate was 2 mL/min.

(3) We used a modulation period of 8 seconds. The first 8 s long slice of the eluent from the ^{1}D column was routed to and trapped by μTI 2A, which were both kept at room temperature (25 ºC). The μTI was then heated to 270 ˚C in 0.6 s and then kept at 250 ˚C for 5 s to inject the trapped analytes to Column 2A. Immediately after injection, the fan on the μTI was turned on to

rapidly lower the μTI back to room temperature in 16 s, as shown in Figure 3.2. Simultaneously, the second 8 s long slice of the eluent from the ^{1}D column was routed to and trapped by μTI 2B, which was subsequently injected into Column 2B. The same operation was repeated for μTI 2C and μTI 2D until the fifth 8 s long slice, which was routed to μTI 2A again. The helium flow was kept at 2 mL/min for all 4 ^{2}D columns.

(4) The analyte underwent ^{2}D separation through one of the 3 m long RTX-200 columns (kept at 60 ºC) and then was detected by μPID 2 (kept at room temperature, 25 ºC). During the separation, the helium flow rate was 2 mL/min. The maximal separation time for each ^{2}D column was 32 s (4 times the modulation period).

3.3 2D μGC calibration

3.3.1 PID module responsivities variation

The 2DGC requires uniform response over all sub-system PIDs, given any concentration of any chemical compounds. However, the PID exhibits different responsivities toward different chemical compounds due to their different ionization potentials. Such responsivity differences for a given PID can be accounted for by calibration with isobutylene to obtain the response factor (or correction factor) [148-150], which is the ratio between the sensitivity of isobutylene to that of a target compound. Additionally, different PID devices may have different responsivities towards the same chemical compound (even at the same concentration or mass) [151]. Such differences result from factors like different aging conditions of PID lamps (due to their finite lifetime and Krypton gas leakage) and PID windows (caused by contamination of gas analytes, water etching, crystal solarization and yellowing effects due to UV damage [148, 152-154]). Another issue is imperfect alignment between the lamp window and the microfluidic channel in the PID during assembly.

Variations in PID responsivity may be detrimental to the employment of multiple PIDs in a GC system, especially in a multi-dimensional GC system.

To calibrate the difference in responsivity of different PIDs, one can always measure each PID's response to all target analytes at all anticipated concentrations (or masses). However, this method is tedious and sometimes impossible to accomplish. The easiest and most practical approach is to compare and calibrate the responses of all PIDs in a GC system with a single analyte at a given concentration. This raises the question of whether or not the calibration factor obtained with this analyte (at the given concentration) can be generally applicable to other analytes of different concentrations. In this section, we systematically investigated the responses of 5 Krypton PIDs (UV photon energy: 10.6 eV) in a 1x4-channel 2-dimensional μGC system to 7 different volatile organic compounds (VOCs) with ionization potentials ranging from 8.45 eV to 10.08 eV and concentrations ranging from ~1 ng to ~2000 ng. Using one of the PIDs as the reference detector, the calibration factor for each of the other four PIDs was obtained. We found the calibration factors to be quite uniform regardless of the analyte, its concentration, or chromatographic peak width. Based on this observation, we were able to quantify coeluted peaks in the 1st-dimension using the signal obtained with a PID array in the 2nd-dimension. This work enables rapid and *in-situ* calibration of PIDs in a multi-dimensional μGC system using a single analyte at a single concentration.

3.3.2 Experimental setup

Benzene (>99.9%), toluene (99.5%), ethylbenzene (99.8%), heptane (99%), styrene (99,9%), chlorobenzene (99.8%) , *p*-xylene (99%), and 2-heptanone (99%) were purchased from Sigma-Aldrich (St. Louis, MO) and used as received. Carbopack^{TM} B (60-80 mesh) was purchased from Supelco (Bellefonte, PA). Compressed helium gas (99.998%) was purchased from Cryogenic

gases (Detroit, MI). The experimental setup for PID characterization is the same as illustrated in Figure 3.9. The setup was arranged in a format resembling a 1x4-channel 2-D GC so that the response of PIDs 2A-D could be calibrated against that of PID 1A. The 1st dimensional module included a microfabricated preconcentrator (μPrcon), one 10 m long RTX-5ms column, and PID 1A. Each of the 2nd dimensional modules included a microfabricated thermal injector (μTI), one 3 m long RTX-200 column, and a PID to be calibrated. The flow routing system between the two separation modules consisted of three microfabricated Deans (μDeans) switches and two three-port solenoid valves to route the analytes from PID 1A to the PIDs in the 2nd dimension.

3.3.3 Calibration procedure

The operation procedure was divided into two steps: detection by PID 1A followed by secondary detection by PIDs 2A-D.

For the first detection, the gas analyte was drawn by a diaphragm pump through a two port valve and adsorbed into Carbopack B inside the μPrcon. After sampling, the two valves were closed and helium gas was flowed through a three-port valve. The μPrcon was heated to 270 ˚C in 0.6 s and then kept at 250 ˚C for 10 s for complete thermal desorption. The analyte was separated by a RTX-5ms column, then detected by PID 1A. During the experiment, the column was heated and kept at 50 ˚C for 1 min and then ramped at a rate of 5˚C min^{-1}, whereas PID 1A was kept at room temperature (25 ˚C).

In the second detection, each of the analytes (either partial or entire amount) passing through PID 1A was routed by the μDeans switches and trapped by the μTI in one of the 2nd dimensional modules. Then, the μTI was heated to 270 ˚C in 0.6 s and kept at 250 ˚C for 5 s.

During the experiment, all columns in the 2nd dimension were kept at 40 ˚C, while PIDs 2A-D were kept at room temperature (25 ˚C).

3.3.4 Analyte dependency

To test and calibrate the PIDs' responses, individual analytes of specific masses were first placed in a Tedlar bag, then collected by the μPCI and injected into the 1st dimensional column. After detected by PID 1A, the analyte was injected into one of the 2nd dimensional columns and detected by the corresponding PIDs (PIDs2A-D). The same procedure was repeated until all four PIDs in the 2nd dimension were tested. Figure 3.10 shows the responses of all five PIDs (PID 1A and PIDs 2A-D) to two representative analytes (ethylbenzene and toluene). Due to the non-destructive nature of the PIDs [155], the same amount of analyte flowed through both PID 1A and one of the PIDs in the 2nd dimension, which allowed for direct comparison of the PID's responsivity in the 2nd dimension with that of PID 1A. For simplicity, we consider PID 1A as the reference and calibrate the responsivity of PIDs 2A-D against that of PID 1A. From Figure 3.10 we can see that the PIDs exhibit quite different responses to the same analyte of the same quantity. The calibration factor, E, for a given PID in the 2nd dimension is defined by the ratio of the peak areas, *i.e.*,

$$E_i = \frac{A_i}{A_{1A}}, \ (i=2A, 2B, 2C \text{ and } 2D) \tag{3.1}$$

where A_i is the peak area obtained from PIDs 2A-D and A_{1A} is the peak area obtained from PID 1A.

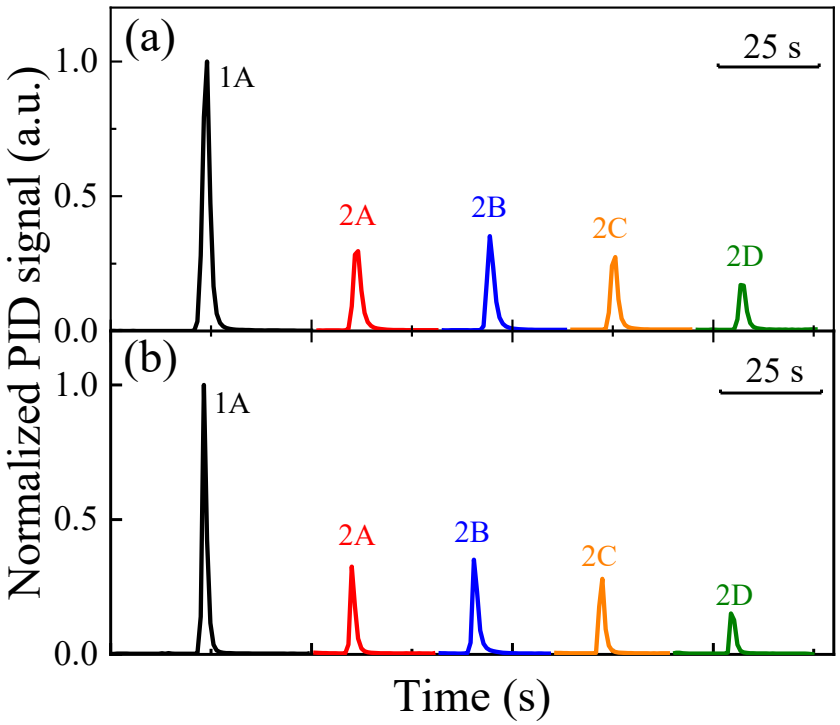

Figure 3.10 The response of 5 PIDs to (a) 85 ng of ethylbenzene and (b) 92 ng of toluene. For comparison purposes, the peaks of PIDs 2A-D are normalized to that of PID 1A for each analyte. Additionally, all the peaks are horizontally shifted for clarity. Therefore, the x-axis does not represent the retention time.

Using the same method, we calibrated the responses of PIDs 2A-D to seven different analytes with ionization potentials ranging widely from 8.45 eV (p-xylene) to 10.08 (heptane)[156]. The results in Figure 3.11 and Table 3.1 show that the calibration factor for each PID are very similar despite the seven analytes having varied physical and chemical properties (such as ionization potential, vapor pressure, polarity, and chromatographic peak width, *etc*.). This result suggests that the PID calibration factor can be obtained by using a single analyte.

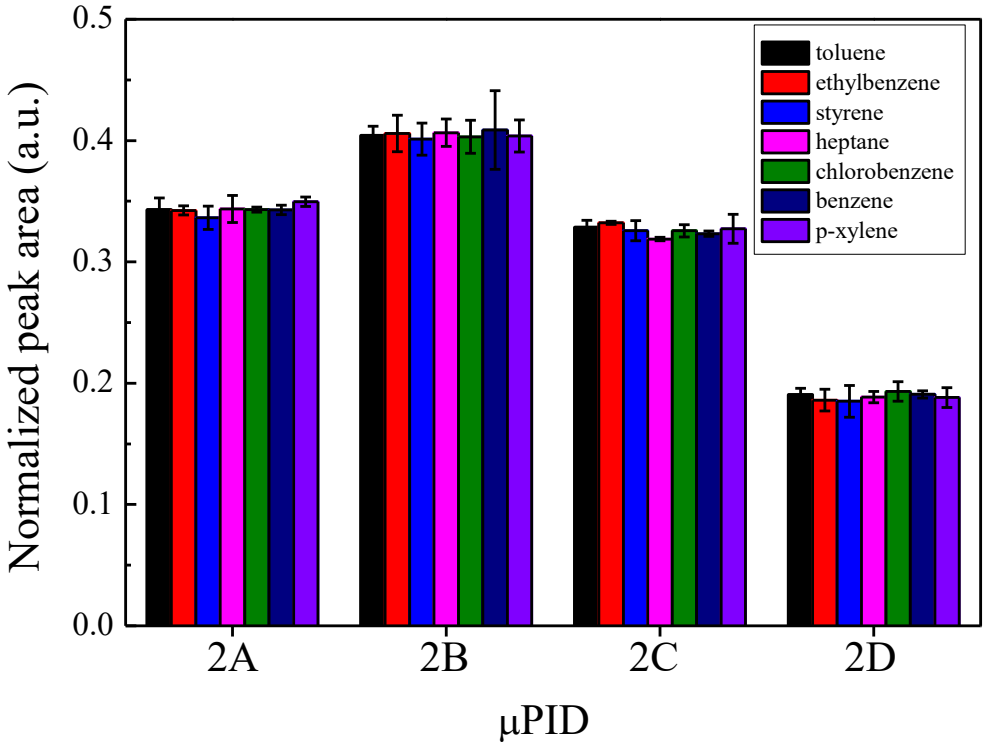

Figure 3.11 Normalized peak area obtained with PIDs 2A-D for toluene (92 ng), ethylbenzene (85 ng), styrene (90 ng), heptane (83 ng), chlorobenzene (75 ng), benzene (80 ng) and p-xylene (80 ng). The peak areas are normalized to that of PID 1A for each analyte. Error bars were obtained with 3 measurements. Related parameters for the analytes and PID calibration factors are given in Table 3.1.

Table 3.1 Comparison of the calibration factors (standard deviation) of PIDs 2A-D for seven different analytes. Averaged calibration factors (standard deviation) are given by E_i.

*Ionization potential (eV)

	Toluene	Ethyl-benzene	Styrene	Heptane	Chloro-benzene	Benzene	*p*-xylene	E_i
IP*	8.82	8.76	8.47	10.08	9.07	9.25	8.49	
2A	0.343 (0.009)	0.342 (0.003)	0.336 (0.009)	0.343 (0.011)	0.343 (0.002)	0.342 (0.003)	0.349 (0.003)	0.343 (0.005)
2B	0.404 (0.007)	0.405 (0.015)	0.401 (0.013)	0.406 (0.011)	0.403 (0.013)	0.408 (0.032)	0.403 (0.013)	0.404 (0.014)
2C	0.328 (0.005)	0.332 (0.001)	0.325 (0.008)	0.318 (0.001)	0.325 (0.005)	0.323 (0.002)	0.327 (0.012)	0.325 (0.004)
2D	0.190 (0.005)	0.186 (0.008)	0.185 (0.013)	0.188 (0.004)	0.193 (0.008)	0.190 (0.002)	0.188 (0.008)	0.189 (0.006)

3.3.5 Concentration dependence

In addition to analyte dependence, we also investigated concentration dependence of the PID's calibration factor. Figure 3.12(a) presents peak areas of toluene signals obtained with PID 1A, 2A, and 2B with injection masses ranging from 1.5 ng to 1800 ng. The peak area shows excellent linear response to the injection mass with an R^2 value of 0.9990-0.9995 from the linear regression analysis (forced zero Y-intercept at zero injection mass). Figure 3.12(b) plots the calibration factors of PIDs 2A and 2B for each injection mass extracted from Figure 3.12 (a), showing high consistency for injection masses ranging over 3 orders of magnitude. The above results suggest that the calibration factor for each PID can be obtained with a single concentration (or mass) of a single analyte.

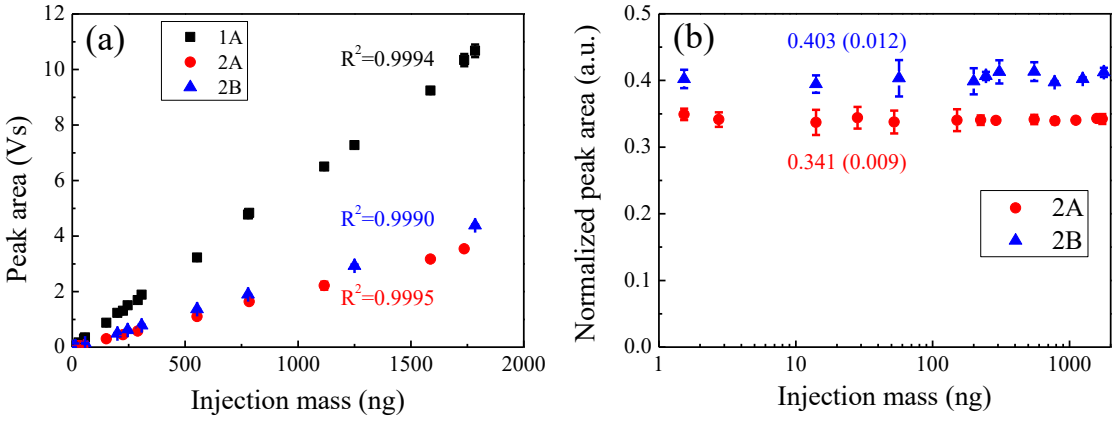

Figure 3.12 (a) Peak area obtained with PID 1A, 2A, and 2B as a function of injection mass of toluene on a linear-linear scale. Error bars were obtained from 3 measurements. (b) The peak areas of signals obtained from PID 2A and PID 2B are normalized to that of PID 1A extracted from (a). Calibration factors for each PID (averaged among different concentrations) and associated standard deviations are labeled in the figure.

3.3.6 Calibration factor validation

To further validate the calibration factors for the PIDs in the 2nd dimension and to demonstrate an important application of using multiple PIDs, we quantitatively reconstructed the coeluted peaks in the 1st dimensional separation using the results obtained from the PIDs in the 2nd dimension. Reconstruction of the 1st dimensional elution peaks is particularly important in comprehensive 2-D GC [157]. Since our instrument had four columns and four PIDs in the 2nd dimension, we were able to alternately route a portion of the eluent from the 1st dimension to the 2nd dimensional columns.

We chose styrene and 2-heptanone as a model system. The black curve in Figure 3.13(a) obtained by PID 1A shows that these two analytes were coeluted from the 1st dimension around 145 seconds. Figure 3.14 illustrates how the eluent was cut and sent into the four 2nd dimensional columns by the flow routing system and subsequently detected by PIDs 2A-D. In order to reconstruct the separation peaks originally overlapped in the 1st dimension, the area under each

peak in the 2nd dimension separation was computed and converted to the response of PID 1A using the corresponding calibration factor. Figure 3.13 (a) and (b) present the reconstructed bars for styrene and 2-heptanone, respectively. The four bars are generated from the signals obtained by PIDs 2A-D. Each bar corresponds to a 5 s slice whose height, h, is computed as follows:

$$h_i = \frac{A_i}{E_i \times 5(s)}, \tag{3.2}$$

where A_i is the peak area obtained by one of the 2nd dimensional PIDs and E_i is the corresponding calibration factor (see Table 3.1). The total area under the bars is 2.575 Vs and 3.03 Vs for styrene and 2-heptanone, respectively. Summations of the two sets of bars are plotted in Figure 3.13 (c) with a total area of 5.605 Vs, which is nearly the same as the area (5.85 Vs) obtained directly by PID 1A (see the black curve in Figure 3.13). In order to verify the reconstruction of the 1st dimension peak, Figure 3.13 (a) and (b) also plot the elution peak of styrene and 2-heptanone detected by PID 1A when they were injected separately (see the red and blue curves in Figure 3.13). The peak area of 2.46 Vs for styrene and 3.006 Vs for 2-heptanone match well with the respective areas obtained from the reconstructed peaks. Details of the peak areas are also given in Table 3.2.

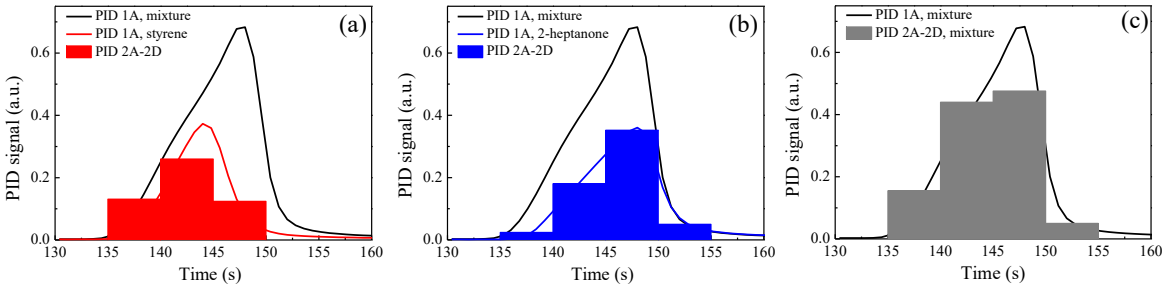

Figure 3.13(a) The coeluted peak of a mixture of styrene (285 ng) and 2-heptanone (420 ng) obtained with PID 1A is given by the black curve. Peak areas of signals from PIDs 2A-2D for styrene is represented by the red bars. The peak of styrene obtained with PID 1A when it was injected individually at 285 ng is given by the red curve. (b) The coeluted peak of a mixture of styrene (285 ng) and 2-heptanone (420 ng) obtained with PID 1A is given by

the black curve. Peak areas the signals from PIDs 2A-2D for 2-heptanone (420 ng) is represented by the blue bars. The peak of 2-heptanone obtained with PID 1A when it was injected individually at 420 ng is given by the blue curve. (c) The coeluted peak of a mixture of styrene (285 ng) and 2-heptanone (420 ng) obtained with PID 1A is provided by the black curve. Black bars are the summation of the red and blue bars in (a) and (b). Details of routing the 1st dimension eluent to the 2nd dimension columns are illustrated in Figure 3.5. Details of the peak areas are given in Table 3.2.

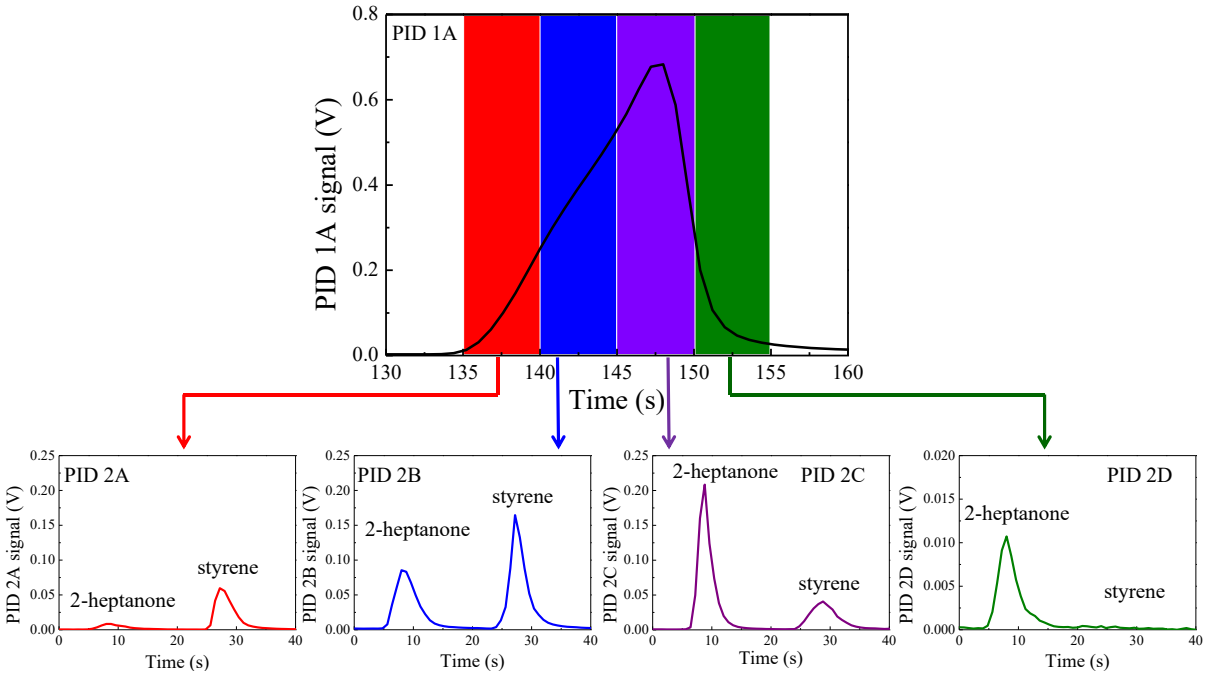

Figure 3.14 (Top panel) Signal from PID 1A when styrene (285 ng) and 2-heptanone (420 ng) were injected together, showing these two analytes coeluted from the 1st dimension around 145 seconds. The routing system cut the eluent into 4 slices (each of which has a 5-second window), and then sent them sequentially to each of the four 2nd dimensional columns. (Bottom panel) Signals from PIDs 2A-D show that styrene and 2-heptanone were separated in the 2nd dimensional column, which allowed us to reconstruct the elution peaks in the 1st dimensional separation.

Table 3.2 Comparison of the total area under red, blue, and black bars obtained with PIDs 2A-2D, and peak areas obtained with PID 1A.

	Styrene (red)	2-Heptanone (blue)	Mixture (Black)
Bar	2.575 (Vs)	3.03 (Vs)	5.605 (Vs)
Curve	2.46 (Vs)	3.006 (Vs)	5.85 (Vs)

With these, we have validated that the calibration factors obtained by calibrating a single analyte at single concentration are applicable to all analytes at any concentrations. We have also validated that by utilizing the peak areas from the ^{2}D PIDs, we can resolve coeluted ^{1}D peaks as long as the peaks can be separated in ^{2}D columns. This work not only enables rapid and *in-situ* calibration of PIDs but facilitates the development of multi-channel, multi-dimensional GC, which will be discussed further in section 3.4.

3.4 2D μGC chromatogram reconstruction algorithm

3.4.1 EMG model based ^{1}D peak reconstruction

While in theory GC x GC enhances a system's peak capacity, in practice, the enhancement is significantly impaired due to the lack of ^{1}D separation information [147]. The retention times or peaks in ^{1}D are deduced from the information obtained from ^{2}D chromatograms. Several methods such as chemometrics have been explored [158-159], but the ^{1}D reconstruction capability is still limited.

Here we demonstrate reconstruction of ^{1}D peaks using the exponentially modified Gaussian (EMG) model with the assistance of the ^{1}D chromatogram obtained with PID 1. The EMG function, which contains both a Gaussian distribution and an exponential decay, is widely used to analyze peaks in chromatography [159-161]. It is defined as:

$$f(t;\mu,\sigma,\lambda)=\frac{\lambda}{2}\exp\left[\frac{\lambda}{2}(2\mu+\lambda\sigma^{2}-2t)\right]\cdot erfc\left(\frac{\mu+\lambda\sigma^{2}-t}{\sqrt{2}\sigma}\right), \tag{3.3}$$

where t is time, λ is the rate of an exponential decay, μ and σ are the mean andstandard deviation of a normal Gaussian function, respectively,and *erfc* is the complementary error function defined as:

$$erfc(x) = \frac{2}{\sqrt{\pi}} \int_x^{\infty} e^{-q^2} dq. \tag{3.4}$$

Note that the total area under the EMG function defined in (3.3) is normalized to unity. The retention time (t_m) of the EMG is defined as:

$$t_m = \mu - \sqrt{2}\sigma \cdot erfcinv(\frac{\sqrt{2}}{\sqrt{\pi}|\lambda|\sigma}) + \lambda\sigma^2, \tag{3.5}$$

where *erfcinv* is the *erfc* inverse function.

Assuming that an analyte from ^{1}D is modulated to ^{2}D n times at t_1, t_2, t_3, ..., t_n, the corresponding normalized peak areas in ^{2}D are a_1, a_2, a_3, …, a_n (*i.e.*, $a_1+a_2+a_3+ \ldots+a_n = 1$). To find the best fit EMG curve for this analyte in ^{1}D, we establish an objective function, e, defined as follows:

$$e = \sum_{i=1}^{n} e_i^2, \tag{3.6}$$

$$e_i = a_i - \int_{t_{i-1}}^{t_i} f(t;\mu,\sigma,\lambda) \cdot dt \ (i = 1, 2, 3, \ldots, n). \tag{3.7}$$

Once the three parameters (μ, σ, and λ) are given, the normalized EMG function $f(t; \mu, \sigma, \lambda)$ is fully defined. To find μ, σ, and λ, we further assume that the retention time for the analyte is located between t_0 and t_n, *i.e.*, $t_0 < t_m < t_n$, which allows us to scan t_m from t_0 to t_n to find the optimal μ, σ, and λ. For a given t_m, there are only two independent parameters, namely σ and λ (μ can be determined by (3.3). Therefore, minimizing the objective function e in the σ-λ plane results in e_{min} (a set of μ, σ, and λ), and hence the corresponding EMG function $f(t; \mu, \sigma, \lambda)$. Repeating the same procedures by scanning over t_m (*i.e.*, $t_m^{(1)}$, $t_m^{(2)}$, …, $t_m^{(p)}$, where p is the number of t_m's used in the scanning), we can obtain a series of e_{min} (*i.e.*, $e_{min}^{(1)}$, $e_{min}^{(2)}$, …, $e_{min}^{(p)}$) and the associated EMG functions, $f(t; \mu^{(1)}, \sigma^{(1)}, \lambda^{(1)})$, $f(t; \mu^{(2)}, \sigma^{(2)}, \lambda^{(2)})$, …, and $f(t; \mu^{(p)}, \sigma^{(p)}, \lambda^{(p)})$.

In the traditional method, which lacks the ^{1}D detector, the best fit EMG function $f(t; \mu, \sigma, \lambda)$ is the one that corresponds to the lowest e_{min}. In contrast, with the information provided by the ^{1}D detector, the EMG functions and hence the ^{1}D peaks can be obtained with much higher accuracy and resolution. Assuming the ^{1}D chromatogram obtained with the ^{1}D detector is $h(t)$, the difference (E) between $h(t)$ and $f(t; \mu, \sigma, \lambda)$ is given as:

$$E = \int_{t_0}^{t_n} \left| h(t) - A \cdot f(t; \mu, \sigma, \lambda) \right| \cdot dt, \tag{3.8}$$

where A represents the total area of the ^{2}D chromatograms. We test Equation (3.8) with the p EMG functions obtained previously. The best fit EMG (and the associated area, A) is the one that minimizes E. Note that here, we use the singlet case (single analyte) in Equation (3.8) to describe the algorithm for the sake of mathematical simplicity and completeness. In practice, if there is only one analyte, $h(t)$ itself can be used to reconstruct the ^{1}D peak. For the doublet (two coeluted analytes) and triplet (three coeluted analytes) cases, Equation (3.8) can be generalized as:

$$E = \int_{t_0}^{t_n} \left| h(t) - A_j \cdot f(t; \mu_j, \sigma_j, \lambda_j) - A_k \cdot f(t; \mu_k, \sigma_k, \lambda_k) \right| \cdot dt, \tag{3.9}$$

$$E = \int_{t_0}^{t_n} \left| h(t) - A_j \cdot f(t; \mu_j, \sigma_j, \lambda_j) - A_k \cdot f(t; \mu_k, \sigma_k, \lambda_k) - A_l \cdot f(t; \mu_l, \sigma_l, \lambda_l) \right| \cdot dt, \tag{3.10}$$

where j, k, l = 1, 2, 3, …, p for different coeluted analytes and $A_{j,k,l}$ are the corresponding total areas obtained from the ^{2}D chromatograms. By minimizing E, the best set of the EMG functions (along with the areas) for the coeluted analytes can be obtained.

We simulated reconstruction of one, two, and three coeluted peaks (singlet, doublet, and triplet) using our algorithm as shown in Figure 3.15(a)(b)(c)and compared it to the traditional method in as shown in Figure 3.15(d)(e)(f). Note that in practice, singlet peaks can be reconstructed directly by the signal from the ^{1}D detector using our method. The singlet example presented in Figure 3.15(a) is to demonstrate the ability of our algorithm to overcome the deficiencies in the

traditional method. Below, we use the doublet case to detail the reconstruction procedures. First, we arbitrarily generated ^{1}D peaks with various combinations of μ, σ, and λ, as shown in (3.3). Red (μ = 5, σ = 1, and λ = 2) and blue (μ = 7, σ = 2, and λ = 1) solid curves in Figure 3.15 (b) represent two analytes. The ^{1}D peaks were modulated every 5 s (P_M = 5 s) and the number of modulations was 4. The scan step size was set to 0.5 s and the t_m range was set from 0 to 20 s, yielding 40 (*i.e.*, p = 40) possible retention times (t_m). Next, the ^{2}D peak areas were calculated (red and blue bars in Figure 3.15 (b)). Based on Equations (3.3) to (3.9), the ^{1}D peaks were reconstructed and shown as red and blue dashed curves. Figure 3.15 shows that our algorithm is able to reconstruct the ^{1}D peaks with high accuracy. In contrast, as shown in Figure 3.15(d)(e)(f), the traditional method that uses the same EMG model, but without the ^{1}D chromatogram (black curves), fails to accurately reconstruct the ^{1}D peaks (see the dashed curves).

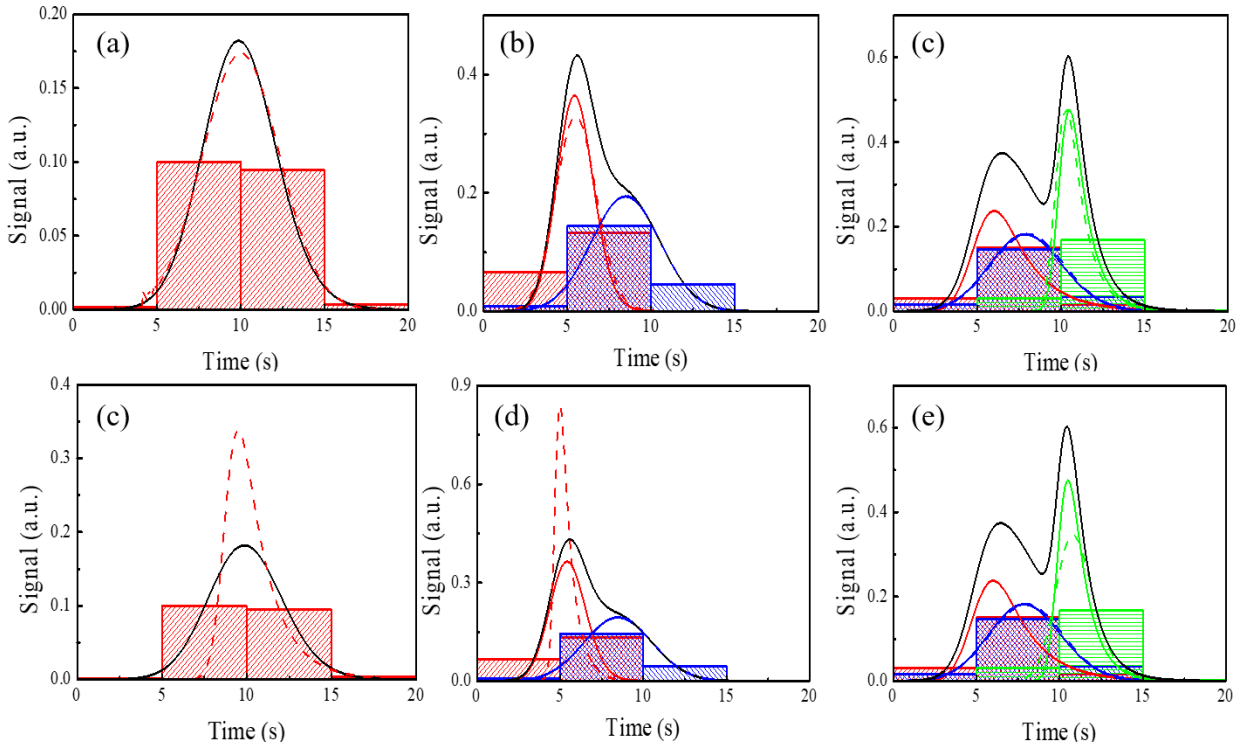

Figure 3.15 Simulation of ^{1}D reconstruction of (a) single peak, (b) coeluted two peaks,

and (c) coeluted three peaks using the EMG model and the ^{1}D chromatogram detected by the ^{1}D detector. Black curves: ^{1}D chromatograms detected by the ^{1}D detector. Black curve in (a): μ =9, σ = 2, and λ = 1 (3.3). Red/blue solid curves in (b): 2 different analytes. μ = 5/7, σ = 1/2, and λ = 2/1 (3.3). Red/blue/green solid curves in (c): 3 different analytes. μ = 5/7/10, σ = 1/2/0.5, and λ = 0.5/1/1 (3.3). The combination of these curves results in the black curves in (b), and (c). Red/blue/green dashed curves: reconstructed ^{1}D peaks using our algorithm. Red/blue/green boxes: the width represents the modulation period (5 s in this case) and the area represents the analyte quantity of each modulation detected by the ^{2}D detector. For comparison, reconstruction of the same ^{1}D peaks without the ^{1}D chromatogram is shown in (c) (d) and (e).

We validated the reconstruction method for the ^{1}D peaks by injecting the sample into our portable 1x4-channel GC x GC system and comparing the experimental peaks with the reconstructed peaks. First, we show the reconstruction of a singlet peak. Cyclohexane was injected by the μPCI in ^{1}D and underwent ^{1}D separation. After detection by μPID 1 (black curve), Figure 3.16(a) shows the ^{2}D separation for modulations at 72 s and 80 s. The ^{1}D peak was reconstructed according to the procedures described in Section 3.4.1 and shown as the red curve in Figure 3.17. Once again, we present the singlet result only to show the capability of our algorithm. In practice, in the singlet case, we would use the ^{1}D peak obtained directly from PID 1.

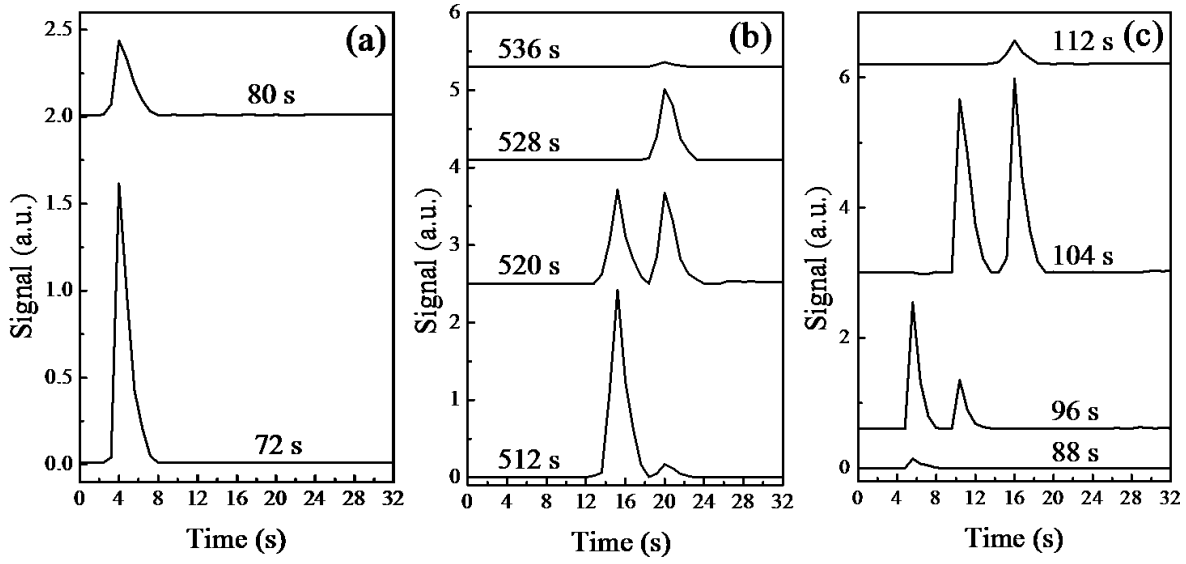

Figure 3.16 ^{2}D separation of (a) cyclohexane for modulations at 72 s and 80 s, (b) 3-

chlorotoluene and 1,3-dichlorobenzene for modulations at 512 s, 520 s, 528 s, and 536 s, and (c) heptane, 1,4-dioxane, and methylisobutylketone for modulations at 88 s, 96 s, 104 s, and 112 s.

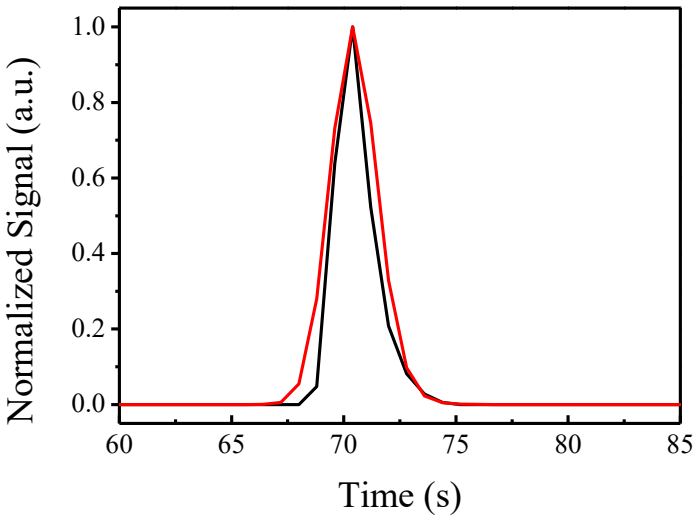

Figure 3.17 Comparison of the normalized peak (black) of cyclohexane obtained with μPID 1 and the reconstructed peak (red).

Next, a coeluted peak containing two analytes was tested. 3-chlorotoluene and 1,3-dichlorobenzene were selected due to their similar retention times. The black curve in Figure 3.18(a) was detected by PID 1, showing that the two analytes were not fully separated in ^{1}D. This ^{1}D peak was then modulated at 512 s, 520 s, 528 s, and 526 s, and further separated in ^{2}D (see Figure 3.16(b), 2D separation for modulations at 512 s, 520 s, 528 s, and 536 s). The ^{1}D peaks were reconstructed according to the procedures described in Section 3.4.1 and shown as the red and blue curves in Figure 3.18(a). To further verify the ^{1}D peak reconstruction, both analytes were injected individually into our system. The corresponding comparison between the normalized original peaks detected by PID 1 and the normalized reconstructed peaks is presented Figure 3.18(b).

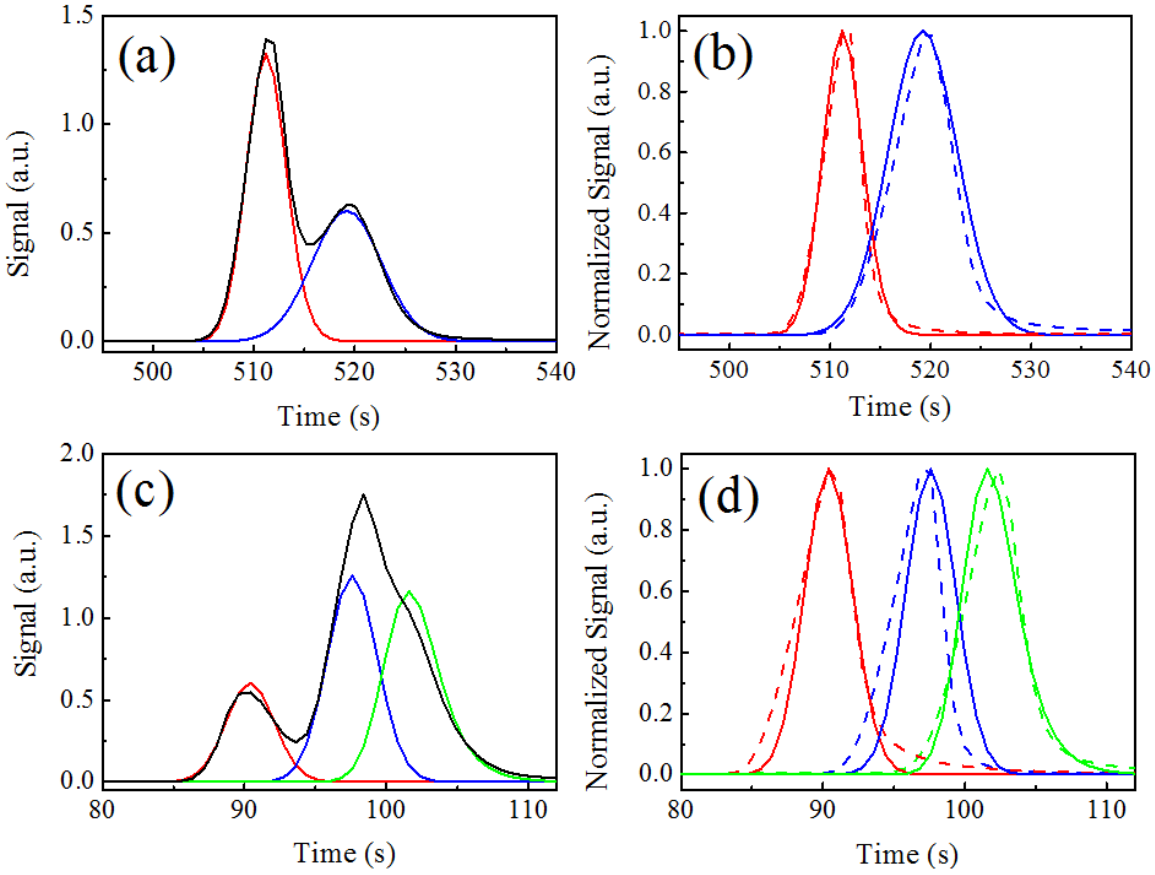

Figure 3.18 (a) ^{1}D chromatogram obtained with µPID 1 for a mixture of 3-chlorotoluene and 1,3-dichlorobenzene (black curve). Reconstructed ^{1}D chromatogram for 3-chlorotoluene (red curve) and 1,3-dichlorobenzene (blue curve). (b) Comparison of the reconstructed ^{1}D chromatograms in (a) for 3-chlorotoluene and 1,3-dichlorobenzene (solid curves) and those obtained with µPID 1 when 3-chlorotoluene and 1,3-dichlorobenzene were injected individually (dashed curves). All curves are normalized to their respective peaks for comparison. (c) ^{1}D chromatogram obtained with µPID 1 for a mixture of heptane, 1,4-dioxane, and methylisobutylketone (black curve). Reconstructed ^{1}D chromatogram for heptane (red curve), 1,4-dioxane (blue curve), and methylisobutylketone (green curve). (d) Comparison of the reconstructed ^{1}D chromatograms in (a) for heptane, 1,4-dioxane, and methylisobutylketone (solid curves) and those obtained with µPID 1 when heptane, 1,4-dioxane, and methylisobutylketone were injected individually (dashed curves). All curves are normalized to their respective peaks for comparison.

Finally, the reconstruction was applied to a coeluted peak containing three analytes (heptane, 1,4-dioxane, and methylisobutylketone). The unresolved ^{1}D chromatogram detected by PID 1 is shown in the black curve in Figure 3.18(c). Modulations took place at 88 s, 96 s, 104 s,

and 112 s. The corresponding ^{2}D separation is given in Figure 3.16(c). The reconstructed peaks are plotted as the red, blue, and green curves in Figure 3.18(c). Comparisons between the normalized peaks of the individually injected analytes and the normalized reconstructed peaks are presented in Figure 3.18(d). These examples suggest that our system and algorithm are able to accurately reconstruct ^{1}D peaks, thus improving ^{1}D resolution and hence peak capacity.

3.4.2 Reconstruction of 2D Chromatogram (contour plot)

One of the distinct characteristics of a GC x GC chromatogram is the 2-D contour plot of well-separated analytes in a mixture. Traditionally, the output of GC x GC is simply a long series of ^{2}D chromatograms[38, 162] since there is no ^{1}D detector. Thus, the resolution of the traditional 2-D contour plot is lost due to modulation and the lack of information on the ^{1}D chromatogram. In contrast, our GC x GC makes use of the information obtained from the reconstructed ^{1}D peaks, allowing for creation of a 2-D contour plot with significantly increased resolution. To generate such a 2-D contour plot, the ^{2}D chromatograms were firstly deconvoluted for each analyte in ^{1}D. Since the 2A-2D PID peak shapes are the same (expect for peak height), we use peak shape within a single modulation (where the ${}^1t_R$ locates) to represent the analyte's ^{2}D peak shape. For analyte *s*, we can define its ^{1}D chromatogram as the area-normalized EMG function, $f_s({}^1t_R)$, the its ^{1}D peak area as A_s and the ^{2}D area-normalized peak as $g_s^{(v)}({}^2t_R)$. $v = \left\lfloor \frac{{}^1t_R}{P_M} \right\rfloor + 1$ (=1, 2, …, n), which represents the v^{th} modulation from ^{1}D to ^{2}D, with $\lfloor \cdot \rfloor$ being the floor function . The 2-D contour plot of $C_s({}^1t_R, {}^2t_R)$ is then:

$$C_s({}^1t_R, {}^2t_R) = A_s f_s({}^1t_R) g_s^{(v)}({}^2t_R) \tag{3.11}$$

Correspondingly, the 2-D contour plot, $C({}^1t_R, {}^2t_R)$, of N analytes can be written as:

$$C({}^1t_R, {}^2t_R) = \sum_{s=1}^{N} C_s({}^1t_R, {}^2t_R). \tag{3.12}$$

Figure 3.19 shows the 2-D and the 3-D contour plots for singlet, doublet, and triplet analytes in Figure 3.17 and Figure 3.18 using the method described in Eqs. (9) and (10), showing well resolved peaks. For comparison, corresponding 2-D and 3-D contour plots using the traditional method are given in Figure 3.20.

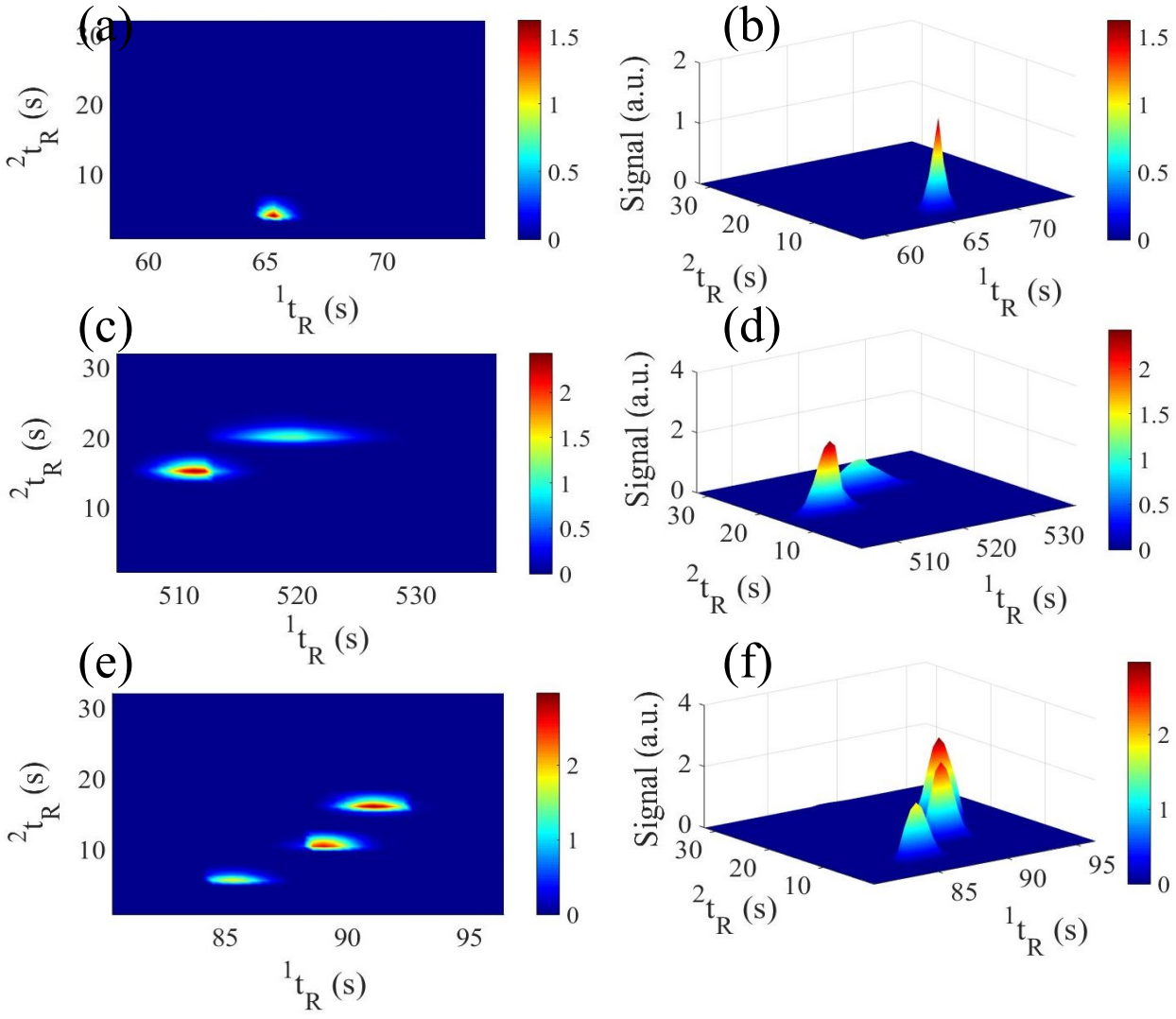

Figure 3.19 2-D and 3-D contour plots of Figure 3.17, and Figure 3.18 using Eqs. (9) and (10). For comparison, the corresponding contour plots using the traditional method are shown in Figure 3.20.

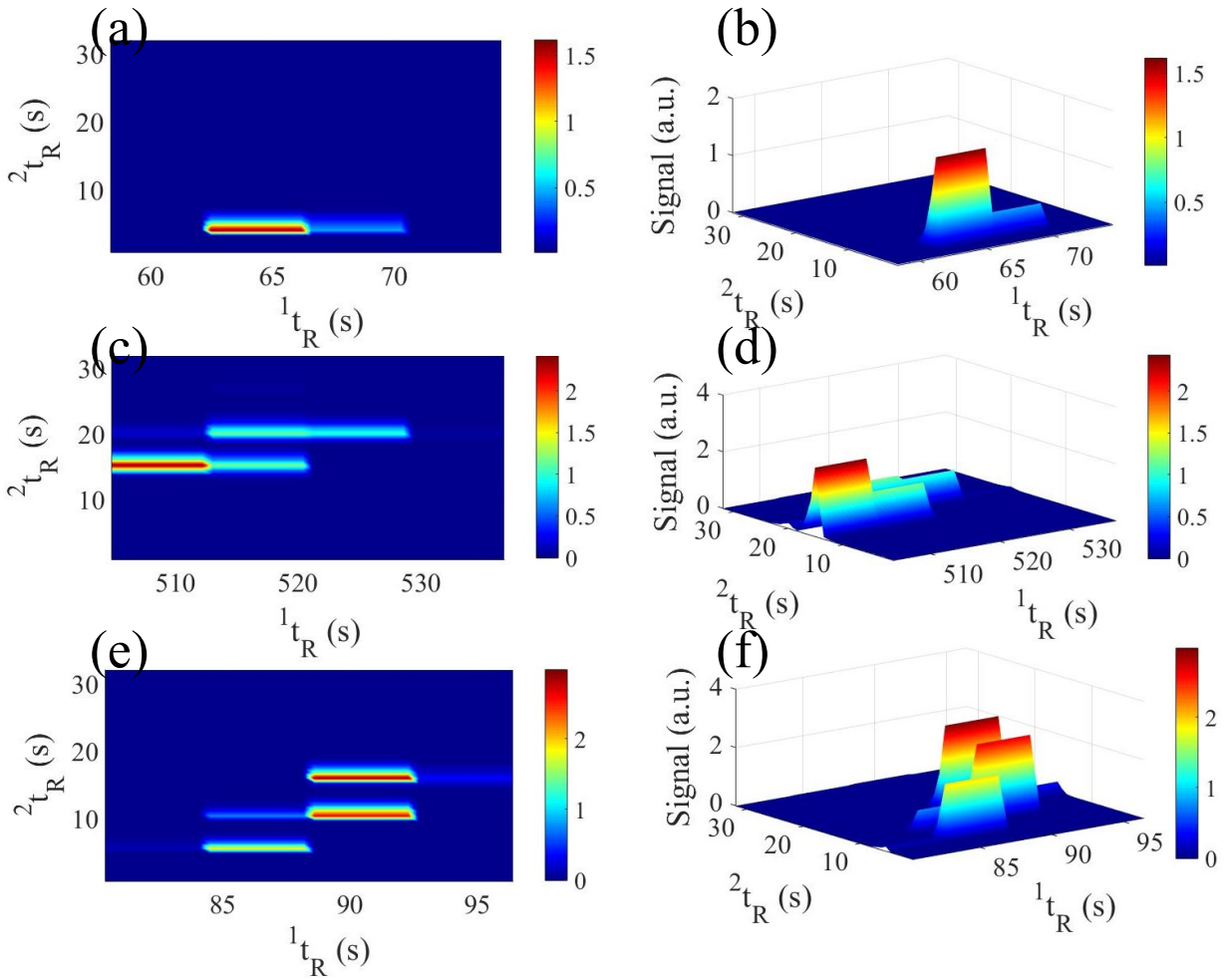

Figure 3.20 2-D and 3-D contour plot corresponding to Figure 3.19 using the traditional method instead.

3.4.3 Demonstration of 2-D separation of 50 VOCs

We employed the portable 1x4-channel GC x GC device to analyze a mixture of 50 VOCs (see Table 3.3). First, the mixture of 50 VOCs was prepared in a Tedlar bag and separated in ^{1}D. The corresponding ^{1}D chromatogram were recorded by μPID 1 (see Figure 3.21). Using a modulation period of 8 s, the analytes were routed to the ^{2}D separation modules and separated in ^{2}D. Figure 3.22 presents the 2-D contour plot of the 50 VOCs using the previously discussed 1D reconstruction and contour plot methods. It can be seen that the 50 VOCs can be completed

separated in only 850 s (or 14.2 minutes). The corresponding reconstructed retention times and peak widths in ^{1}D and retention times and peak widths in ^{2}D are listed in Table 3.

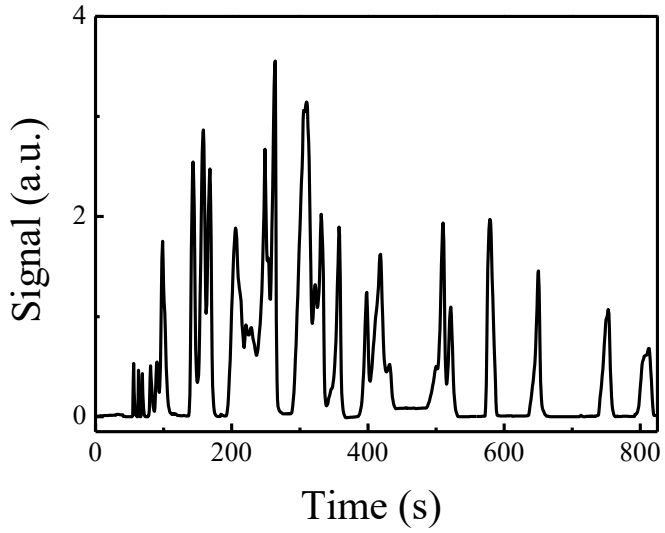

Figure 3.21 ^{1}D chromatogram of the 50 VOCs detected by PID 1.

Table 3.3 List of 50 VOCs and their ^{1}D and ^{2}D retention times and peak widths.

	Analyte	$^{1}t_R$	^{1}FWHM	$^{2}t_R$	^{2}FWHM		Analyte	$^{1}t_R$	^{1}FWHM	$^{2}t_R$	^{2}FWHM
1	Hexane	56	1.5	5.7	1	26	Nonane	310	10.9	10.4	1.4
2	2-methylfuran	63	1	10.3	1	27	1,2-dichlorobenzene	323	10.2	19.2	1.6
3	Cyclohexane	70	1.7	4	1.3	28	Cumene	331	9.2	18.4	1.22
4	Benzane	80	3.2	8	1.25	29	2-ethoxyethyl acetate	333	7.2	24.7	1.2
5	Heptane	90	4	5.6	1	30	Propylbenzene	355	9.03	16	1.56
6	1.4-dioxane	97	4.2	10	0.95	31	(+)-α-pinene	357	6.18	12	1.12
7	Methylisobutylketone	102	4.5	16	1.34	32	4-ethyltoluene	396	5.8	11.9	1.4
8	Methylcyclohexane	142	4.6	5.57	1.23	33	Benzaldehyde	401	9	16	1.1
9	Toluene	144	6.91	8.8	1.12	34	2-chlorotoluene	411	7.92	22.4	1.5
10	Cyclopentanone	156	5.99	11.1	1.34	35	Mesitylene	418	11.8	20	1.2
11	2-hexanone	160	8.1	14	1.45	36	4-chlorotoluene	419	6	16	1.4
12	Hexanal	168	8.8	12.8	1.12	37	Phenol	427	5.5	12	1.34
13	Octane	168	7.1	7.9	1.1	38	2-ethlytoluene	500	10.3	19	1.31
14	Trans-2-hexen-1-al	202	10.7	12	1.23	39	1,2,4-trimentylbenzene	508	7.2	22.4	1.6
15	Chlorobenzene	206	8.37	19.1	1.33	40	3-chlorotoluene	511	5.5	15.2	1.5
16	Ethylbenzene	213	7.53	8.8	1.24	41	1,3-dichlorobenzene	519	8.5	19.8	1.6
17	Xylene	221	5.36	12	1.34	42	1-heptanol	522	8	21.6	1.29
18	1-hexanol	228	4.1	15.3	1.09	43	2-octanone	577	6	22.4	1.3
19	Cyclohexanol	236	8.7	17.5	1.2	44	Decane	581	8.3	12	1.8
20	Styrene	248	10.8	13.5	1.17	45	(R)-(+)-limonene	646	9.45	15.2	1
21	Cyclohexanone	250	11	12	1.3	46	3-octanol	650	7	21.6	1.26
22	2-heptanone	260	6.7	20	1.14	47	Nonanal	749	12.3	21.5	1.36
23	Anisol	264	11	22.3	1.2	48	Undecane	752	11	16	1.6
24	Heptanal	300	10	12.7	1.34	49	1-octen-3-ol	805	10.5	20	1.81
25	2,5-hexadione	305	11.4	16.8	1.8	50	Dodecane	812	11	16	1.57

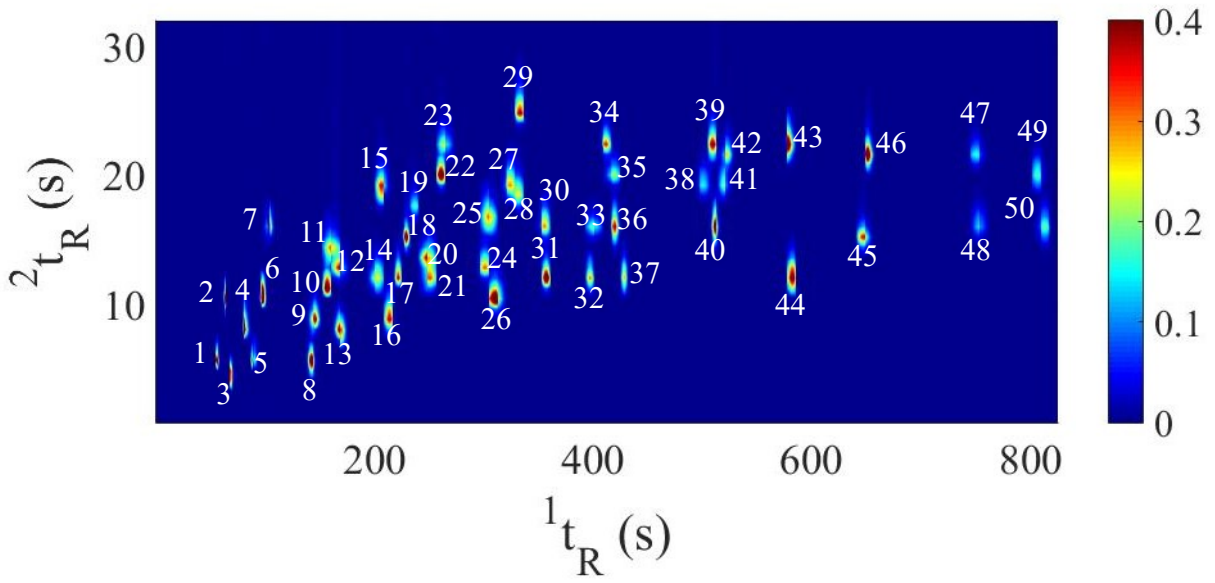

Figure 3.22 2-D contour plot of the 50 VOCs generated with the portable 1x4-channel GC x GC device.

3.4.4 System performance evaluation

The GC x GC peak capacity is defined as:

$$n_{GC\chi GC}=n_1 x n_2, \tag{3.13}$$

where n_1 and n_2 are the peak capacities for ^{1}D and ^{2}D, respectively. With a chromatographic resolution Rs of 1, (3.13) can be written as [163]:

$$n_{GC\chi GC} = 0.35\cdot(^1t_R/^1\text{FWHM}) \text{ x } (CP_M/^2\text{FWHM}) \tag{3.14}$$

where ^1t_R is the analyte retention time in ^{1}D, ^{1}FWHM and ^{2}FWHM are the FWHMs in ^{1}D and ^{2}D, respectively, P_M is the modulation period, and C is the number of ^{2}D channels. Correspondingly, the peak capacity production is as follows [163]:

$$n_{GC\chi GC}/^1t_R = 0.35/^1\text{FWHM} \text{ x } (CP_M/^2\text{FWHM}) \tag{3.15}$$

We evaluate the 1x4-channel GC x GC performance using three example analytes: 2-ethoxyethyl acetate, benzaldehyde, and dodecane. Table 3.4 presents the peak capacity and peak capacity production of 2-ethoxyethyl acetate, benzaldehyde, and dodecane. The peak capacity production ranges from 40/min to 80/min, which is similar to values obtained by conventional GC x GC [147, 163-166]. For comparison, the peak capacity productions for benzaldehyde and dodecane in a hybrid μGC x μGC system are 31/min and 14/min, respectively, (assuming ^{1}FWHM is 17.5 s and 12 s for benzaldehyde and dodecane, respectively).

Table 3.4 Calculation of peak capacity and peak capacity production of the portable 1x4-channel GC x GC device based on equation (3.14) and (3.15)

	Analyte	$^{1}t_R$	^{1}FWHM	^{2}FWHM	n_{GCXGC}	$n_{GCXGC}/^{1}t_R$
#29	2-ethoxyethyl acetate	333 s	7.2 s	1.2 s	430	77/min
#33	Benzaldehyde	401 s	9 s	1.1 s	455	68/min
#50	Dodecane	812 s	11 s	1.57 s	526	40/min

3.5 Conclusions

Compared to conventional GC x GC, our GC x GC design has several advantages. First, in conventional GC x GC, the ^{2}D separation time is limited by the short modulation period (to avoid wrap-around), thus resulting in lower ^{2}D peak capacity. In contrast, our multiple channel design allows for much longer separation times, resulting in significantly increased ^{2}D peak capacity. Second, in conventional GC x GC, the ^{1}D elution peaks are not detected directly. Instead, they are reconstructed using the modulation period and information obtained by the detector at the end of the ^{2}D column. This leads to deteriorated resolution (and hence lower ^{1}D peak capacity) [147]. In contrast, in our GC x GC, μPID 1 monitors elutions from the ^{1}D column so that the elution peaks in ^{1}D can be reconstructed more accurately, thus increasing the ^{1}D peak capacity. Third, this system uses a μDS and μTI for modulation, focusing, and injection of analytes. These devices are

mechanically robust and can be operated at room temperature without the need for a TEC. Furthermore, neither coating bleeding nor analyte breakthrough occurs. Fourth, our GC x GC system is highly scalable, and additional μDSs, μTIs, PIDs, and ^{2}D columns can be easily used. Finally, this system exhibits high versatility and can operate in heart-cutting mode (rather than GC x GC mode) with minimal modification (in control software). The major challenges that still remain in in this multi-channel GC x GC are higher system complexity and requirement PID calibration [167].

In summary, we have developed a new, fully automated, portable 1x4-channel GC x GC device. The device is compact (60 cm × 50 cm × 10 cm, and < 5 kg), robust (μTI and μDS), provides rapid analysis (50 VOCs in 14 minutes), and provides excellent peak capacity and peak capacity production. This system can be used for a plethora of field applications, such as *in-situ* continuous environmental monitoring, workplace safety monitoring, industrial in-line monitoring, food and agriculture analysis, and breath analysis.

3.7 References

1. Whiting, J. J.; Fix, C. S.; Anderson, J. M.; Staton, A. W.; Manginell, R. P.; Wheeler, D. R.; Myers, E. B.; Roukes, M. L.; Simonson, R. J. In *High-speed two-dimensional gas chromatography using microfabricated GC columns combined with nanoelectromechanical mass sensors*, TRANSDUCERS 2009 - 2009 International Solid-State Sensors, Actuators and Microsystems Conference, 21-25 June 2009; 2009; pp 1666-1669.
2. Kim, S. J.; Reidy, S. M.; Block, B. P.; Wise, K. D.; Zellers, E. T.; Kurabayashi, K., Microfabricated thermal modulator for comprehensive two-dimensional micro gas chromatography: design, thermal modeling, and preliminary testing. *Lab chip* **2010,** *10* (13), 1647-1654.
3. Serrano, G.; Dibyadeep, P.; Kim, S.-J.; Kurabayashi, K.; Zellers, E. T., Comprehensive Two-Dimensional Gas Chromatographic Separations with a Microfabricated Thermal Modulator. *Anal. Chem.* **2012,** *84* (16), 6973–6980.
4. Kim, S.-J.; Serrano, G.; Wise, K. D.; Kurabayashi, K.; Zellers, E. T., Evaluation of a Microfabricated Thermal Modulator for Comprehensive Two-Dimensional Microscale Gas Chromatography. *Anal. Chem.* **2011,** *83* (14), 5556-5562.
5. Collin, W. R.; Bondy, A.; Paul, D.; Kurabayashi, K.; Zellers, E. T., μGC × μGC: Comprehensive Two-Dimensional Gas Chromatographic Separations with Microfabricated Components. *Anal. Chem.* **2015,** *87*, 1630−1637.
6. Blumberg, L. M., Potentials and Limits of Comprehensive GC X GC. *Anal. Chem.* **2002,** *74*, 503A.
7. Blumberg, L. M.; David, F.; Klee, M. S.; Sandra, P., Comparison of one-dimensional and comprehensive two-dimensional separations by gas chromatography. *J. Chromatogr. A* **2008,** *1188* (2), 2-16.
8. Zhu, H.; Nidetz, R.; Zhou, M.; Lee, J.; Buggaveeti, S.; Kurabayashi, K.; Fan, X., Flow-through microfluidic photoionization detectors for rapid and highly sensitive vapor detection. *Lab Chip* **2015,** *15* (14), 3021-3029.
9. Inc., R. S., *The PID Handbook: Theory and applications of direct reading photoionization detectors (3rd Edn.)*. San Jose, CA, 2013; Vol. 3.
10. Langhorst, M. L., Photoionization Detector Sensitivity of Organic Compounds. *J. Chromatogr. Sci.* **1981,** *19* (2), 98-103.
11. Freedman, A. N., Photoionization detector response. *J. Chromatogr. A* **1982,** *236* (1), 11-15.
12. Drummond, I., On-the-Fly Calibration of Direct Reading Photoionization Detectors. *American Industrial Hygiene Association Journal* **1997,** *58* (11), 820-822.
13. Peng, F. M.; Xie, P. H.; Shi, Y. G.; Wang, J. D.; Liu, W. Q.; Li, H. Y., Photoionization detector for portable rapid GC. *Chromatographia* **2007,** *65* (5-6), 331-336.
14. Davenport, J. N.; Adlard, E. R., Photoionization detectors for gas chromatography. *J. Chromatogr. A* **1984,** *290*, 13-32.
15. Edgett, L. B.; Stotlar, S. C. In *Study Of Possible Solarization - Related Impurities In CaF2 And Other Fluorides*, 1985; pp 134-139.
16. Driscoll, J. N., Evaluation of a new photoionization detector for organic compounds. *J. Chromatogr. A* **1977,** *134* (1), 49-55.
17. Freedman, A. N., The photoionization detector: Theory, performance and application as a low-level monitor of oil vapour. *J. Chromatogr. A* **1980,** *190* (2), 263-273.
18. Blomberg, J.; Schoenmakers, P. J.; Beens, J.; Tijssen, R., Compehensive two-dimensional gas chromatography (GC×GC) and its applicability to the characterization of complex (petrochemical) mixtures. *J. High Resolut. Chromatogr.* **1997,** *20* (10), 539-544.
19. Zeng, Z.-D.; Hugel, H. M.; Marriott, P. J., Simultaneous estimation of retention times of overlapping primary peaks in comprehensive two-dimensional GC. *J Sep. Sci.* **2013,** *36* (17), 2728-2737.

20. Kong, H.; Ye, F.; Lu, X.; Guo, L.; Tian, J.; Xu, G., Deconvolution of overlapped peaks based on the exponentially modified Gaussian model in comprehensive two-dimensional gas chromatography. *J. Chromatogr. A* **2005,** *1086* (1–2), 160-164.
21. Jeansonne, M. S.; Foley, J. P., Review of the Exponentially Modified Gaussian (EMG) Function Since 1983. *J. Chromatogr. Sci.* **1991,** *29* (6), 258-266.
22. Jung, K. H.; Yun, S. J.; Kang, S. H., Characterization of peak shape parameters with normal and derivative chromatograms. *Anal. Chem.* **1984,** *56* (3), 457-462.
23. Kallio, M.; Hyötyläinen, T., Quantitative aspects in comprehensive two-dimensional gas chromatography. *J. Chromatogr. A* **2007,** *1148* (2), 228-235.
24. Dallüge, J.; Beens, J.; Brinkman, U. A. T., Comprehensive two-dimensional gas chromatography: a powerful and versatile analytical tool. *J. Chromatogr. A* **2003,** *1000* (1–2), 69-108.
25. Siegler, W. C.; Crank, J. A.; Armstrong, D. W.; Synovec, R. E., Increasing selectivity in comprehensive three-dimensional gas chromatography via an ionic liquid stationary phase column in one dimension. *J. Chromatogr. A* **2010,** *1217* (18), 3144-3149.
26. Sinha, A. E.; Prazen, B. J.; Fraga, C. G.; Synovec, R. E., Valve-based comprehensive two-dimensional gas chromatography with time-of-flight mass spectrometric detection: instrumentation and figures-of-merit. *J. Chromatogr. A* **2003,** *1019* (1–2), 79-87.
27. Fitz, B. D.; Wilson, R. B.; Parsons, B. A.; Hoggard, J. C.; Synovec, R. E., Fast, high peak capacity separations in comprehensive two-dimensional gas chromatography with time-of-flight mass spectrometry. *J. Chromatogr. A* **2012,** *1266*, 116-123.
28. Klee, M. S.; Cochran, J.; Merrick, M.; Blumberg, L. M., Evaluation of conditions of comprehensive two-dimensional gas chromatography that yield a near-theoretical maximum in peak capacity gain. *J. Chromatogr. A* **2015,** *1383*, 151-159.
29. Lee, J.; Zhou, M.; Zhu, H.; Nidetz, R.; Kurabayashi, K.; Fan, X., In situ calibration of micro-photoionization detectors in a multi-dimensional micro-gas chromatography system. *Analyst* **2016,** *141* (13), 4100-4107.

Chapter 4 Rapid Breath Analysis for Acute Respiratory Distress Syndrome Diagnostics Using a Portable 2D GC

4.1 Introduction

Acute respiratory distress syndrome (ARDS) is an inflammatory condition of the lung producing severe lung damage. It is one of the most severe forms of acute lung injury and responsible for high mortality (40%) and long-term morbidity[168-170]. An estimated 200,000 Americans develop ARDS each year, of which more than 74,000 cases are fatal[168]. Patients who survive ARDS experience long-term deficits in physical and neurocognitive function[171-172]. Both primary hospitalizations and increased health service utilization among survivors are associated with high healthcare costs[168, 171]. For example, the average cost of an Intensive Care Unit (ICU) patient requiring mechanical ventilation ranges between $7,000 and $11,000 per day with an incremental cost of $1,000-1,500 per day for mechanical ventilation[173].

Numerous predisposing factors for ARDS have previously been identified (*e.g.*, sepsis, aspiration, and trauma)[174]. However, our understanding of patient susceptibility to ARDS is incomplete and disease onset is poorly predicted by current risk models. Among patients with multiple established risk factors, the majority do not develop ARDS, while a minority develop severe, life-threatening disease[175-176]. The most commonly used ARDS risk model (Lung Injury Prediction Score, LIPS) has strong negative predictive value (97%) and is effective at identifying

patients at low risk for ARDS, but has a weak positive predictive value (18%),[168, 175] implying poor ability to predict disease onset. The clinical diagnosis of ARDS is established based on the radiological, physiological, and clinical criteria summarized in the Berlin definition (Table 4.1)[176]. However, these criteria show only a moderate correlation with real time and post-mortem tissue pathological findings[177-178] and temporally lag the acute, dynamic inflammatory processes responsible for ARDS. Thus the Berlin criteria cannot be used for early diagnosis and trajectory monitoring of ARDS. Therefore, there is a significant unmet clinical need for early, rapid detection and diagnosis, as well as clinical trajectory monitoring of ARDS.

Table 4.1. The Berlin Definition of Acute Respiratory Distress Syndrome (ARDS).

Acute Respiratory Distress Syndrome	
Timing	Within 1 week of a known clinical insult or new worsening respiratory symptoms
Chest imaging (Chest radiograph)	Bilateral opacities – not fully explained by effusion, lobar/lung collapse, or nodules
Origin of edema	Respiratory failure not fully explained by cardiac failure or fluid overload. Need objective assessment (e.g., Echocardiography) to exclude hydrostatic edema if no risk factor is present.
Oxygenation	
Mild	200 mmHg < PaO_2 / FiO_2 ≤ 300 mm Hg with PEEP or CPAP ≥ 5 cm H_2O
Moderate	100 mmHg < PaO_2 / FiO_2 ≤ 200 mm Hg with PEEP ≥ 5 cm H_2O
Severe	PaO_2 / FiO_2 ≤ 100 mm Hg with PEEP ≥ 5 cm H_2O
Abbreviation: CPAP, continuous positive airway pressure; FiO_2, fraction of inspired oxygen; PaO_2, partial pressure of arterial oxygen; PEEP, positive end-expiratory pressure.	

Exhaled breath condensate (non-volatile compounds) of ARDS patients have been studied actively for years to aid in understanding the natural history, pathophysiology, and prognosis of ARDS[179-180]. For example, a novel and non-invasive sampling method using a heat-moisture exchanger (HME) filter[181] was recently developed to accurately sample the distal airspace in patients with ARDS. The HME filter is an inline hygroscopic sponge placed between the patient and the ventilator; the moisture from the patient's exhaled breath condenses on this filter. The filter is changed every few hours, at which time condensed fluid can be collected from the used filter

and analyzed using liquid chromatography coupled tandem mass spectrometry (LC-MS). While potentially useful in ARDS diagnosis, this technology is focused on proteomic analysis of the breath condensates and requires long analysis times.

Hundreds of volatile organic compounds (VOCs) are also contained in exhaled breath. Many VOCs (such as pentane, isoprene, and ethane) are related to inflammatory processes occurring in the lungs and systemically in blood from remote organ injury[182-185]. These and other VOCs could potentially be used as biomarkers to predict the onset and severity of certain critical lung diseases such as ARDS as well as systemic inflammation such as sepsis. These VOCs also have potential in guiding therapy if simultaneous, precise, real-time measurement can be performed[186-189]. Unlike blood-based analysis, breath is unlimited in its sampling potential and can be noninvasively and continuously collected and analyzed. Technologies designed for the real-time analysis of VOCs in a point-of-care (POC) fashion could allow for the identification of breathomic signatures that enable the early diagnosis of ARDS, stratification, and trajectory monitoring, allowing for precision treatments.

Table 4.2 summarizes the major technologies used in breath analysis. A more comprehensive overview of the different technologies can also be found in Saalberg et al.[190] and Cao et al.[191]. Gas chromatography in tandem with mass spectrometer (GC-MS) is the gold standard for the analysis of complex vapor mixtures such as breath samples. In practice, breath from a subject is collected in a thermal desorption tube or sampling bag, and then transferred to GC-MS by thermal desorption device or by solid phase microextraction (SPME). Comprehensive 2-dimensional (2D) GC has improved the peak capacity over the traditional GC[192-193]. VOC analytes are subject to two independent separation processes, first by their vapor pressures in the 1st-dimensional column and then by their polarities in the 2nd-dimensional column. It has also been

used for detection of diseases such as cancer, tuberculosis and human volatome[194-196]. Due to the bulky size and the long turn-around times, GC-MS and comprehensive 2D GC are not suitable for POC applications and cannot be used to continuously monitor the subject to detect dynamic changes. SIFT-MS (selected-ion flow-tube mass spectrometry) and PTR-MS (Proton Transfer Reaction tube mass spectrometry) has high sensitivity and can be used for real time breath VOC monitoring[197-199]. However, the bulky size, heavy weight (>200 kg), and high cost limit its wide acceptance. Ion mobility spectrometry (IMS)[193, 200-201] can be operated under ambient pressure, thus avoid the use of a cumbersome vacuum pump. The portability and short analysis time (usually a few minutes) makes IMS suitable for POC application. Recently exploratory tests using FAIMS (Field Asymmetric Ion Mobility Spectrometry) technology in diagnosis of lung cancer, asthma, and inflammatory bowel disease have been reported[193, 201]. However, its limited VOC separation capability may affect the diagnostic accuracy. Electronic nose (e-Nose) relies on various vapor sensor arrays (such as colorimetric, gold nanoparticles, carbon nanotubes) and pattern recognition for breath analysis[188, 202-203]. Although portable, fast and easy to use, E-nose has poor chemical selectivity, device-to-device repeatability, and stability, as well as high susceptibility to background or interference VOCs[188-189]. Portable GC systems are also used in breath analysis [204]. However, current commercial portable GC systems are 1D devices and have limited separation capability (or peak capacity), which, again, may affect the diagnostic accuracy for given diseases. In addition, most of the 1D GC devices are not customized to operate in a fully automated mode, which hinders its clinical applications.

Table 4.2. A Summary of Breath Analysis Technologies.

Analysis Method	Instru-ment	Sampling Method	LOD	Time	Advantages	Limitations	Suit-able for POC
Benchtop GC[205-206]	GC-FID/TCD[a]; GC-MS; GCxGC-MS;	Sorbent trap SPME	ppt[f]	Long	Most widely used; High separation capability; Compound identification available;	Bulky size; Heavy weight; Dedicated personnel needed; Sample preparation needed;	No
Selected Ion Flow Tube[197-199]	SIFT-MS	Direct input	ppb[g] to ppt	Real time	Rapid analysis; High sensitivity; Allow breath-by-breath analyses; No sample preparation needed;	Bulky size; Heavy weight; High cost; Dedicated personnel needed;	No
Proton Transfer Reaction [207]	PTR-MS	Direct input	ppb to ppt	Real time	Rapid analysis; High sensitivity; Allow breath-by-breath analyses; No sample preparation needed;	Bulky size; Heavy weight; High cost; Dedicated personnel needed;	No
Ion Mobility Spectro-metry[193, 200-201]	FAIMS[b]	Direct input	ppm[h] to ppb	Short	Portable; Fast; No sample preparation needed;	Low separation capability; Background VOC interference;	Yes
Electro-nic Nose[188, 202-203]	AuNPs[c]; CNTs[d]; CPs[e]; Color-metric;	Direct input	ppm to ppb	Short	Easy to use; Highly portable; Low cost; No sample preparation needed;	Low separation capability; Sensors drift overtime; Background VOC interference;	Yes
Portable GC[208]	Portable GC; Proposed portable 2D GC;	Sorbent trap	sub-ppb	Moder ate	Portable; Fully automated; High separation capability and sensitivity; No sample preparation needed;	More complicated than 1D portable GC	Yes

[a] Flame ionization detector/Thermal conductivity detector
[b] Field Asymmetric Ion Mobility Spectrometry
[c] Gold nanoparticles
[d] Carbon nanotubes
[e] Conducting polymers
[f] parts-per-trillion, 10^{-12}
[g] parts-per-billion, 10^{-9}
[h] parts-per-million, 10^{-6}

We have developed a fully automated portable GC device with a sub-ppb sensitivity that can be operated simultaneously as a 1D GC and comprehensive 2D GC[209]. The 2-dimensional separation allows for further separation of co-eluted peaks that are not separated from the 1st-dimensional column. The aim of this study was to further adapt this portable GC for use on a mechanical ventilator in ICUs and develop related algorithms for rapid analysis of breath from patients undergoing mechanical ventilation. This would allow us to understand our method's (GC and algorithms) ability to detect the presence of ARDS and compare it to clinician adjudication.

Figure 4.1 is a schematic of the GC device connected to a ventilator. In our work, breath was collected and analyzed every 33 minutes via a small tube connected to the exhalation port of the ventilator. A total of 97 peaks were separated out from human breath. Through principal component analysis (PCA) and linear discriminant analysis (LDA), 9 out of 97 peaks were selected as a VOC subset for discrimination between ARDS and non-ARDS respiratory failure. 48 ARDS and non-ARDS patients with a total of 85 different breath chromatograms were evaluated. From the 48 patients, we used 28 patients (43 sets of breath) as the training set and 20 patients (42 sets of breath) as the testing set. Using blind physician adjudication of patient records based on the Berlin criteria as the gold standard, our breath analysis achieved an overall accuracy of 87.1% with 94.1% positive predictive value and 82.4% negative predictive value.

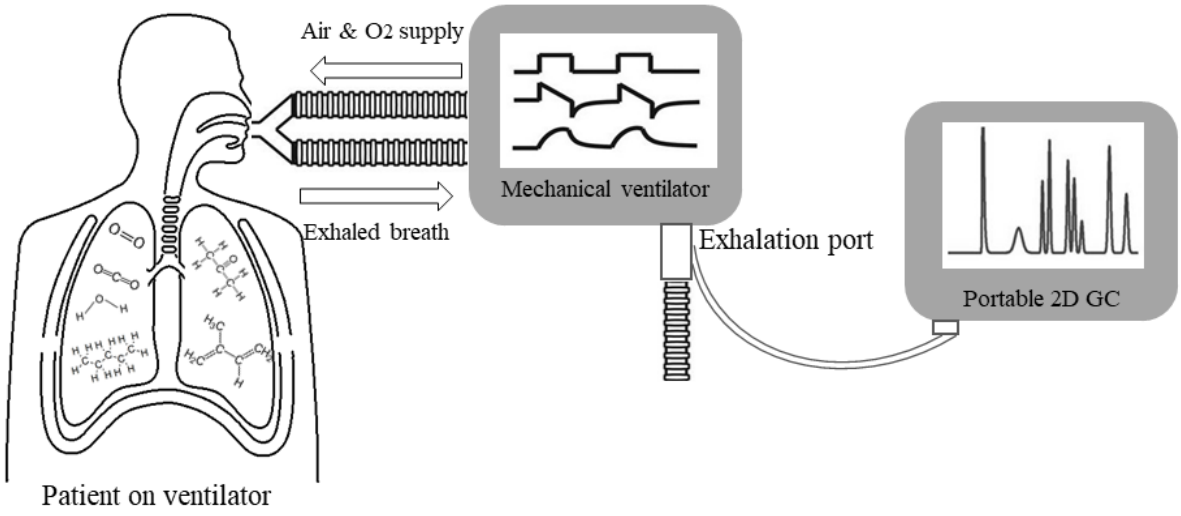

Figure 4.1. Schematic of a portable GC device for breath analysis from a patient on a mechanical ventilator.

4.2 Portable 2D µGC system for breath analysis

4.2.1 Device components and operation

Materials

DB-1ms Agilent J&W, nonpolar column (length 10 m, i.d. 250 µm, film thickness 0.25 µm) was purchased form Agilent Technologies (P/N: 122-0162, Agilent Technologies). SUPELCOWAX® 10 polar column (length 3 m, i.d. 250 µm, film thickness 0.25 µm) was purchased from Sigma Aldrich (P/N: 24077, Sigma-Aldrich). Copper tube (length 10 cm, i.d. 1 mm, o.d. 1.5 mm) was purchased from Swagelok and glass wool was purchased from Sigma Aldrich. Teflon tape was purchased from Grainger (Ann Arbor, MI). Shrink tube was purchased from Digi-Key Electronics. Other materials are the same as those described in Section 3.2.

Device components

Various microfabricated components were used in the portable 1 x 2 channel 2D GC device, including a thermal desorption tube, micro-fabricated thermal injector (μTI), micro-Deans switch (μDS), and micro-photoionization detector (μPID). All of these components were fabricated and characterized in-house. The details of the μTI, μDS, and μPID can be found in Section 3.2.The thermal desorption tube was made of a 5 cm long copper tube with an inner diameter of 1 mm. 10 mg each of Carbopack^{TM} X and B granules were loaded into the hollow, cylindrical copper tube using a diaphragm pump. Glass wool was used to separate the Carbopack^{TM} X and B as well as to seal the copper tube from both ends. Swagelok fittings were used to connect a stainless steel tube of i.d. 250 μm at both the ends of the copper tube. Nickel wire was wrapped around the entire length of the copper tube for column heating. The nickel wire was insulated from the copper tube using Kapton tape. A type K thermocouple was attached to the copper tube using Kapton tape to monitor the temperature in real time. Finally, the thermal desorption tube was preconditioned at 300 °C for 12 h under helium flow.

The portable 1 x 2 channel 2D GC device is similar to the 1 x 4 channel 2D GC device described in Section 3.2. As illustrated in Figure 4.2, the 2D GC consisted of a sampling module, a 1st-dimensional separation module, and a 2nd-dimensional separation module. The sampling module consisted of a sampling tube, a thermal desorption tube loaded with Carbopack^{TM} X and B, valves, and a pump. The 1st-dimensional module consisted of a μTI loaded with Carbopack^{TM} X and B, a 10 m long Agilent J&W DB-1ms, and a μPID. The 2nd-dimensional module had two identical channels consisting of a μTI, a 3 m long SUPELCOWAX® 10 column, and a μPID. The eluent from the ^{1}D column was transferred to one of the ^{2}D columns via a μDS. All the modules and components were connected via tubings, universal connectors, and Y-connectors. The entire

device was housed in a customized plastic case (see Figure 4.3) and had a total weight less than 5 kg, including the weight of the He gas cartridge (231 g). LabVIEW™ based software was developed in-house for the user interface, device control, and automation.

The portable GC can be operated as a 1D GC alone (in which case the 2nd-dimensional module was disabled or detached) or comprehensive 2D GC. Operation as 1D GC is straightforward (the same as a regular GC). Operation as comprehensive 2D GC is described below.

Device operation

Figure 4.2 shows the layout of the portable 1x2-channel 2D GC and its flow direction. The 2D GC device consisted of three detachable modules: sampling module, 1st-dimensional separation module, and 2nd-dimensional separation module. The 1st-dimensional module further consisted of a home-made micro-thermal injector (μTI), a 10 m long on-polar DB-1ms column (250 μm x 0.25 μm, Agilent J&W Scientific), and a home-made micro-photoionization detector (μPID)[210]. The 2nd-dimensional module consisted of two identical channels, each of which had a 3 m long polar SUPELCOWAX® 10 column (250 μm x 0.25 μm, Sigma Aldrich). Note that while polar columns have been used in the 2nd-dimensional column in 2D GC analysis of breath[194-195], mid-polar columns can also be used[196]. The 1x2-channel 2D GC can be operated as a 1D GC alone when the 2nd-dimensional module is either disabled or detached or as comprehensive 2D GC. To increase the separation capability, in this work we chose to operate our portable GC in a comprehensive 2D GC mode, which required additional but negligible 20 seconds compared to 1D GC operation alone. In the comprehensive 2D GC mode, eluted analytes from the ^{1}D column were sliced by the micro-Deans switch, loaded onto the one of the μTIs (μTI 2A or μTI 2B in Figure 4.2), then injected into the corresponding ^{2}D column (^{2}D column 2A or ^{2}D column 2B in Figure 4.2). The

modulation time was 10 seconds, yielding a maximal separation time on each ^{2}D column of 20 seconds[209]. The ^{1}D column was temperature programmed from 25 ºC held for 2 min to 80 ºC with a ramping rate of 10 ºC/min. The temperature was then raised to 120 ºC with a ramping rate of 20 ºC/min and finally kept at 120 ºC for 4 min. Both ^{2}D columns were kept at 75 ºC. In our 1x2-channel 2D GC, we used 3 flow-through µPIDs, one at the end of the ^{1}D column (µPID 1 in Figure 4.2) and two at the end of the ^{2}D columns (µPID 2A and µPID 2B in Figure 4.2). The use of a detector at the end of ^{1}D column allows us to monitor the elution of the analytes from the ^{1}D column to produce the 1D chromatogram (if the GC device is operated as 1D GC alone) or to avoid potential under-sampling that may be caused by the 10 s modulation time (if the GC device is operated as comprehensive 2D GC).

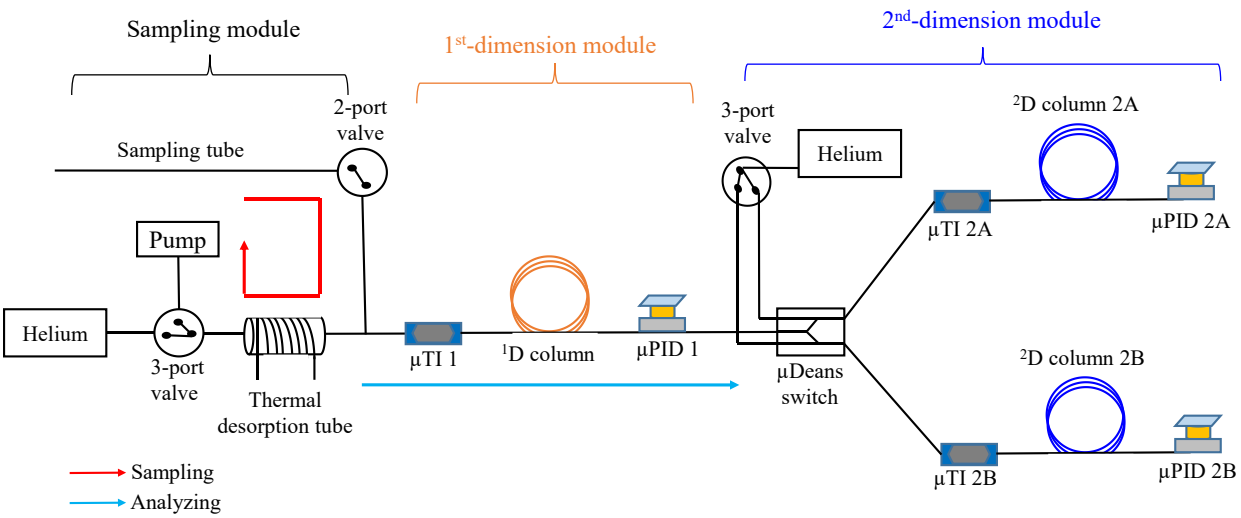

Figure 4.2. Layout of the portable 1x2-channel 2D GC device. It consisted of three detachable modules: sampling module, 1st-dimensional separation module, and 2nd-dimensional separation module.

Operation of the portable GC in comprehensive 2D GC mode and relevant parameters are described as follows.

(1) Sampling: The exhaled breath of the patient was drawn by the diaphragm pump through the 2-port valve at a flow rate of 70 mL/min for 5 min and adsorbed by the thermal desorption tube.

(2) Desorption and injection: The 2-port valve was closed and helium gas was flowed through the 3-port valve at a flow rate of 2 mL/min, simultaneously the thermal desorption tube was heated to 300 °C for 5 min to transfer the analytes onto the μTI 1. After 5 min, μTI 1 was heated to 270 °C in 0.6 s, then kept at 250 °C for 30 s for complete thermal desorption and injection of the analytes into the ^{1}D column.

(3) Separation: The analytes underwent separation through the 10 m long ^{1}D column and were detected by μPID 1. During separation, the column was kept at 25 °C for 2 min, then ramped at a rate of 10 °C min^{-1} to 80 °C, followed by ramping at a rate of 20 °C min^{-1} to 120 °C, and finally holding at 120 °C for 4 min. The flow rate was 2 mL/min for the ^{1}D column.

We used a modulation period of 10 s to inject the eluent from the ^{1}D column into the ^{2}D columns. The first 10 s long slice of the eluent from the ^{1}D column was routed to and trapped by μTI 2A. μTI 2A was then heated to 270 °C in 0.6 s, then kept at 250 °C for 5 s to inject the trapped analytes to Column 2A. Concurrently, the second 10 s long slice of the eluent from the ^{1}D column was routed to and trapped by μTI 2B, which was subsequently injected into Column 2B. The same process was repeated between Columns 2A and 2B alternatively throughout the analysis. Analytes underwent ^{2}D separation through one of ^{2}D columns (held isothermally at 75 °C) and were detected by μPID 2. The helium flow was 3 mL/min for each of ^{2}D columns.

(4) Cleaning: After analysis, the outlet of μTI 1 was disconnected from the inlet of the ^{1}D column so that it was open to the ambient air. The thermal desorption tube was then heated to 300 ºC for 5 min followed by heating μTI 1 to 270 °C in 0.6 s and holding at 250 °C for 30 s at a

helium flow rate of 25 mL/min. This process was repeated twice in order to completely remove residual analytes (if any) trapped in the thermal desorption tube and μTI 1. Cleaning of μTI 2A and 2B was not needed. The total assay time was 33 minutes, which included 5 minutes of sample collection, 5 minutes of desorption/transfer, 13 minutes of separation, and 10 minutes of cleaning.

Multiple μPIDs were used to measure the analytes eluted from the ^{1}D column and ^{2}D columns. The responsivities of these μPIDs may be different due to variations in aging and amplification. During the experiment, μPID 2A and 2B were calibrated against μPID 1 using toluene (50 ppb), as discussed in detail in Section 3.3. This calibration was carried out approximately every 300 hours of operation.

Operation of the portable GC as a 1D GC is similar to the steps in (1)-(4) above, except that the inlet of the μDS is detached from the outlet of μPID 1. Alternatively, the 2nd-dimensional module may be powered off.

4.2.2 Patient tests

Patient enrollment criteria and ARDS adjudication

This study was approved by the University of Michigan Institutional Review Board (IRB) to consenting adult patients 18 years or older undergoing mechanical ventilation for both hypoxic and non-hypoxic respiratory failure or requiring mechanical ventilation for other life-support issues in various intensive care unit settings. Etiologies for the need for intubation and mechanical ventilation included ARDS, pneumonia, sepsis, pulmonary embolism, traumatic brain injury, cardiac arrest, severe chronic obstructive pulmonary disease exacerbations, or combinations of these conditions.

The final diagnosis of ARDS was adjudicated retrospectively by a multi-physician panel blinded to portable GC data. The adjudication was based on the Berlin Criteria[176], which relies on

a combination of medical history, chest radiography findings, and oxygenation parameters[176]. Details regarding this ARDS adjudication process have been previously reported[211].

An adjudication was performed on each day each patient was studied using the portable GC. If a patient was studied at more than one-time point, a separate adjudication was made on those days. The adjudication of ARDS was binary (present/not present) and no attempt was made to score ARDS (if present) as mild, moderate, or severe. If patient subjects were successfully liberated from mechanical ventilations, no additional GC testing was performed.

In order to identify and populate the algorithm with breath signatures from individuals with no acute illness or injury requiring mechanical ventilation, we also recruited five laboratory members with no history of pulmonary conditions or acute illnesses as volunteer controls (denoted as Patients #1, 2, 3, 4, and 38 in Figure 4.9, Figure 4.13 and Figure 4.16). Their breath samples were collected in Tedlar bags through a moisture filter and immediately withdrawn into the GC device for analysis. Patients #1, 2, 3, and 4 were used in the training set, while Patient #38 was used in the testing set.

A total of 21 ARDS patients and 27 non-ARDS control patients were recruited for 85 sets of breath chromatograms.

IRB Statement: This clinical research study (HUM00103401) was approved by the University of Michigan Medical School's Institutional Review Board (a component of the University of Michigan's Human Research Protection Program). Consent was required from patient subjects or their legally authorized representative prior to enrollment.

Breath sampling via mechanical ventilator

As shown in Figure 4.3, patient breath was collected via 2 m long polytetrafluoroethylene (PTFE) tubing (0.64 cm i.d.) connected to the exhalation port of the ventilator. In order to maintain

not to break the already-established respiratory circuits of the patients, we used direct sampling (sampling from the ventilator exhalation port) rather than end-tidal air collection (in which a CO_2 sensor is needed close to the tracheal tube to monitor the real time CO_2 concentration). As a result, the collected breath sample contains some dead space volume. The sampling rate was 70 mL/min and the sampling time was 5 minutes.

During measurement, the device was secured on a rolling cart (see Figure 4.3) and placed outside the ventilated patient's room. 2 m long PTFE tubing (0.64 cm i.d.) was used to connect the output of the ventilator to the GC device, through the 7.6 mm port of a 22M-22F straight connector (Figure 4.3). The straight connector was discarded after a single use and the PTFE tube was cleaned (rinsed with 70% 2-propanol, then flushed with deionized water, and finally dried with pressured air to eliminate pathogenic microorganisms and remove residual VOCs) after each sampling to avoid patient-to-patient transmission as well as cross contamination between patient breath samples.

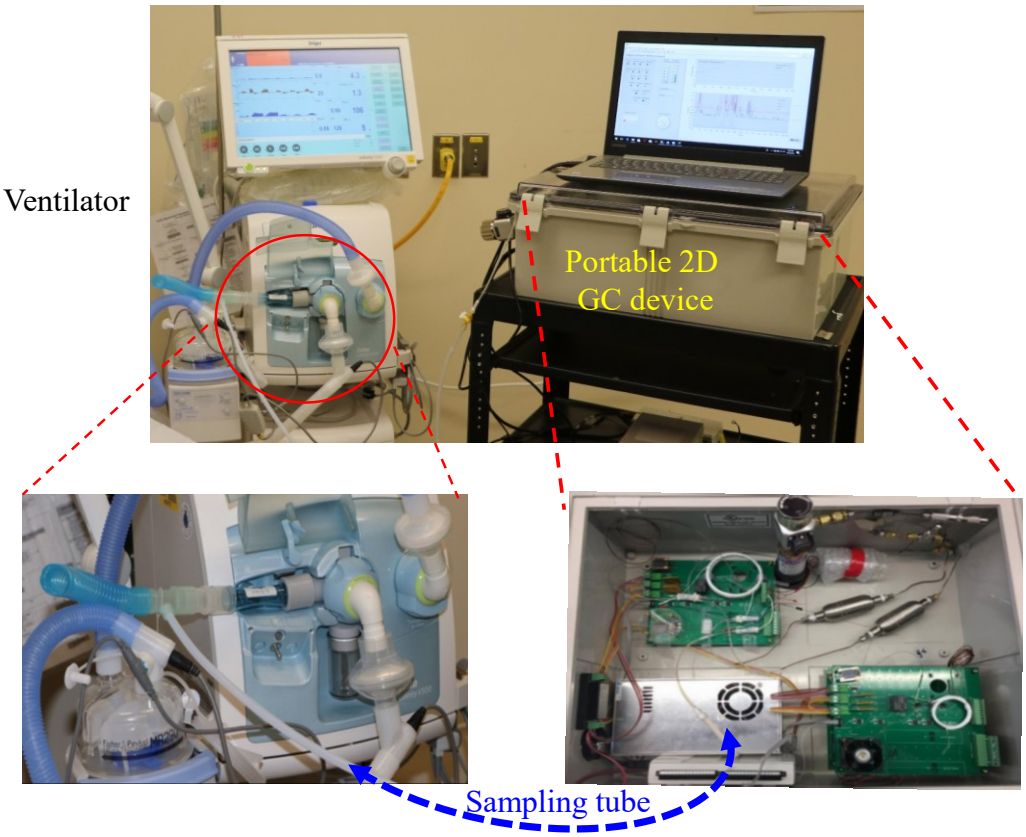

Figure 4.3 The portable MDGC device and connection to mechanical ventilator. The portable GC was connected to the output of a ventilator via 2 m long PTFE tubing (0.64 cm i.d.). The portable GC weighed less than 5 kg. Patient breath was drawn into and captured by the thermal desorption tube in the GC device at a flow rate of 70 mL/min for 5 minutes. The total assay time was 33 minutes, which included 5 minutes of sample collection time, 5 minutes of desorption/transfer time, 13 minutes of separation time, and 10 minutes of cleaning time.

4.2.3 Chromatogram analysis

2D chromatogram pre-processing and reconstruction

Following analysis completion, two-dimensional gas chromatograms were generated from all three channels' (1D, 2A, 2B) PID signals. The signals from each channel were first preprocessed for baseline correction and peak detection. After preprocessing, all ^{2}D peaks were traced back to corresponding ^{1}D peaks based on the ^{1}D period they were sampled from so that both ^{1}D and ^{2}D retention times and peak shapes could be found. Third, the ^{1}D chromatogram was aligned to the reference chromatogram to fix the ^{1}D retention time drift. Finally, the two-

dimensional gas chromatogram for each peak was generated by multiplying its ^{1}D peak shape by its ^{2}D peak shape. Combining all individual peak's two-dimensional gas chromatogram yielded the completed two-dimensional gas chromatogram. All algorithms were implemented in the Matlab™ programming environment with a user-friendly graphical interface. The detailed algorithms are described as below:

(1) Baseline correction: Gas chromatogram baselines drift slowly due to column bleeding at high temperatures, flow fluctuation, and detector performance. This baseline drift can negatively affect quantitative analytical results and should be corrected before performing further data analysis[212]. We use adaptive iterative reweighted Penalized Least Squares (airPLS) algorithms, developed by Zhang et al.[213], which iteratively change weights of sum squared errors (SSE) between the original signals and fitted baseline until the termination criteria is met. This method requires no user intervention and has previously been applied to chromatograms, NMR, and Raman spectra.

(2) Peak detection: After baseline correction, peak detection is applied to both ^{1}D and ^{2}D chromatograms. Peak apexes are found via a method developed by Morris et al.[214]. The signal is first denoised via wavelet regression using the undecimated discrete wavelet transform (UDWT), then scanned for all local maxima and associated peak endpoints. Peaks that do not meet the peak height and FWHM criteria are eliminated [214-218]. Once the peak apexes are found (including single and co-eluted peaks), peak shapes are fitted by the exponentially modified Gaussian (EMG) model. This peak fitting method has been described previously[1].

(3) Peak assignment: Within each modulation, the ^{1}D peak will be injected into either a 2A or 2B subsystem. Each ^{2}D peak is assigned to one or multiple ^{1}D peak IDs, depending on the total number of peaks within each modulation. For each individual peak, multiplying its ^{1}D peak

shape by its normalized ^{2}D peak shape yields a two-dimensional chromatogram for this individual peak.

(4) Peak alignment: Gas chromatograms may contain distortions of retention times due to column aging, changes in temperature, or other unknown deviations in instrumental conditions. Fluctuations in retention times across various measurements obscure statistical analysis and discovery of relevant patterns in the data[219]. Since retention time shifts are observed in our ^{1}D chromatogram, we applied the correlation optimized wrapping (COW) algorithm[220] for peak alignment. This method is a piecewise or segmented data preprocessing method (operating on one sample record at a time) aimed at aligning a sample data vector towards a reference vector by allowing limited changes in segment lengths on the sample vector. The output of this method contains the correlation between the reference chromatogram retention time and the new chromatogram retention time. With this correlation, a shift time can be found for each peak based on its original retention time and the single peak two-dimensional gas chromatogram can be shifted on the ^{1}D based on this shift time.

(5) Summation of individual two-dimensional chromatograms: Adding all individual peaks' two-dimensional chromatograms together after applying the shift time yields the complete two-dimensional chromatogram.

With these steps, a 2D chromatogram can be generated for each patient's breath, which can be converted to a table of peak areas at different retention times. The ^{1}D and ^{2}D retention times are defined by the peak identity, while the peak area is defined by the breath VOCs' abundance.

Relevant peak selection

While more than 1200 VOCs are currently known to exist within human exhaled breath (typical patient breath contains 150-200 VOCs), not all of these breath VOCs are relevant to

ARDS. For example, some of the peaks may be from the indoor air background, normal metabolic activities, or other patient conditions. These irrelevant peaks interfere in the correct classification of ARDS and non-ARDS groups. We therefore developed a machine learning based algorithm to select relevant peaks from all breath VOCs and use these relevant peaks for ARDS diagnosis.

To distinguish ARDS and non-ARDS patients based on their breath chromatograms, linear discriminant analysis (LDA) was applied to find a linear function that could be used to separate these two groups. LDA can only be applied if the number of samples (patient chromatograms) is much larger than the number of features[221] (i.e., the number of VOCs, which was 97 in our study). To overcome this limitation and to decrease the computational complexity of the pattern classifier, principal component analysis (PCA) was applied prior to LDA to reduce the dimensionality of the feature space. Since PCA is an unsupervised dimensionality reduction method, it only performs a linear mapping of the data to a lower-dimensional space in such a way that the variance of the data point is maximized. Direct application of PCA to the overall VOC dataset, the VOCs relevant to ARDS may get overlooked and the interference VOCs that have bigger variance among patients. Therefore, to produce the best classification result with PCA-LDA, it is critical to find the features (VOCs) that are relevant to ARDS and discard all other interference features. The detailed algorithm is described as follows:

Step 1. Generation of possible peak subsets

We first assume that there are a total of m different peaks found in all patients' 2D chromatograms with different quantities. For a particular patient, not all m peaks are present. The quantities of those missing peaks are assigned to 0. All m peaks and their quantities form the entire dataset and can be expressed as:

$$\begin{pmatrix} x_{11} & \cdots & x_{1m} \\ \vdots & \ddots & \vdots \\ x_{p1} & \cdots & x_{pm} \end{pmatrix}, \tag{4.1}$$

where x_{ij} is the quantity of the j^{th} peak of the i^{th} patient. In total, there are m peaks and p patients. We further assume that there are N peaks relevant to ARDS and non-ARDS classification. Consequently, there are C_m^N possible peak combinations (subsets) that can be selected from the dataset in Equation (4.1). One such subset can be written as:

$$\begin{pmatrix} x_{1k_1} & \cdots & x_{1k_N} \\ \vdots & \ddots & \vdots \\ x_{pk_1} & \cdots & x_{pk_N} \end{pmatrix}, \tag{4.2}$$

where $(k_1, k_2, \ldots, k_N)$ is the subset formed by N peaks.

Step 2. Criteria of peak subset selection

PCA was first used for data reduction of the N peak VOC subsets. LDA was then applied to the primary two principal component scores for classification. The total accuracy (true positive plus true negative rate) of classification was used as the criteria for peak subset relevancy to ARDS. For each possible peak subset, PCA was first applied to the p-by-N dataset to produce p-by-N principal component scores. Then, the primary two principal component scores (p-by-2) and the classifier (1 as ARDS and 0 as non-ARDS) for each patient were used to train an LDA model and yield a linear boundary between the ARDS and non-ARDS groups. The total accuracy (number of patients falling in the correct side of the boundary divided by the total patients) was calculated and used as the criteria of the relevancy of this VOC subset. Equations (4.3) and (4.4) illustrate the methods and processes described above.

$$\begin{pmatrix} x_{1k_1} & \cdots & x_{1k_N} \\ \vdots & \ddots & \vdots \\ x_{pk_1} & \cdots & x_{pk_N} \end{pmatrix} \xrightarrow{PCA} \begin{pmatrix} s_{11} & \cdots & s_{1N} \\ \vdots & \ddots & \vdots \\ s_{p1} & \cdots & s_{pN} \end{pmatrix}, \tag{4.3}$$

where s_{ij} is the j^{th} principal component score of the i^{th} patient.

$$\begin{pmatrix} s_{11} & s_{12} \\ \vdots & \vdots \\ s_{p1} & s_{p2} \end{pmatrix} with \begin{pmatrix} c_1 \\ \vdots \\ c_p \end{pmatrix} \xRightarrow{LDA} linear\ boundary \xrightarrow{yields} Classification\ accuracy, \tag{4.4}$$

where c_i is the classifier (1 for ARDS and 0 for non-ARDS) of the i^{th} patient. Finally, the peak combinations (i.e., subsets) with the highest accuracy were selected. For each of these selected peak combinations (subsets), the patients' coordinates on the PCA plot were determined by their principal component scores. The mean distance of the closest patients (closest 20%) to the boundary line, normalized by the mean distance, was calculated. The peak subset with highest boundary distance was chosen as the optimal peak subset.

Step 3. Iterative peak subset selection

Since human breath is a complex mixture, the total peak number *m* is large and the total number of possible combinations of peaks (i.e., peak subsets), $\sum_{N=1}^{m} C_m^N$, is enormous. As a result, it requires a great amount of computation time to evaluate all the peak subsets. To expedite the selection process, we started with peak subsets formed by a small number of peaks (e.g., *n* peaks, which resulted in C_m^n subsets to be evaluated). Once the most relevant peak subset was determined, more peaks were added to this selected subset, aiming to achieve higher accuracy.

Assuming that there are *n'* more peaks that are relevant to ARDS (*n'* is another small number of VOCs in order to save computation time), $C_{m-n}^{n'}$ possible peak combinations (subsets) can be found and added to the previously optimized VOC subset to form a new peak subset, i.e.,

$$\begin{pmatrix} x_{1k_1} & \cdots & x_{1k_n} & x_{1l_1} & \cdots & x_{1l_{n'}} \\ \vdots & \ddots & \vdots & \vdots & \ddots & \vdots \\ x_{pk_1} & \cdots & x_{pk_n} & x_{pl_1} & \cdots & x_{pl_{n'}} \end{pmatrix}, \tag{4.5}$$

where $(l_1, l_2, \ldots, l_{n'})$ is the peak subset with n' peaks.

With this new peak subset, PCA and LDA were applied to calculate the accuracy and the boundary distance. If the classification accuracy increased or the boundary distance increased, the

n' peaks were kept and more peaks out of *m-n-n'* peaks would be added iteratively in the same manner described above. If accuracy no longer increased or the boundary distance no longer increased, then the iteration process was ended, and the final optimal peak subset was determined. A flow chart of the subset selection process is provided in Figure 4.4.

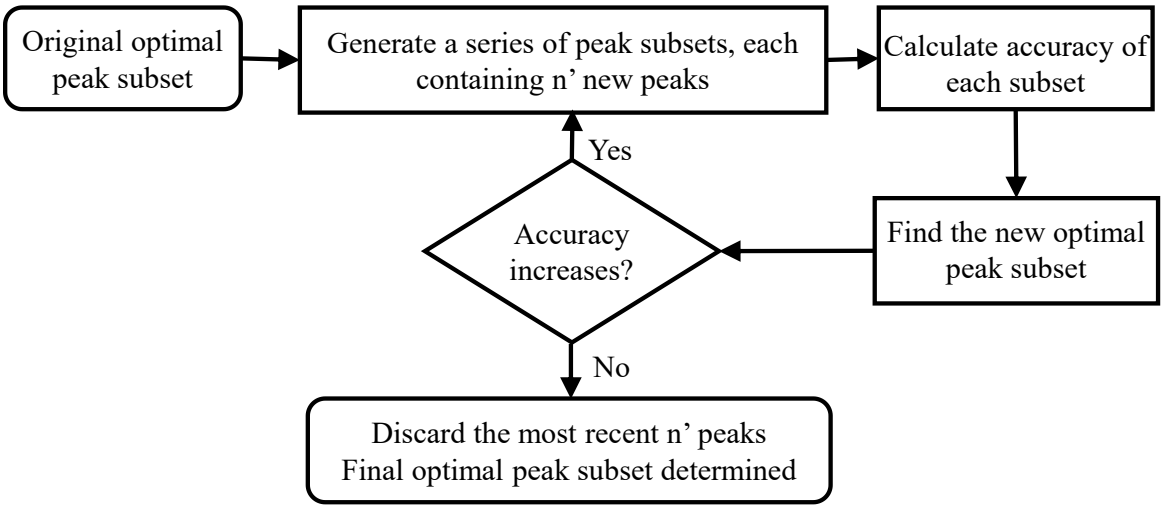

Figure 4.4. Iterative peak subset selection procedure.

Step 4. Training and testing with ARDS and non-ARDS patients

The entire patient data set was divided into two sets: training set (*p* patients) and testing set (*q* patients). The training set was used to select the optimal peak subset for best classification and to determine the linear boundary, whereas the testing set was used to validate the selected subset and the boundary on the PCA plot.

Assuming the final optimal peak subset contains *N* peaks, PCA analysis yields an *N*-by-*N* PCA coefficient and a linear boundary line between ARDS and non-ARDS groups.

$$\begin{pmatrix} x_{t_1 k_1} & \cdots & x_{t_1 k_N} \\ \vdots & \ddots & \vdots \\ x_{t_p k_1} & \cdots & x_{t_p k_N} \end{pmatrix} \xrightarrow{PCA} \begin{pmatrix} Coeff_{11} & \cdots & Coeff_{1N} \\ \vdots & \ddots & \vdots \\ Coeff_{N1} & \cdots & Coeff_{NN} \end{pmatrix} \tag{4.6}$$

and $\begin{pmatrix} s_{t_1 1} & \cdots & s_{t_1 N} \\ \vdots & \ddots & \vdots \\ s_{t_p 1} & \cdots & s_{t_p N} \end{pmatrix}$

where $(t_1, t_2, \ldots t_p)$ is the p training set patients.

$$\begin{pmatrix} s_{t_1 1} & s_{t_1 2} \\ \vdots & \vdots \\ s_{t_p 1} & s_{t_p 2} \end{pmatrix} with \begin{pmatrix} c_{t_1} \\ \vdots \\ c_{t_p} \end{pmatrix} \xrightarrow{LDA} linear\ boundary \tag{4.7}$$

With the N-by-N PCA coefficients acquired from the training set, the PC scores of the testing set can be calculated by multiplying the PCA coefficients by the N peak subset for all testing patients. With the linear boundary line acquired from the training set, the final classification accuracy can be calculated.

$$\begin{pmatrix} x_{v_1 k_1} & \cdots & x_{v_1 k_N} \\ \vdots & \ddots & \vdots \\ x_{v_q k_1} & \cdots & x_{v_q k_N} \end{pmatrix} \begin{pmatrix} Coeff_{11} & \cdots & Coeff_{1N} \\ \vdots & \ddots & \vdots \\ Coeff_{N1} & \cdots & Coeff_{NN} \end{pmatrix} \xrightarrow{yields} \begin{pmatrix} s_{v_1 1} & \cdots & s_{v_1 N} \\ \vdots & \ddots & \vdots \\ s_{v_q 1} & \cdots & s_{v_q N} \end{pmatrix}, \tag{4.8}$$

where $(v_1, v_2, \ldots, v_q)$ is the q testing set patients;

$$\begin{pmatrix} s_{v_1 1} & s_{v_1 2} \\ \vdots & \vdots \\ s_{v_q 1} & s_{v_q 2} \end{pmatrix} \text{with } linear\ boundary \xrightarrow{yields} final\ classification\ accuracy \tag{4.9}$$

4.3 Breath chromatograms

4.3.1 System peak capacity

Table 4.3 lists the peak capacities estimated from three example peaks. For GC × GC, the peak capacity is defined as $n_{GC\times GC} = n_1 \times n_2$, where n_1 and n_2 are the peak capacities for ^{1}D and ^{2}D, respectively[209]. The conventional method for calculation of peak capacity using 4σ - bottom-to-bottom-width $w_{4\sigma}$ is given by: $n_{4\sigma} = (t_R^1/w_{4\sigma}^1)(CP_M/w_{4\sigma}^2)$, where C is the number of channels in ^{2}D and P_M is the modulation period. The peak capacities for three selected peaks are listed in the table below as $n_{4\sigma}$.

Table 4.3. Peak capacities for the portable 2D GC calculated for three example peaks.

Peak #	t_R^1	$w_{4\sigma}^1$	t_R^2	$w_{4\sigma}^2$	$n_{4\sigma}$
16	154.0 s	4.8 s	5.0 s	1.5 s	428
35	315.7 s	6.6 s	6.0 s	2.5 s	383
58	544.3 s	7.0 s	10.4 s	6.8 s	229

t_R^1: 1D retention time
t_R^2: 2D -dimensional retention time
$w_{4\sigma}^1$: 1D peak width (4σ - bottom-to-bottom)
$w_{4\sigma}^2$: 2D peak width (4σ - bottom-to-bottom)
C: Number of 2D channels (in our case: C = 2)
P_M: modulation time (in our case: P_M = 10 s)

4.3.2 Chromatograms for ARDS and non-ARDS patients

Figure 4.5 shows the representative 1D and 2D chromatograms for an ARDS and a non-ARDS control. Figure 4.5 shows that 2D GC provides additional separation capabilities compared to the 1D GC (3-10 times higher in terms of peak capacity). In the zoomed-in 2D chromatogram for the control patient, four co-eluted ^{1}D peaks are separated into eight peaks in the 2D chromatogram. Other zoomed-in portions of (b) and (d) can be found in Figure 4.5(i) and (j).

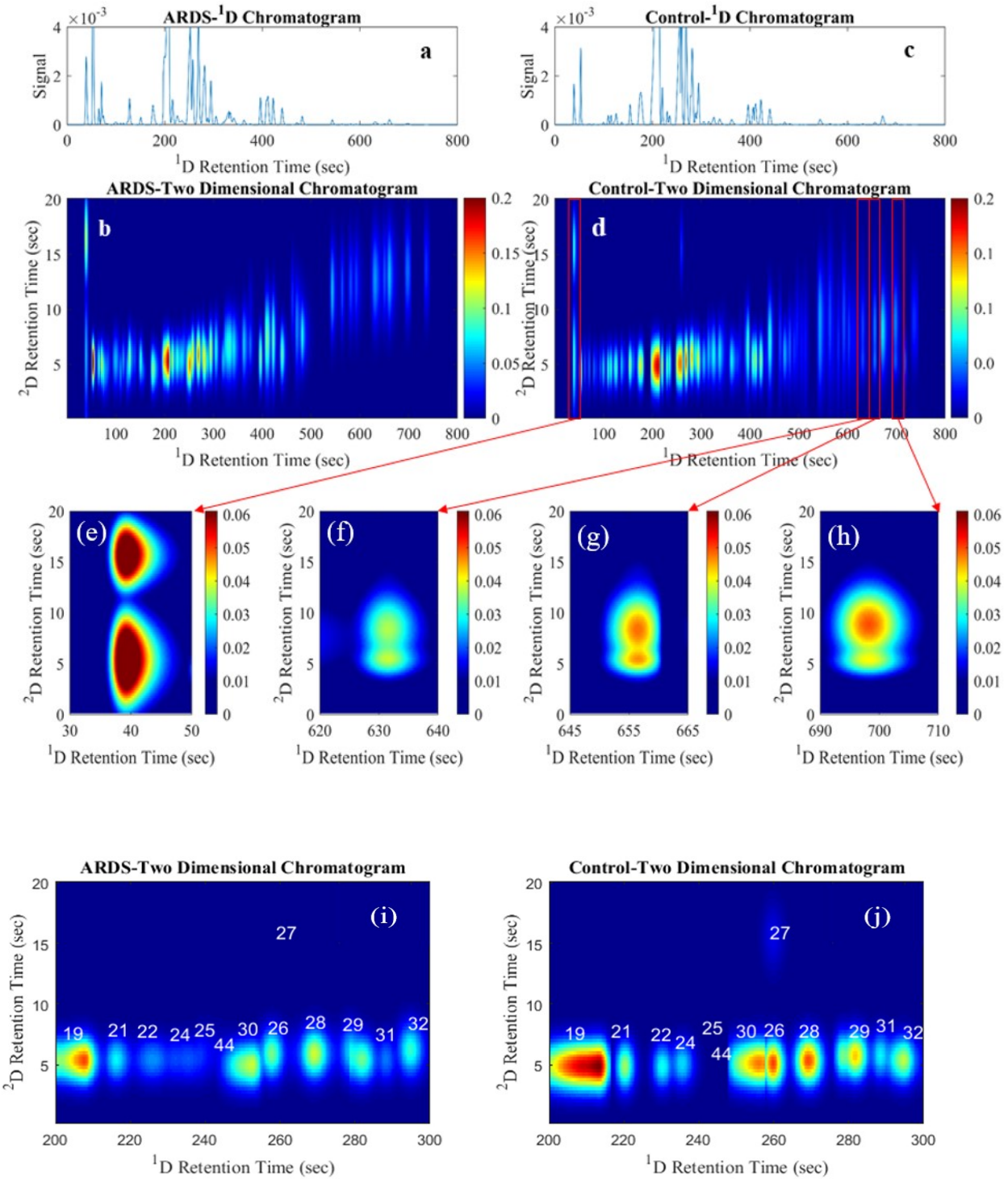

Figure 4.5. (a)(b) Representative 1D chromatogram and 2D chromatogram for an ARDS patient, respectively. (c)(d) Representative 1D chromatogram and 2D chromatogram for a non-ARDS (control) patient, respectively. (e) - (h) shows 4 co-eluted ^{1}D peaks are separated into 8 peaks in the 2D chromatogram. (i) Zoomed-in portion of (b). (j) Zoomed-in portion of (d).

Figure 4.6 shows that a total 97 peaks were found collectively in the 85 2D chromatograms from the patients under study, among which nearly 70% of the peaks are co-eluted or partially coeluted in the ^{1}D column. Note that not all 97 peaks appear in a 2D chromatogram for a particular patient, as some peaks are either not present in that patient's breath or below the detection limit of our μPIDs. Although our portable 2D GC does not generate as many peaks as the high-end bench-top 2D GC in tandem with MS[196], it is still sufficient for distinguishing between ARDS and non-ARDS as shown later. In total, among all recruited and adjudicated patients, we were able to monitor 9 ARDS patients and 9 non-ARDS patients for multiple days.

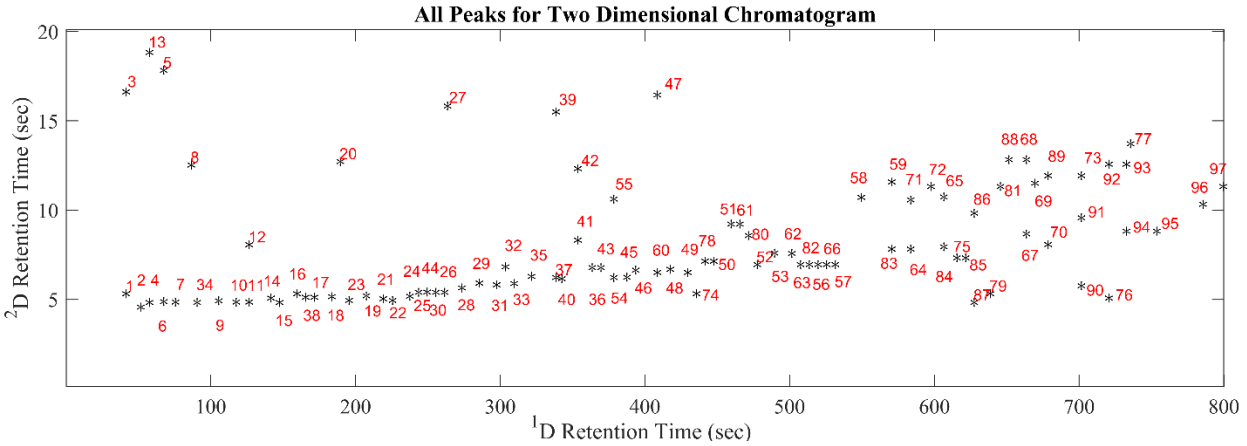

Figure 4.6. All 97 peaks found collectively in 85 breath samples from 48 patients plotted in a 2D chromatogram, among which 18 pairs (36 peaks) are co-eluted and approximately another 30 peaks are partially co-eluted (with doublets or triplets and separation of adjacent peaks is less than 2σ) from the ^{1}D column. Each dot represents the center of a peak in the contour plot (see, for example, Figure 4.5, for a peak contour plot). Note that not all 97 peaks appear in a 2D chromatogram for a particular patient.

Figure 4.7 shows, as an example, 2D chromatograms for an ARDS patient tested over 3 days, from which we can see clearly that breath VOC peaks change quantitatively (e.g., Peak #2 and #44). ARDS trajectory tracking is given in Figure 4.15.

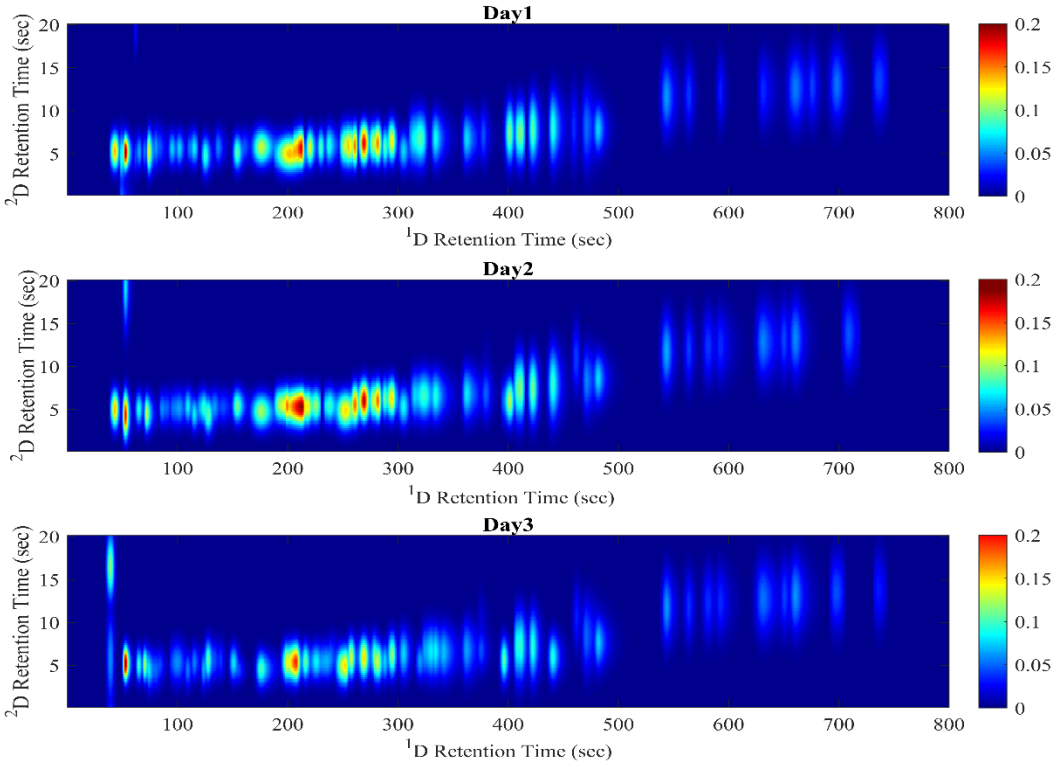

Figure 4.7. Evolution of the 2D chromatogram of an ARDS patient (Patient #11) over 3 days of monitoring.

4.3.3 Identified breath compounds: Mass Spectrometry analysis

To identify the VOC compounds contained in our breath samples, we coupled our GC (operated in 1D mode) with a Thermo Scientific Single Quadrupole Mass Spectrometer (ISQ^{TM} Series, from the Analytical Chemistry Lab at the University of Michigan Biological Station in Pellston, Michigan) and analyzed several breath samples. The mass spectrometer (MS) data was analyzed with Chromeleon^{TM} 7 Software, and the details of the identified compounds are shown in Figure 4.8, Table 4.4, and Table 4.5. Noted that only the 1st hits of the identified chemicals are presented.

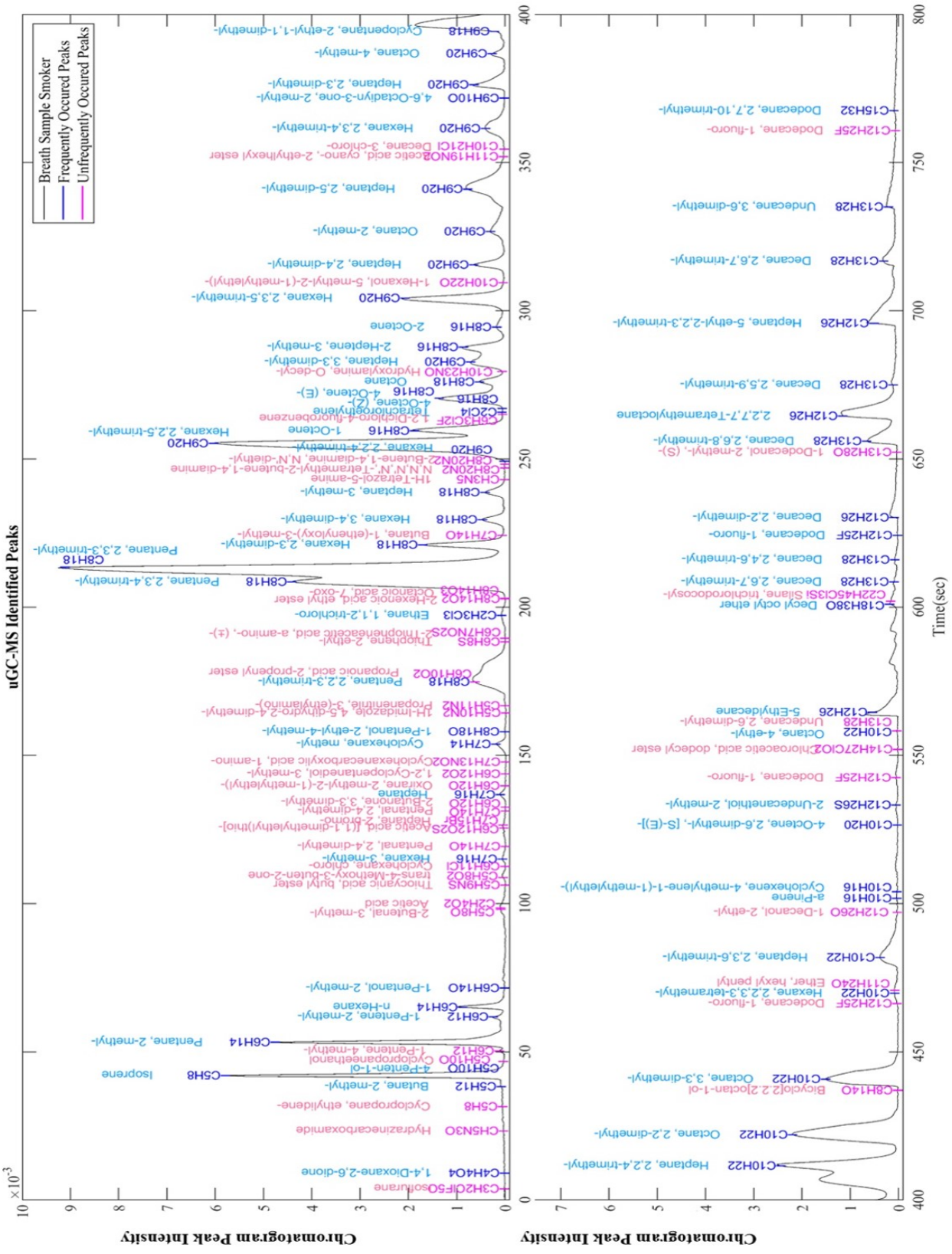

Figure 4.8 MS identified peaks within human breath.

Table 4.4 MS identified common peaks within human breath.

T_R (sec)	Library Compound	CAS #	MW	Formula	Structure
9	1,4-Dioxane-2,6-dione	4480-83-5	116	C4H4O4	O=C1COCC(=O)O1
38	Butane, 2-methyl-	78-78-4	72	C5H12	CCC(C)C
42	Isoprene	78-79-5	68	C5H8	CC(=C)C=C
47	4-Penten-1-ol	821-09-0	86	C5H10O	OCCCC=C
53	Pentane, 2-methyl-	107-83-5	86	C6H14	CCCC(C)C
62	1-Pentene, 2-methyl-	763-29-1	84	C6H12	CCCC(C)=C
65	n-Hexane	110-54-3	86	C6H14	CCCCCC
72	1-Pentanol, 2-methyl-	105-30-6	102	C6H14O	CCCC(C)CO
115	Hexane, 3-methyl-	589-34-4	100	C7H16	CCCC(C)CC
137	Heptane	142-82-5	100	C7H16	CCCCCCC
154	Cyclohexane, methyl-	108-87-2	98	C7H14	CC1CCCCC1
158	1-Pentanol, 2-ethyl-4-methyl-	106-67-2	130	C8H18O	CCC(CO)CC(C)C
175	Pentane, 2,2,3-trimethyl-	564-02-3	114	C8H18	CCC(C)C(C)(C)C
197	Ethane, 1,1,2-trichloro-	79-00-5	133	C2H3Cl3	ClCC(Cl)Cl
209	Pentane, 2,3,4-trimethyl-	565-75-3	114	C8H18	CC(C)C(C)C(C)C
214	Pentane, 2,3,3-trimethyl-	560-21-4	114	C8H18	CCC(C)(C)C(C)C
221	Hexane, 2,3-dimethyl-	584-94-1	114	C8H18	CCCC(C)C(C)C
230	Hexane, 3,4-dimethyl-	583-48-2	114	C8H18	CCC(C)C(C)CC
239	Heptane, 3-methyl-	589-81-1	114	C8H18	CCCCC(C)CC
249	Hexane, 2,2,4-trimethyl-	16747-26-5	128	C9H20	CCC(C)CC(C)(C)C
255	Hexane, 2,2,5-trimethyl-	3522-94-9	128	C9H20	CC(C)CCC(C)(C)C
260	1-Octene	111-66-0	112	C8H16	CCCCCCC=C
266	Tetrachloroethylene	127-18-4	166	C2Cl4	ClC(Cl)=C(Cl)Cl
267	4-Octene, (Z)-	7642-15-1	112	C8H16	CCC\C=C/CCC
271	4-Octene, (E)-	14850-23-8	112	C8H16	CCC/C=C/CCC
276	Octane	111-65-9	114	C8H18	CCCCCCCC
283	Heptane, 3,3-dimethyl-	4032-86-4	128	C9H20	CCCCC(C)(C)CC
288	2-Heptene, 3-methyl-	3404-75-9	112	C8H16	CCCC\C(C)=C\C
295	2-Octene	111-67-1	112	C8H16	CCCCC\C=C/C
304	Hexane, 2,3,5-trimethyl-	1069-53-0	128	C9H20	CC(C)CC(C)C(C)C
316	Heptane, 2,4-dimethyl-	2213-23-2	128	C9H20	CCCC(C)CC(C)C
327	Octane, 2-methyl-	3221-61-2	128	C9H20	CCCCCCC(C)C
341	Heptane, 2,5-dimethyl-	2216-30-0	128	C9H20	CCC(C)CCC(C)C
362	Hexane, 2,3,4-trimethyl-	921-47-1	128	C9H20	CCC(C)C(C)C(C)C
372	4,6-Octadiyn-3-one, 2-methyl-	N/A	134	C9H10O	CC#CC#CC(=O)C(C)C
376	Heptane, 2,3-dimethyl-	3074-71-3	128	C9H20	CCCCC(C)C(C)C
387	Octane, 4-methyl-	2216-34-4	128	C9H20	CCCCC(C)CCC

394	Cyclopentane, 2-ethyl-1,1-dimethyl-	54549-80-3	126	C9H18	CCC1CCCC1(C)C
412	Heptane, 2,2,4-trimethyl-	14720-74-2	142	C10H22	CCCC(C)CC(C)(C)C
422	Octane, 2,2-dimethyl-	15869-87-1	142	C10H22	CCCCCCC(C)(C)C
441	Octane, 3,3-dimethyl-	4110-44-5	142	C10H22	CCCCCC(C)(C)CC
470	Hexane, 2,2,3,3-tetramethyl-	13475-81-5	142	C10H22	CCCC(C)(C)C(C)(C)C
482	Heptane, 2,3,6-trimethyl-	4032-93-3	142	C10H22	CC(C)CCC(C)C(C)C
502	a-Pinene	80-56-8	136	C10H16	CC1=CCC2CC1C2(C)C
504	Cyclohexene, 4-methylene-1-(1-methylethyl)-	99-84-3	136	C10H16	CC(C)C1=CCC(=C)CC1
527	4-Octene, 2,6-dimethyl-, [S-(E)]-	N/A	140	C10H20	CCC(C)C=CCC(C)C
533	2-Undecanethiol, 2-methyl-	10059-13-9	202	C12H26S	CCCCCCCCCC(C)(C)S
558	Octane, 4-ethyl-	15869-86-0	142	C10H22	CCCCC(CC)CCC
565	5-Ethyldecane	17302-36-2	170	C12H26	CCCCCC(CC)CCCC
601	Decyl octyl ether	N/A	270	C18H38O	CCCCCCCCCCOCCCCCCCC
609	Decane, 2,6,7-trimethyl-	62108-25-2	184	C13H28	CCCC(C)C(C)CCCC(C)C
616	Decane, 2,4,6-trimethyl-	62108-27-4	184	C13H28	CCCCC(C)CC(C)CC(C)C
624	Dodecane, 1-fluoro-	334-68-9	188	C12H25F	CCCCCCCCCCCCF
630	Decane, 2,2-dimethyl-	17302-37-3	170	C12H26	CCCCCCCCC(C)(C)C
665	2,2,7,7-Tetramethyloctane	1071-31-4	170	C12H26	CC(C)(C)CCCCC(C)(C)C
656	Decane, 2,6,8-trimethyl-	62108-26-3	184	C13H28	CCC(C)CC(C)CCCC(C)C
675	Decane, 2,5,9-trimethyl-	62108-22-9	184	C13H28	CC(C)CCCC(C)CCC(C)C
696	Heptane, 5-ethyl-2,2,3-trimethyl-	62199-06-8	170	C12H26	CCC(CC)CC(C)C(C)(C)C
717	Decane, 2,6,7-trimethyl-	62108-25-2	184	C13H28	CCCC(C)C(C)CCCC(C)C
735	Undecane, 3,6-dimethyl-	17301-28-9	184	C13H28	CCCCCC(C)CCC(C)CC
768	Dodecane, 2,7,10-trimethyl-	74645-98-0	212	C15H32	CCC(C)CCC(C)CCCCC(C)C

Table 4.5 MS identified uncommon peaks within human breath

T_R (sec)	Library Compound	CAS #	MW	Formula	Structure
4	Isoflurane	26675-46-7	184	C3H2ClF5O	FC(F)OC(Cl)C(F)(F)F
23	Hydrazinecarboxamide	57-56-7	75	CH5N3O	NNC(N)=O
32	Cyclopropane, ethylidene-	18631-83-9	68	C5H8	CC=C1CC1
47	Cyclopropaneethanol	2566-44-1	86	C5H10O	OCCC1CC1
50	1-Pentene, 4-methyl-	691-37-2	84	C6H12	CC(C)CC=C
99	2-Butenal, 3-methyl-	107-86-8	84	C5H8O	CC(C)=CC=O
98	Acetic acid	64-19-7	60	C2H4O2	CC(O)=O
106	Thiocyanic acid, butyl ester	628-83-1	115	C5H9NS	CCCCSC#N

109	trans-4-Methoxy-3-buten-2-one	51731-17-0	100	C5H8O2	CO/C=C/C(C)=O
113	Cyclohexane, chloro-	542-18-7	119	C6H11Cl	ClC1CCCCC1
119	Pentanal, 2,4-dimethyl-	27944-79-2	114	C7H14O	CC(C)CC(C)C=O
126	Acetic acid, [(1,1-dimethylethyl)thio]-	24310-22-3	148	C6H12O2S	CC(C)(C)SCC(O)=O
127	Heptane, 2-bromo-	1974-04-5	179	C7H15Br	CCCCCC(C)Br
131	Pentanal, 2,4-dimethyl-	27944-79-2	114	C7H14O	CC(C)CC(C)C=O
133	2-Butanone, 3,3-dimethyl-	75-97-8	100	C6H12O	CC(=O)C(C)(C)C
140	Oxirane, 2-methyl-2-(1-methylethyl)-	72221-03-5	100	C6H12O	CC(C)C1(C)CO1
144	1,2-Cyclopentanediol, 3-methyl-	27583-37-5	116	C6H12O2	CC1CCC(O)C1O
148	Cyclohexanecarboxylic acid, 1-amino-	2756-85-6	143	C7H13NO2	NC1(CCCCC1)C(O)=O
148	1,4-Butanediamine, N,N'-diethyl-	19435-68-8	144	C8H20N2	CCNCCCCNCC
164	1H-Imidazole, 4,5-dihydro-2,4-dimethyl-	930-61-0	98	C5H10N2	CC1CN=C(C)N1
167	Propanenitrile, 3-(ethylamino)-	21539-47-9	99	C5H11N2	CC[NH2+]CCC#N
175	Propanoic acid, 2-propenyl ester	2408-20-0	114	C6H10O2	CCC(=O)OCC=C
188	Thiophene, 2-ethyl-	872-55-9	112	C6H8S	CCc1sccc1
190	2-Thiopheneacetic acid, a-amino-, (±)-	21124-40-3	157	C6H7NO2S	[NH3+][C@H](C([O-])=O)c1sccc1
203	2-Hexenoic acid, ethyl ester	1552-67-6	142	C8H14O2	CCC/C=C/C(=O)OCC
203	Octanoic acid, 7-oxo-	14112-98-2	158	C8H14O3	CC(=O)CCCCCC(=O)O
224	Butane, 1-(ethenyloxy)-3-methyl-	39782-38-2	114	C7H14O	CC(C)CCOC=C
225	1-Piperidinyloxy, 4-amino-2,2,6,6-tetramethyl-	14691-88-4	173	C9H21N2O	CC1(C)CC([NH3+])CC(C)(C)N1O
243	1H-Tetrazol-5-amine	4418-61-5	85	CH3N5	Nc1n[nH]nn1
244	N-Allyl-N,N-dimethylamine	2155-94-4	85	C5H11N	CN(C)CC=C
247	N,N,N',N',-Tetramethyl-2-butene-1,4-diamine	4559-79-9	144	C8H20N2	C[NH+](C)C\C=C\C[NH+](C)C
248	2-Butene-1,4-diamine, N,N'-diethyl-	112-21-0	144	C8H20N2	CC[NH2+]C\C=C\C[NH2+]CC
265	1,2-Dichloro-4-fluorobenzene	1435-49-0	165	C6H3Cl2F	Fc1ccc(Cl)c(Cl)c1
280	Hydroxylamine, O-decyl-	29812-79-1	173	C10H23NO	CCCCCCCCCCON
310	1-Hexanol, 5-methyl-2-(1-methylethyl)-	2051-33-4	158	C10H22O	CC(C)CCC(CO)C(C)C
352	Acetic acid, cyano-, 2-ethylhexyl ester	13361-34-7	197	C11H19NO2	CCCCC(CC)COC(=O)CC#N
355	Decane, 3-chloro-	1002-11-5	177	C10H21Cl	CCCCCCCC(Cl)CC

437	Bicyclo[2.2.2]octan-1-ol	20534-58-1	126	C8H14O	OC12CCC(CC1)CC2
466	Dodecane, 1-fluoro-	334-68-9	188	C12H25F	CCCCCCCCCCCCF
471	Ether, hexyl pentyl	32357-83-8	172	C11H24O	CCCCCCOCCCCC
497	1-Decanol, 2-ethyl-	21078-65-9	186	C12H26O	CCCCCCCCC(CC)CO
543	Dodecane, 1-fluoro-	334-68-9	188	C12H25F	CCCCCCCCCCCCF
552	Chloroacetic acid, dodecyl ester	6316-04-7	263	C14H27ClO2	CCCCCCCCCCCCOC(=O)CCl
602	Silane, trichlorodocosyl-	7325-84-0	444	C22H45Cl3Si	CCCCCCCCCCCCCCCCCCCCCC[Si](Cl)(Cl)Cl
558	Undecane, 2,6-dimethyl-	17301-23-4	184	C13H28	CCCCCC(C)CCCC(C)C
652	1-Dodecanol, 2-methyl-, (S)-	57289-26-6	200	C13H28O	CCCCCCCCCCC(C)CO
761	Dodecane, 1-fluoro-	334-68-9	188	C12H25F	CCCCCCCCCCCCF

4.3.4 ARDS diagnosis based on 2D chromatograms

There were a total of 97 peaks found in about 800 seconds of 2D separation (~800 seconds of 1st-dimensional separation and 20 seconds of 2nd-dimensional separation). Each of the peaks may represent a single analyte (no co-elution) or multiple analytes (co-elution). Note that the 2D chromatogram of a particular patient may contain only a subset of the 97 peaks. Also note that the volume (analyte mass) of each peak is normalized to the total peak volume of the entire 2D chromatogram, which is one of the most commonly used normalization techniques[221-226]. To select the optimal subset of peaks, 28 patients (11 ARDS, 17 control, and a total of 43 tests) were used as the training set, whereas the remaining 20 patients (10 ARDS, 10 controls, and a total of 42 tests) were used as the testing set.

Selection of the optimal subset of peaks relevant to ARDS

In our study, a total of *m=97* peaks were found in 2D chromatograms. We first assumed that there are n=4 peaks relevant to classification of ARDS and non-ARDS. We found that the 4-peak subset of Peaks #(2, 44, 72, 79) provides the best 4-peak subset classification with a total accuracy of 88.4% (see the corresponding peaks on the 2D GC chromatogram in Figure 4.10 and

the PCA-LDA results in Figure 4.9(a)). n'=5 peaks were then added and we found that the 9-peak subset of [(2, 44, 72, 79) + (34, 38, 62, 66, 81)] provides the best 9-peak subset classification with a total accuracy of 93.0% (see the corresponding peaks on a 2D GC chromatogram in Figure 4.10 and the PCA-LDA results in Figure 4.9(b)). Subsequently, yet another n'=5 peaks were added and we found that the 14-peak subset of [(2, 44, 72, 79) + (34, 38, 62, 66, 81) + (54, 61, 63, 71, 75)] provides the best classification with a total accuracy of 93.0% (see the corresponding peaks on a 2D GC chromatogram in Figure 4.10 and the PCA-LDA results in Figure 4.9(c)). Since the classification accuracy and the boundary distance does not improve from the 9-peak subset to the 14-peak subset (i.e., the ARDS and non-ARDS groups are not clustered/separated better), the 9-peak subset was selected as the final optimal peak subset, which consists of Peaks #(2, 44, 72, 79, 34, 38, 62, 66, 81) in the 2D chromatogram.

These 9 peaks were tentatively identified by coupling our portable GC with the Thermo Scientific Single Quadrupole Mass Spectrometer (ISQ™ Series) and analyzing with Chromeleon™ 7 Software. Their names, CAS numbers, and formulas are presented in Table 4.6.

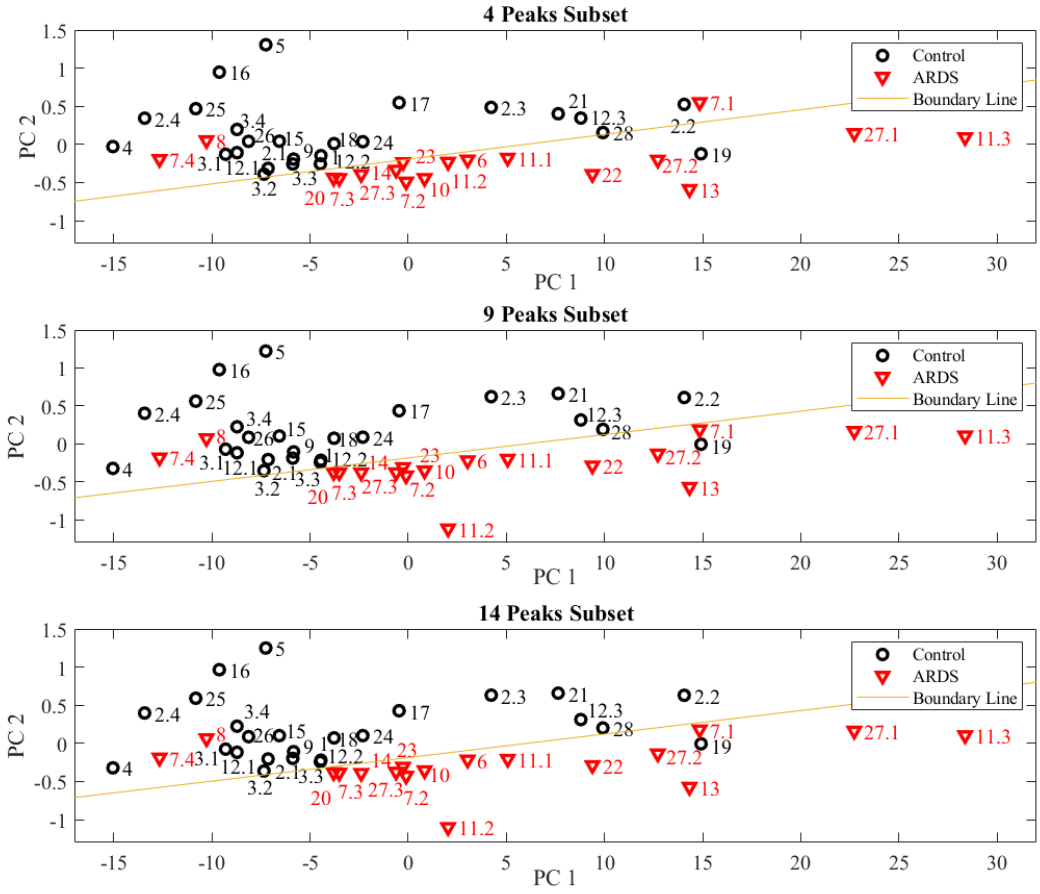

Figure 4.9. PCA plots using the subset containing 4 peaks, 9 peaks, and 14 peaks for the training set. The red and black symbols denote, respectively, the ARDS and non-ARDS patients adjudicated by physicians using the Berlin criteria. The patient numbers are given by the labels. For example, "11.1" and "11.3" denote Patient #11, Day 1 and Day 3 results, respectively. The bottom/top zone below/above the boundary line represents respectively the ARDS/non-ARDS region.

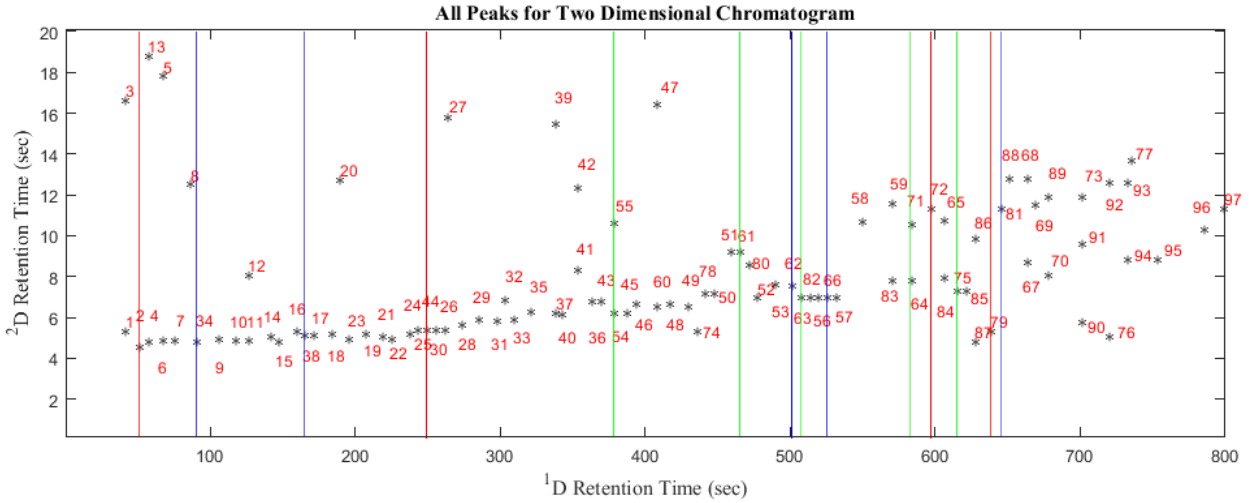

Figure 4.10. Selection of the optimal subset of peaks relevant to ARDS. Red lines mark the 1D retention time of the 4 peaks selected in the first iteration. Blue lines mark the ^{1}D retention time of the additional 5 peaks selected in the second iteration. Green lines mark the ^{1}D retention time of the additional 5 peaks selected in the third iteration. Peak #34 in the 9-peak subset nearly co-elutes with Peak #8. Peak #54 and #71 in the 14-peak subset co-elutes with Peak #55 and Peak #64, respectively.

Table 4.6. Tentative chemical identification for the 9-peak subset.

Peak ID	Chemical Name	CAS Number	Formula
2	Pentane, 2-methyl-	107-83-5	C_6H_{14}
44	Heptane, 3-methyl-	589-81-1	C_8H_{18}
72	Heptane, 2,3,5-trimethyl-	20278-85-7	$C_{10}H_{22}$
79	2,2,7,7-Tetramethyloctane	1071-31-4	$C_{12}H_{26}$
34	Pentane, 2,4-dimethyl-	108-08-7	C_7H_{16}
38	Cyclohexane, methyl-	108-87-2	C_7H_{14}
62	α-Pinene	80-56-8	$C_{10}H_{16}$
66	3-Octene, 2,2-dimethyl-	86869-76-3	$C_{10}H_{20}$
81	1-Decanol, 2-ethyl-	21078-65-9	$C_{12}H_{26}O$

Table 4.7 Tentative chemical identification for all peaks.

Peak ID	Library Compounda	CAS #	MW	Formula	Structure
1 or 3	Butane, 2-methyl-	78-78-4	72	C5H12	CCC(C)C
1 or 3	Isoprene	78-79-5	68	C5H8	CC(=C)C=C
2	Pentane, 2-methyl-	107-83-5	86	C6H14	CCCC(C)C
4	unidentified				

5 or 6	1-Pentene, 2-methyl-	763-29-1	84	C6H12	CCCC(C)=C
5 or 6	n-Hexane	110-54-3	86	C6H14	CCCCCC
7	1-Pentanol, 2-methyl-	105-30-6	102	C6H14O	CCCC(C)CO
8	unidentified				
9	2-Butenal, 3-methyl-	107-86-8	84	C5H8O	CC(C)=CC=O
10	Hexane, 3-methyl-	589-34-4	100	C7H16	CCCC(C)CC
11 or 12	Acetic acid, [(1,1-dimethylethyl)thio]-	24310-22-3	148	C6H12O2S	CC(C)(C)SCC(O)=O
11 or 12	Heptane, 2-bromo-	1974-04-5	179	C7H15Br	CCCCCC(C)Br
13	unidentified				
14	Heptane	142-82-5	100	C7H16	CCCCCCC
15	1,2-Cyclopentanediol, 3-methyl-	27583-37-5	116	C6H12O2	CC1CCC(O)C1O
16	Cyclohexanecarboxylic acid, 1-amino-	2756-85-6	143	C7H13NO2	NC1(CCCCC1)C(O)=O
17	1-Pentanol, 2-ethyl-4-methyl-	106-67-2	130	C8H18O	CCC(CO)CC(C)C
18	unidentified				
19	2-Hexenoic acid, ethyl ester	1552-67-6	142	C8H14O2	CCC/C=C/C(=O)OCC
20	Thiophene, 2-ethyl-	872-55-9	112	C6H8S	CCc1sccc1
21	Pentane, 2,3,3-trimethyl-	560-21-4	114	C8H18	CCC(C)(C)C(C)C
22	Hexane, 2,3-dimethyl-	584-94-1	114	C8H18	CCCC(C)C(C)C
23	unidentified				
24	Hexane, 3,4-dimethyl-	583-48-2	114	C8H18	CCC(C)C(C)CC
25	unidentified				
26	Hexane, 2,2,5-trimethyl-	3522-94-9	128	C9H20	CC(C)CCC(C)(C)C
27	1-Octene	111-66-0	112	C8H16	CCCCCCC=C
28	4-Octene, (E)-	14850-23-8	112	C8H16	CCC/C=C/CCC
29	Heptane, 3,3-dimethyl-	4032-86-4	128	C9H20	CCCCC(C)(C)CC

30	Hexane, 2,2,4-trimethyl-	16747-26-5	128	C9H20	CCC(C)CC(C)(C)C
31	2-Octene	111-67-1	112	C8H16	CCCCC\C=C/C
32	unidentified				
33	Hexane, 2,3,5-trimethyl-	1069-53-0	128	C9H20	CC(C)CC(C)C(C)C
34	Pentane, 2,4-dimethyl-	108-08-7	100	C7H16	CC(C)CC(C)C
35	Heptane, 2,4-dimethyl-	2213-23-2	128	C9H20	CCCC(C)CC(C)C
36	unidentified				
37	unidentified				
38	Cyclohexane, methyl-	108-87-2	98	C7H14	CC1CCCCC1
39	unidentified				
40	Heptane, 2,5-dimethyl-	2216-30-0	128	C9H20	CCC(C)CCC(C)C
41 or 42	Acetic acid, cyano-, 2-ethylhexyl ester	13361-34-7	197	C11H19NO2	CCCCC(CC)COC(=O)CC#N
41 or 42	Decane, 3-chloro-	1002-11-5	177	C10H21Cl	CCCCCCCC(Cl)CC
43	Hexane, 2,3,4-trimethyl-	921-47-1	128	C9H20	CCC(C)C(C)C(C)C
44	Heptane, 3-methyl-	589-81-1	114	C8H18	CCCCC(C)CC
45	Octane, 4-methyl-	2216-34-4	128	C9H20	CCCCC(C)CCC
46	Cyclopentane, 2-ethyl-1,1-dimethyl-	54549-80-3	126	C9H18	CCC1CCCC1(C)C
47	unidentified				
48	Heptane, 2,2,4-trimethyl-	14720-74-2	142	C10H22	CCCC(C)CC(C)(C)C
49	Octane, 2,2-dimethyl-	15869-87-1	142	C10H22	CCCCCCC(C)(C)C
50	Octane, 3,3-dimethyl-	4110-44-5	142	C10H22	CCCCCC(C)(C)CC
51	unidentified				
52	Ether, hexyl pentyl	32357-83-8	172	C11H24O	CCCCCCOCCCCC
53	Heptane, 2,3,6-trimethyl-	4032-93-3	142	C10H22	CC(C)CCC(C)C(C)C
54 or 55	4,6-Octadiyn-3-one, 2-methyl-	N/A	134	C9H10O	CC#CC#CC(=O)C(C)C

54 or 55	Heptane, 2,3-dimethyl-	3074-71-3	128	C9H20	CCCCC(C)C(C)C
56	unidentified				
57	4-Octene, 2,6-dimethyl-, [S-(E)]-	N/A	140	C10H20	CCC(C)C=CCC(C)C
58	unidentified				
59 or 83	5-Ethyldecane	17302-36-2	170	C12H26	CCCCCC(CC)CCCC
60	unidentified				
61	unidentified				
62	a-Pinene	80-56-8	136	C10H16	CC1=CCC2CC1C2(C)C
63	Cyclohexene, 4-methylene-1-(1-methylethyl)-	99-84-3	136	C10H16	CC(C)C1=CCC(=C)CC1
64	unidentified				
65 or 84	Decyl octyl ether	N/A	270	C18H38O	CCCCCCCCCCOCCCCCCCC
65 or 84	Silane, trichlorodocosyl-	7325-84-0	444	C22H45Cl3Si	CCCCCCCCCCCCCCCCCCCCCC[Si](Cl)(Cl)Cl
66	3-Octene, 2,2-dimethyl-	86869-76-3	140	C10H20	CCCC/C=C/C(C)(C)C
67 or 68	Decane, 2,6,8-trimethyl-	62108-26-3	184	C13H28	CCC(C)CC(C)CCCC(C)C
69	unidentified				
70 or 89	Decane, 2,5,9-trimethyl-	62108-22-9	184	C13H28	CC(C)CCCC(C)CCC(C)C
71	unidentified				
72	Heptane, 2,3,5-trimethyl-	20278-85-7	142	C10H22	CCC(C)CC(C)C(C)C
73 or 90	Heptane, 5-ethyl-2,2,3-trimethyl-	62199-06-8	170	C12H26	CCC(CC)CC(C)C(C)(C)C
74	unidentified				
75	Decane, 2,6,7-trimethyl-	62108-25-2	184	C13H28	CCCC(C)C(C)CCCC(C)C
76	unidentified				
77	Undecane, 3,6-dimethyl-	17301-28-9	184	C13H28	CCCCCC(C)CCC(C)CC
78	Bicyclo[2.2.2]octan-1-ol	20534-58-1	126	C8H14O	OC12CCC(CC1)CC2

79	2,2,7,7-Tetramethyloctane	1071-31-4	170	C12H26	CC(C)(C)CCCCC(C)(C)C
80	Hexane, 2,2,3,3-tetramethyl-	13475-81-5	142	C10H22	CCCC(C)(C)C(C)(C)C
81	1-Decanol, 2-ethyl-	21078-65-9	186	C12H26O	CCCCCCCCC(CC)CO
82	unidentified				
85	Decane, 2,4,6-trimethyl-	62108-27-4	184	C13H28	CCCCC(C)CC(C)CC(C)C
86 or 87	Dodecane, 1-fluoro-	334-68-9	188	C12H25F	CCCCCCCCCCCCF
86 or 87	Decane, 2,2-dimethyl-	17302-37-3	170	C12H26	CCCCCCCCC(C)(C)C
88	1-Dodecanol, 2-methyl-, (S)-	57289-26-6	200	C13H28O	CCCCCCCCCCC(C)CO
90 or 91	Heptane, 5-ethyl-2,2,3-trimethyl-	62199-06-8	170	C12H26	CCC(CC)CC(C)C(C)(C)C
92	unidentified				
93	unidentified				
94	unidentified				
95	unidentified				
96	unidentified				
97	unidentified				

Classification accuracy

With this algorithm, we selected the 9-peak subset as the final optimal peak subset, which yields the best classification accuracy (93.0%) and the maximum boundary distance. The final PCA scores for all recruited patients are shown in Figure 4.11. The final PCA model achieved an overall accuracy of 87.1% with 94.1% positive predictive value and 82.4% negative predictive value. The corresponding specificity, sensitivity, positive predictive value (PPV), and negative predictive value (NPV) are presented in Table 4.8. The corresponding Q-residuals for all recruited patients are shown in Figure 4.12. Separate PCA scores and corresponding statistics (specificity, sensitivity, PPV and NPV) for the training and testing sets are presented in Figure 4.13 and Table 4.9, respectively. Receiver operating characteristic curves for the training set, testing set, and all

patients are presented in Section 4.3.4.2 and Figure 4.14. 4-fold cross-validation was performed, in which original datasets were randomly divided into 4 subsets of equal size and 4 cross-validation models were generated using one subset as a testing set and the rest as the training set. The 4 models yielded a classification accuracy of 85.3% ± 0.7%, which supports the robustness of the model. The statistics (specificity, sensitivity, PPV, and NPV) of the 4 models are presented in Table 4.10.

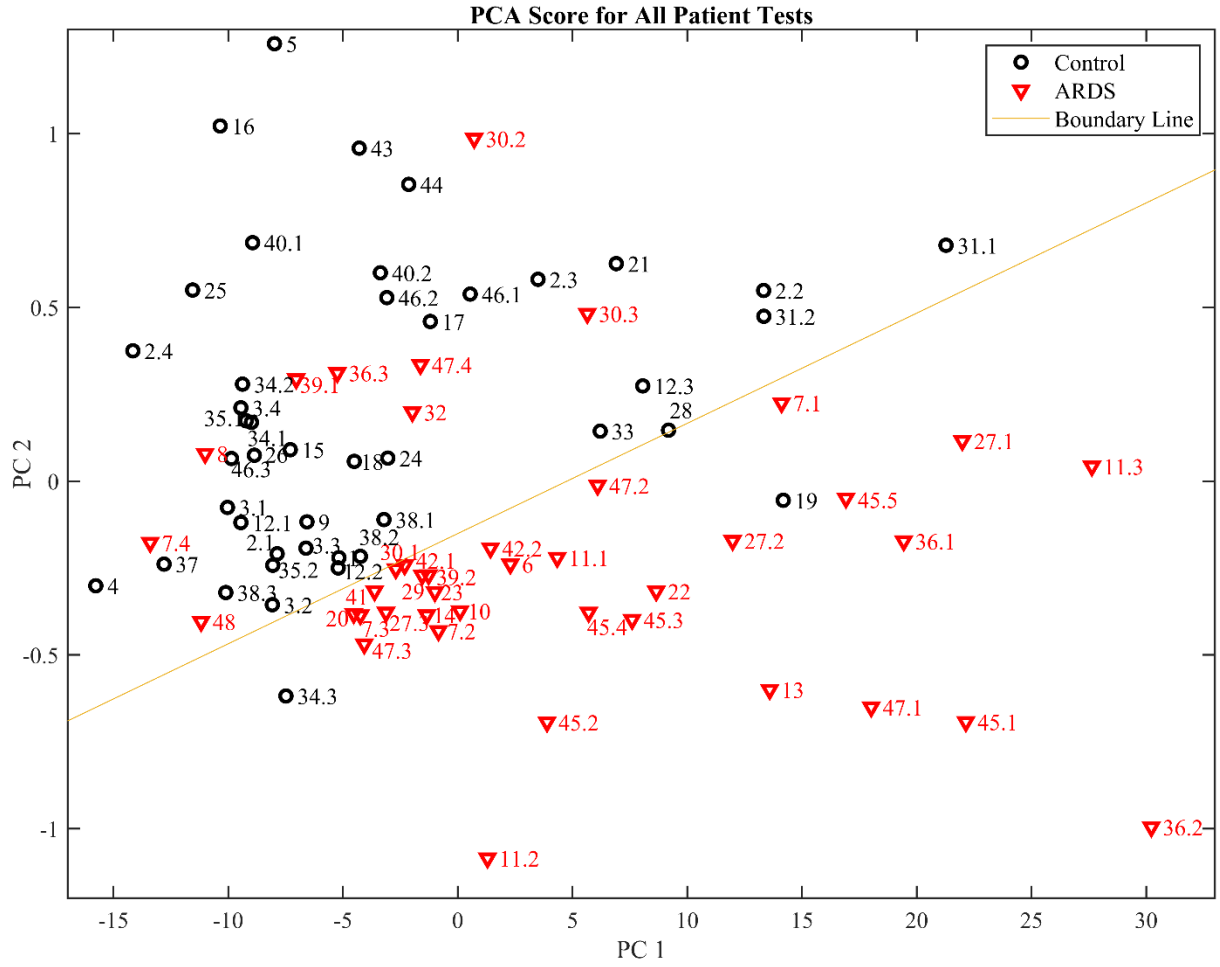

Figure 4.11. PCA plot of all recruited patients. The X-axis (PC 1) is the 1st principal component and the Y-axis (PC 2) is the 2nd principal component. The red and black symbols denote, respectively, the ARDS and non-ARDS patients adjudicated by physicians using the Berlin criteria. The patient numbers are given by the labels. For example, "11.1" and "11.3" denote Patient #11, Day 1 and Day 3 results, respectively. The bottom/top zone below/above the boundary line represents, respectively, the ARDS/non-ARDS region using the breath

analysis method. The corresponding Q-residuals for this PCA model are shown in Figure 9.

Table 4.8. Statistics of breath analysis for ARDS.

	ARDS	Non-ARDS	Total
Positive (our results)	32	2	34
Negative (our results)	9	42	51
Column total	41	44	85
Specificity	95.5 %		
Sensitivity	78.0 %		
Positive predictive value	94.1 %		
Negative predictive value	82.4 %		
Total accuracy	87.1%		

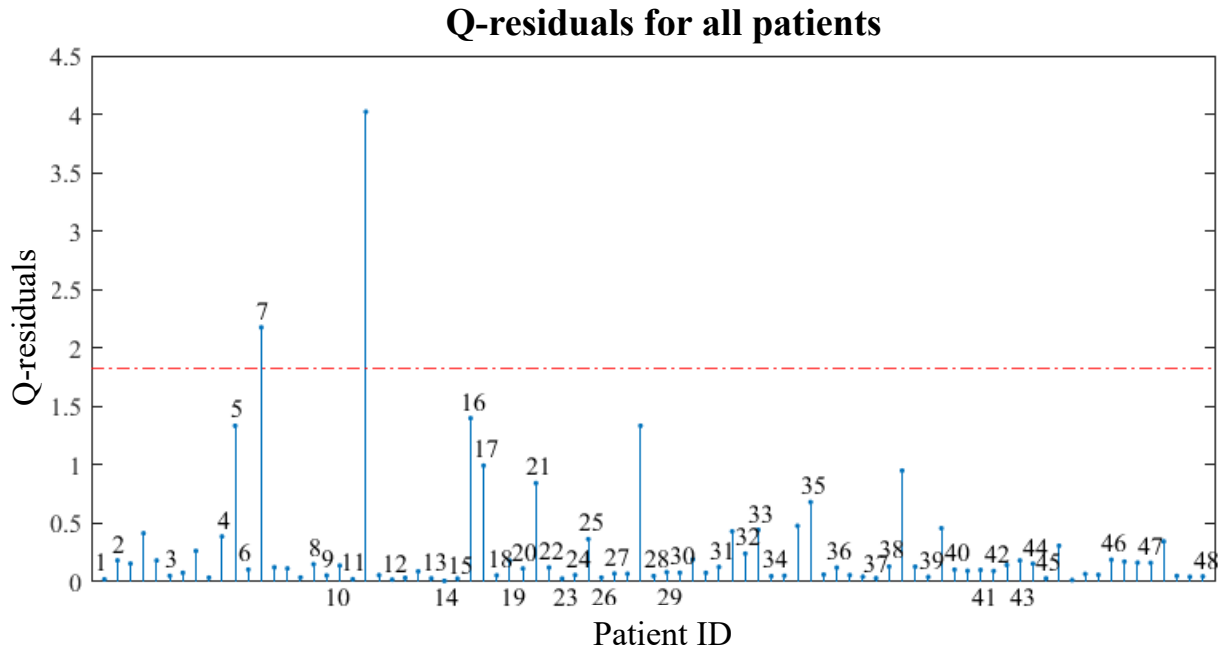

Figure 4.12. Q-residuals of the PCA model (Figure 8) for all recruited patients. For patients with time series tests, only the 1st test day is marked with the patient ID. The red dashed line represents a 99% confidence level.

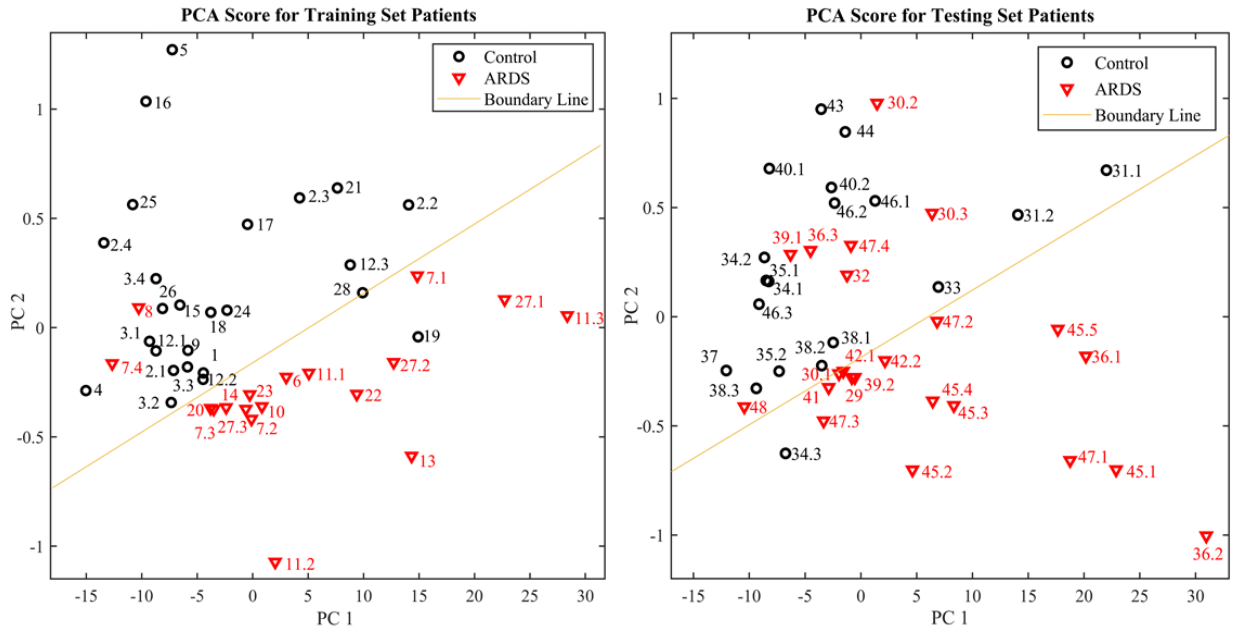

Figure 4.13. PCA plot for the training and testing set of patients. Corresponding statistics are given in Table 4.9.

Table 4.9. Statistics for the training and testing sets.

Training Set	ARDS	Non-ARDS	Total
Positive (our results)	16	1	17
Negative (our results)	2	24	26
Column total	18	25	43
Specificity	96.0%		
Sensitivity	88.9 %		
Positive predictive value	94.1%		
Negative predictive value	92.3%		
Total accuracy	93.0%		
Testing Set	ARDS	Non-ARDS	Total
Positive (our results)	16	1	17
Negative (our results)	7	18	25
Column total	23	19	42
Specificity	94.7 %		
Sensitivity	69.6 %		
Positive predictive value	94.1%		
Negative predictive value	72.0%		
Total accuracy	80.9%		

Receiver Operating Characteristic (ROC) curve analysis

With the LDA model acquired from the training set, the posterior probability can be calculated for any given $\boldsymbol{S}_p$:

$$P(ARDS|\boldsymbol{S}_p) = \frac{P(\boldsymbol{S}_p|ARDS)P(ARDS)}{P(\boldsymbol{S}_p|ARDS)P(ARDS)+P(\boldsymbol{S}_p|non-ARDS)P(non-ARDS)} \quad , \tag{4.10}$$

where $\boldsymbol{S}_p$ is a vector of the principal component scores (S_{p1} S_{p2}) for any given patient p. $P(ARDS)$ and $P(non-ARDS)$ are the prior probability (fraction of ARDS and non-ARDS patients within the training set), respectively. $P(\boldsymbol{S}_p|ARDS)$ and $P(\boldsymbol{S}_p|non-ARDS)$ are the ARDS and non-ARDS multivariate Gaussian distribution density functions, with $\boldsymbol{\mu}_{ARDS}$ and $\boldsymbol{\mu}_{non-ARDS}$ being the means and $\boldsymbol{\Sigma}$ being the shared covariance matrix across ARDS and non-ARDS.

$$P(\boldsymbol{S}_p|ARDS) = \frac{1}{(2\pi|\boldsymbol{\Sigma}|)^{\frac{1}{2}}} e^{-\frac{1}{2}(\boldsymbol{S}_p-\boldsymbol{\mu}_{ARDS})^T\boldsymbol{\Sigma}^{-1}(\boldsymbol{S}_p-\boldsymbol{\mu}_{ARDS})}, \tag{4.11}$$

$$P(\boldsymbol{S}_p|non-ARDS) = \frac{1}{(2\pi|\boldsymbol{\Sigma}|)^{\frac{1}{2}}} e^{-\frac{1}{2}(\boldsymbol{S}_p-\boldsymbol{\mu}_{non-ARDS})^T\boldsymbol{\Sigma}^{-1}(\boldsymbol{S}_p-\boldsymbol{\mu}_{non-ARDS})} \tag{4.12}$$

With the ARDS/non-ARDS labels and the posterior probability of the patients in the training set, testing set, and all patients, their ROC curves and the corresponding AUC (area under curve) were computed and shown in Figure 4.14.

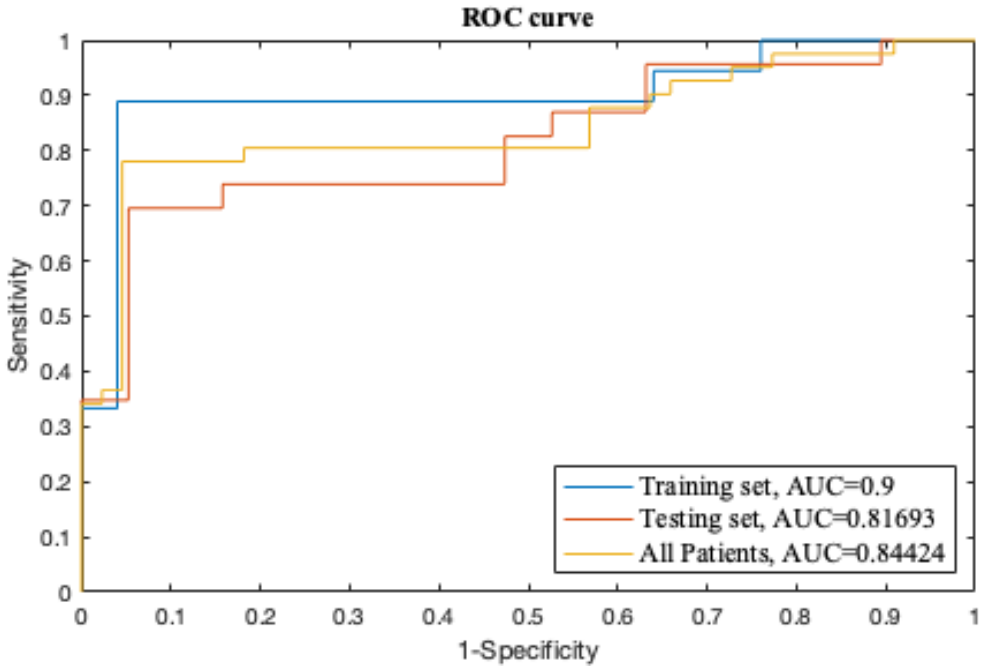

Figure 4.14. Receiver operating characteristic (ROC) curves for the training set, testing set, and all patients.

Table 4.10. Statistics for the 4-fold cross-validation

Cross Validation - 4 fold	Model 1	Model 2	Model 3	Model 4
Specificity	93.2%	93.2%	93.2%	93.2%
Sensitivity	78.0%	75.6%	78.0%	75.6%
Positive predictive value	91.4%	91.2%	91.4%	91.2%
Negative predictive value	82%	80.4%	82%	80.4%
Total accuracy	85.9%	84.7%	85.9%	84.7%

Time series measurement of ARDS patients

One of important advantages of breath analysis is the potential to non-invasively monitor the development of ARDS, the severity of ARDS (if present), and the resolution of ARDS. This would allow the technology to map the trajectory of the disease and potentially guide therapy and decision making. Among the 9 ARDS patients and 9 non-ARDS patients whom we monitored on multiple days, some ARDS patients were noted to clinically progress to a non-ARDS status and vice versa, as determined by both 2D GC and clinical adjudication. Our results demonstrated that

breath analysis may be able to predict the ARDS trajectory 12-48 hours in advance. Below, we show some examples, whose trajectories on the PCA plot are shown in Figure 4.15.

(1) Upgrade cases:

Patient #11 (see also Figure 4.7 for the corresponding time-series chromatograms) was a potential and undetermined ARDS patient (meaning that the clinician suspected that the patient might develop ARDS, but was not certain at the time of diagnosis: the patient was closely monitored) on the 1st test day, then upgraded to ARDS on the second day. The breath test suggested a diagnosis of ARDS from the 1st test day to the 3rd test day (#11.1, #11.2, and #11.3).

Patient #27 was a potential and undetermined ARDS patient on the 1st test day and upgraded to ARDS on the second day. The breath test suggested a diagnosis of ARDS from the 1st test day to the 3rd test day (#27.1, #27.2, and #27.3).

(2) Recovery cases:

Patient #36 was sampled for 3 days. On the 3rd day, the patient was still listed as ARDS based on the Berlin Criteria. The patient was extubated (liberated from mechanical ventilation) and discharged from the ICU on the 5th day. The breath tests for the first 2 days suggested ARDS (#36.1 and #36.2). The breath test for the 3rd day demonstrated a non-ARDS pattern (#36.3).

Patient #47 was sampled for 4 days and was liberated from mechanical ventilation and discharged on the 6th day. Based on the Berlin Criteria, this patient had ARDS for the first four days. The breath tests for the first three days show an ARDS pattern (#47.1, # 47.2, and #47.3) and the fourth day breath test shows a non-ARDS pattern (#47.4).

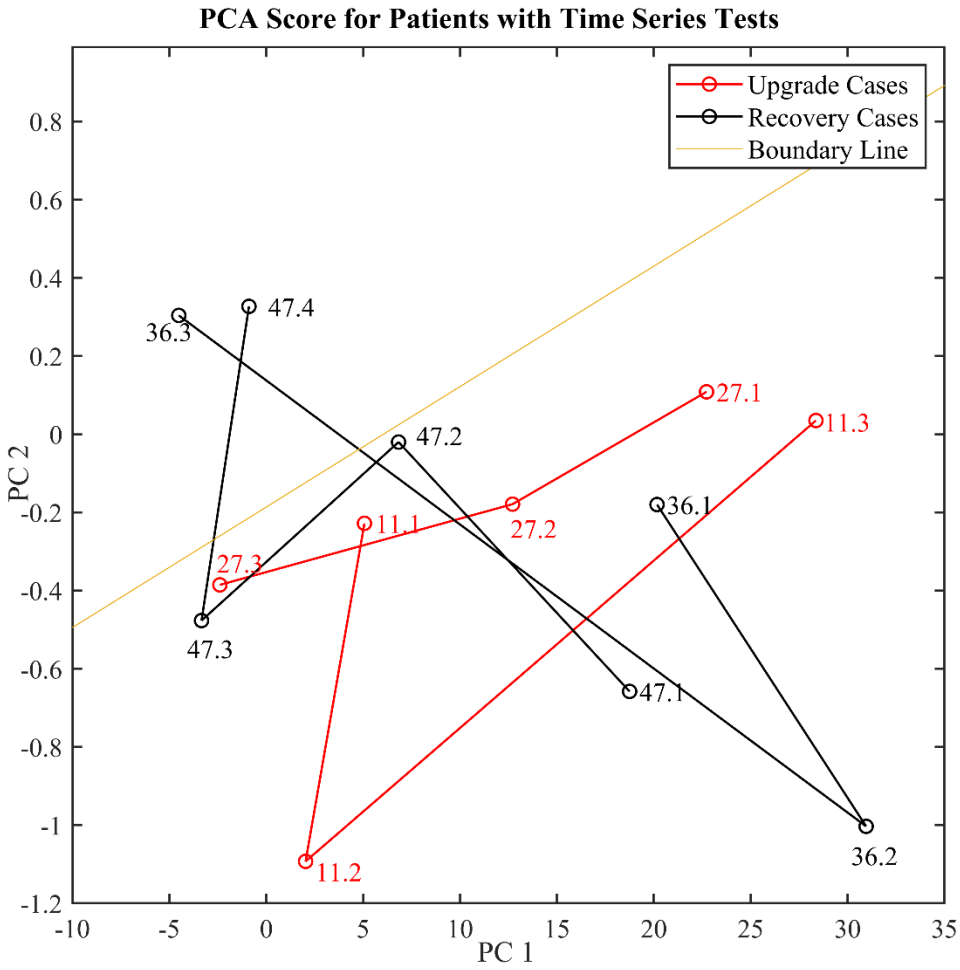

Figure 4.15. Trajectories on the PCA plot for patient #11, #27, #36, and #47. #11 and #27 are the upgrade case (initially listed as potential ARDS on the first day) and #36 and #47 are recovery cases (extubated and discharged from ICU 24-48 hours after the last test). The bottom/top zone below/above the boundary line represents, respectively, the ARDS/non-ARDS region using the breath analysis method.

Note: If the breath test results do not match the clinical adjudication, we consider the test as "misclassification" when calculating the overall classification accuracy, even for cases like #36.3 and #47.4, which suggest that the breath analysis was able to correctly predict the trajectory of ARDS (i.e., earlier diagnosis).

With further evidence on subsequent days, the two potential and undetermined ARDS cases mentioned above (#11.1 and #27.1) were finally determined as ARDS based on the Berlin Criteria. The trajectories of all 18 patients and their medical histories can be found in Figure 4.16.

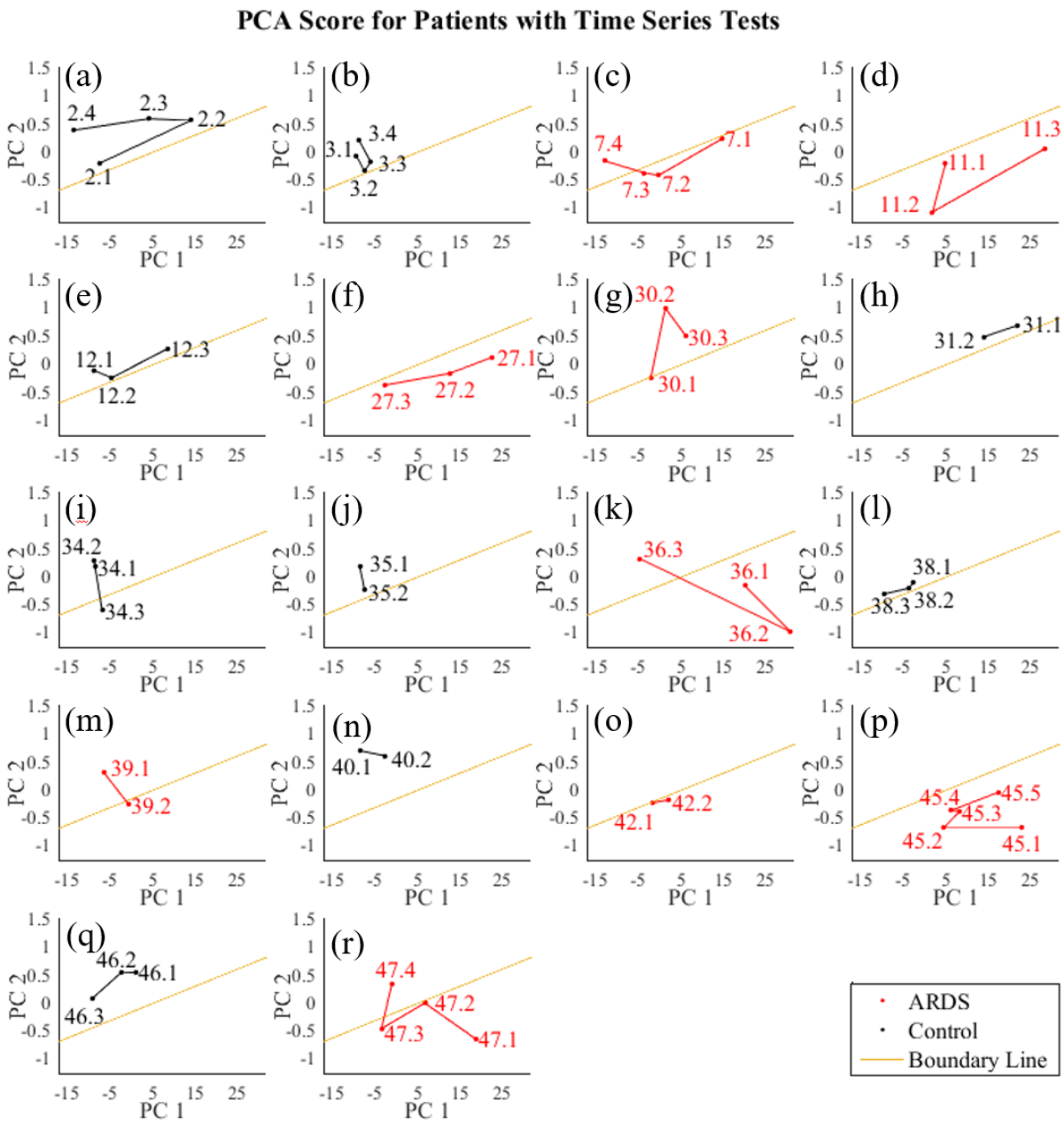

Figure 4.16 Individual trajectories of all 18 patients with time series tests on the PCA plot. Patient medical histories are shown below.

.

Patient medical histories during time series testing dates:

Patient #2 was a healthy subject tested for 4 days.

Patient #3 was a healthy subject tested for 4 days.

Patient #7 was sampled for 4 days and had ARDS by the Berlin Criteria from the first testing day. No signs of recovery for at least 4 days after the last testing day.

Patient #11 was a potential and undetermined ARDS patient on the first test day and was upgraded to ARDS on the second day. By the Berlin Criteria, the patient had ARDS for all 3 days.

Patient #12 was suspected to have pneumonia on the first testing day. This patient was tested for 3 days and no ARDS was developed during this period based on the Berlin Criteria.

Patient #27 was a potential and undetermined ARDS patient on the first test day and was upgraded to ARDS on the second day. Based on the Berlin Criteria, the patient had ARDS for all 3 days.

Patient #30 had pneumonia and ARDS based on the Berlin Criteria from the first test day. The patient was tested for 3 days. No signs of recovery and was shifted to comfort care after the last testing day.

Patient #31 had acute respiratory failure on the first testing day, but no ARDS based on the Berlin Criteria for the two testing days.

Patient #34 had hypoxemic respiratory failure on the first testing day, but no ARDS based on the Berlin Criteria for the three testing days.

Patient #35 had no ARDS based on the Berlin Criteria for the two testing days.

Patient #36 had ARDS from the first sampling day. On the third, day the patient was still listed as ARDS based on the Berlin Criteria. The patient was extubated and discharged from ICU on the 5^{th} day.

Patient #38 was a healthy subject tested for three days.

Patient #39 had ARDS based on the Berlin Criteria for the two testing days. No signs of recovery.

Patient #40 had pneumonia on the first testing day but no ARDS based on the Berlin Criteria for the two testing days.

Patient #42 had ARDS based on the Berlin Criteria for the two testing days. No signs of recovery.

Patient #45 had ARDS based on the Berlin Criteria for the five testing days. No signs of recovery and was shifted to comfort care on the last testing day.

Patient #46 had no ARDS based on the Berlin Criteria for the three testing days.

Patient #47 was sampled for 4 days and was extubated and discharged on the sixth day. Based on the Berlin Criteria, this patient had ARDS for the first four days.

4.4 Discussion

To our knowledge, the portable 2D GC device described here is the first of its kind for facile use in POC to continuously monitor patient breath. Using this portable GC device, along with its corresponding machine learning algorithms, we are able to distinguish ARDS and non-ARDS with high accuracy compared to clinical expert adjudication. As a dynamic syndrome with multiple etiologies, the real-time diagnosis of ARDS is challenging. There are currently no technologies allowing its real-time diagnosis or tracking. The only widely available tool in use in assisting in ARDS diagnostics is LIPS. However, LIPS was designed as a screening tool that incorporates a series of risk factors and risk modifiers to predict whether ARDS will occur at a future point. While a small subset of data using the 2D GC technology indicates the potential to predict onset or resolution, much more testing will be needed. An interesting possibility would be to utilize LIPS in conjunction with this technology to improve screening[187, 189].

It should be noted that, based on current results obtained, the 9-peak subset (Peak #2, 34, 38, 44, 62, 66, 72, 79, and 81 in Figure 4.6) that was selected for ARDS detection can be almost

completely separated using the ^{1}D column in our current 2D GC device (except for Peak #34, which is nearly co-eluted with Peak #8, see Figure 4.10). Therefore, the portable GC's 1D GC mode may be sufficient to distinguish between ARDS and non-ARDS. However, we believe that 2D GC operation is still preferred, since potential co-elution of Peak #34 and #8 may affect ARDS detection. More significantly, 2D GC operation is critical to sub-typing ARDS and analyzing complications. For example, the peaks (#3, 5, 13, and 27) in Figure 4.6 do not belong to the ARDS-relevant 9-peak subset, but have different concentrations between the ARDS patient and the healthy control (see Figure 4.5), suggesting that the ARDS patient in Figure 4.5(b) might have other health conditions besides ARDS, which may change during medical treatment. For future applications (in detection of ARDS and ARDS with complications, and in detection of other diseases such as asthma and pneumonia), it is still preferred to continue to use comprehensive 2D GC to separate as many peaks as possible, which makes the device much more flexible for various diseases and medical conditions, rather than being dedicated to monitoring of ARDS alone.

This study has a number of important limitations. First and foremost, the histopathologic examination of lung tissue for changes consistent with diffuse alveolar damage (DAD) was not used to make the diagnosis of ARDS. Even in patients dying of respiratory failure, autopsies were not obtained. While DAD on histopathology is the pathologic gold standard, obtaining serial lung biopsies for diagnosis is not feasible for clinical standard of care. Although the clinical consensus for the diagnosis of ARDS is the Berlin criteria, Kao and others have demonstrated that of patients clinically diagnosed as having ARDS using the Berlin criteria, less than 60% have DAD on lung histopathology when lung biopsies can be obtained[178]. In the absence of tissue biopsy, we employed the best available method (multi-physician adjudication) for identifying ARDS[211].

This limitation is not only restricted to our study, but is present in any clinical research or clinical trial in the field of ARDS and further underscores the need for new diagnostics. Despite this, we observed VOC patterns in ARDS patients that were clearly distinguishable from patterns seen in subjects who were mechanically ventilated for non-hypoxic respiratory failure such as sepsis (without ARDS) and cardiac arrest, as well as those intubated for hypoxic respiratory failure, whose PaO_2/FiO_2s (after intubation and mechanical ventilation) were clearly not indicative of ARDS (COPD exacerbation, pulmonary embolism, and unilateral pneumonia). In cases of divergence in clinical scoring and breath analysis, differences could be due to mis-diagnosis of ARDS by clinical scoring, the ability of breath analysis to detect earlier onset or resolution of ARDS than clinical adjudication, or mixed lung and systemic pathologies existing in the same patients.

Finally, we note that in the current study, only 48 patients (and 85 sets of breath samples) were used as a proof of concept demonstration. Larger groups of patients are required to further validate our method.

We have developed an automated portable 2D GC device and machine learning algorithm for breath analysis that is capable of distinguishing ARDS from non-ARDS. Particularly, the 94.1% positive predicative value suggests that our breath analysis method can accurately diagnose ARDS, which is critical to its treatment. In the several subjects studied, the technology was found to indicate the presence of ARDS prior to the development of traditional indicators used for ARDS diagnosis, which opens up the potential for earlier interventions. The non-invasive nature of breath analysis may also allow for continuous monitoring of ARDS trajectories as evidenced by several subjects who demonstrated changing breathomic patterns from ARDS to non-ARDS statuses prior to changes in traditional indicators.

The potential to leverage exhaled breath for the identification of breathomic patterns used for early diagnosis, disease trajectory tracking, and outcome prediction monitoring of ARDS can have significant impacts on changing medical practices and improving patient outcomes. The device is envisioned for use for ARDS patients in emergency departments, operating rooms, and intensive care units. Additionally, our device holds the potential to dramatically improve the molecular characterization of ARDS and its competing diagnoses. The clinical ambiguity of ARDS diagnosis compared with histopathology impairs the field's ability to develop and study targeted, disease-specific therapies. Exhaled breath VOC analysis could significantly enhance our molecular phenotyping of patients with hypoxic respiratory failure, enable more straightforward diagnoses, and dramatically improve our ability to tailor treatments to patients with true ARDS pathophysiology.

4.5 References

1. Guiochon, G.; Guillemin, C. L., Gas chromatography. *Review of Scientific Instruments* **1990,** *61* (11), 3317-3339.
2. McNair, H. M.; Miller, J. M.; Snow, N. H., *Basic gas chromatography*. John Wiley & Sons: 2019.
3. Camino-Sánchez, F. J.; Zafra-Gómez, A.; Pérez-Trujillo, J. P.; Conde-González, J. E.; Marques, J. C.; Vílchez, J. L., Validation of a GC–MS/MS method for simultaneous determination of 86 persistent organic pollutants in marine sediments by pressurized liquid extraction followed by stir bar sorptive extraction. *Chemosphere* **2011,** *84* (7), 869-881.
4. Bristow, T.; Harrison, M.; Sims, M., The application of gas chromatography/atmospheric pressure chemical ionisation time-of-flight mass spectrometry to impurity identification in Pharmaceutical Development. *Rapid Communications in Mass Spectrometry* **2010,** *24* (11), 1673-1681.
5. Wolthers, B. G.; Kraan, G. P. B., Clinical applications of gas chromatography and gas chromatography–mass spectrometry of steroids. *Journal of Chromatography A* **1999,** *843* (1), 247-274.
6. de Koning, S.; Janssen, H.-G.; Brinkman, U. A. T., Modern Methods of Sample Preparation for GC Analysis. *Chromatographia* **2009,** *69* (1), 33.
7. Lara-Gonzalo, A.; Sánchez-Uría, J. E.; Segovia-García, E.; Sanz-Medel, A., Critical comparison of automated purge and trap and solid-phase microextraction for routine determination of volatile organic compounds in drinking waters by GC–MS. *Talanta* **2008,** *74* (5), 1455-1462.
8. Vreuls, J. J.; de Jong, G. J.; Brinkman, U. A. T., On-line coupling of liquid chromatography, capillary gas chromatography and mass spectrometry for the determination and identification of polycyclic aromatic hydrocarbons in vegetable oils. *Chromatographia* **1991,** *31* (3), 113-118.
9. Aragón, M.; Borrull, F.; Marcé, R. M., Thermal desorption-gas chromatography–mass spectrometry method to determine phthalate and organophosphate esters from air samples. *Journal of Chromatography A* **2013,** *1303*, 76-82.
10. Marcillo, A.; Jakimovska, V.; Widdig, A.; Birkemeyer, C., Comparison of two common adsorption materials for thermal desorption gas chromatography – mass spectrometry of biogenic volatile organic compounds. *Journal of Chromatography A* **2017,** *1514*, 16-28.
11. Jaillais, B.; Bertrand, V.; Auger, J., Cryo-trapping/SPME/GC analysis of cheese aroma. *Talanta* **1999,** *48* (4), 747-753.
12. Basic Overview on Gas Chromatography Columns. In *Analytical Separation Science*, pp 823-834.
13. McWilliam, I. G.; Dewar, R. A., Flame Ionization Detector for Gas Chromatography. *Nature* **1958,** *181* (4611), 760-760.
14. Camin, D. L.; King, R. W.; Shawhan, S. D., Capillary Gas Chromatography Using Micro-Volume Thermal Conductivity Detectors. *Anal. Chem.* **1964,** *36* (7), 1175-1178.
15. Klee, M. S., Chapter 12: Detectors. In *Gas Chromatography*, Poole, C. F., Ed. Elsevier: New York, 2012.
16. Sun, J.; Guan, F.; Cui, D.; Chen, X.; Zhang, L.; Chen, J., An improved photoionization detector with a micro gas chromatography column for portable rapid gas chromatography system. *Sens. Actuators B.* **2013,** *188*, 513– 518.

17. Akbar, M.; Restaino, M.; Agah, M., Chip-scale gas chromatography: From injection through detection. *Nat. Microsys. Nanoeng.* **2015,** *1*.
18. Zhu, H.; Nidetz, R.; Zhou, M.; Lee, J.; Buggaveeti, S.; Kurabayashi, K.; Fan, X., Flow-through microfluidic photoionization detectors for rapid and highly sensitive vapor detection. *Lab Chip* **2015,** *15* (14), 3021-3029.
19. Narayanan, S.; Rice, G.; Agah, M., A micro-discharge photoionization detector for micro-gas chromatography. *Microchim. Acta* **2014,** *181*, 493-499.
20. Cai, Q. Y.; Zellers, E. T., Dual-chemiresistor GC detector employing layer-protected metal nanocluster interfaces. *Anal. Chem.* **2002,** *74* (14), 3533-3539.
21. Lin, H. B.; Shih, J. S., Fullerene C60-cryptand coated surface acoustic wave quartz crystal sensor for organic vapors. *Sens. Actuators B: Chemical* **2003,** *92* (3), 243-254.
22. Lewis, P. R.; Manginell, R. P.; Adkins, D. R.; Kottenstette, R. J.; Wheeler, D. R.; Sokolowski, S. S.; Trudell, D. E.; Byrnes, J. E.; Okandan, M.; Bauer, J. M.; Manley, R. G.; Frye-Mason, G. C., Recent advancements in the gas-phase MicroChemLab. *IEEE Sens. J.* **2006,** *6* (3), 784-795.
23. Shopova, S. I.; White, I. M.; Sun, Y.; Zhu, H.; Fan, X.; Frye-Mason, G.; Thompson, A.; Ja, S.-j., On-Column Micro Gas Chromatography Detection with Capillary-Based Optical Ring Resonators. *Anal. Chem.* **2008,** *80*, 2232-2238.
24. Liu, J.; Sun, Y.; Fan, X., Highly versatile fiber-based optical Fabry-Pérot gas sensor. *Opt. Express* **2009,** *17* (4), 2731-2738.
25. Liu, J.; Sun, Y.; Howard, D. J.; Frye-Mason, G.; Thompson, A. K.; Ja, S.-j.; Wang, S.-K.; Mengjun Bai; Taub, H.; Almasri, M.; Fan, X., Fabry-Perot Cavity Sensors for Multipoint On-Column Micro Gas Chromatography Detection. *Anal. Chem.* **2010,** *82*, 4370–4375.
26. Sun, Y.; Liu, J.; Howard, D. J.; Fan, X.; Frye-Mason, G.; Ja, S.-j.; Thompson, A. K., Rapid tandem-column micro-gas chromatography based on optofluidic ring resonators with multi-point on-column detection. *Analyst* **2010,** *135*, 165-171.
27. Reddy, K.; Guo, Y.; Liu, J.; Lee, W.; Khaing Oo, M. K.; Fan, X., Rapid, sensitive, and multiplexed on-chip optical sensors for micro-gas chromatography. *Lab Chip* **2012,** *12*, 901-905.
28. Reddy, K.; Liu, J.; Khaing Oo, M. K.; Fan, X., Integrated Separation Columns and Fabry-Perot Sensors for Microgas Chromatography Systems. *IEEE JMEMS* **2013,** *22*, 1174-1179.
29. Scholten, K.; Fan, X.; Zellers, E. T., Microfabricated optofluidic ring resonator structures. *Appl. Phys. Lett.* **2011,** *99* (14), -.
30. Scholten, K.; Fan, X.; Zeller, E. T., A microfabricated optofluidic ring resonator for sensitive, high-speed detection of volatile organic compounds. *Lab Chip* **2014,** *14*, 3873-3880.
31. McCorkle, D. L.; Warmack, R. J.; Patel, S. V.; Mlsna, T.; Hunter, S. R.; Ferrell, T. L., Ethanol vapor detection in aqueous environments using micro-capacitors and dielectric polymers. *Sens. Actuators B: Chemical* **2005,** *107* (2), 892-903.
32. Patel, S. V.; Hobson, S. T.; Cemalovic, S.; Mlsna, T. E., Detection of methyl salicylate using polymer-filled chemicapacitors. *Talanta* **2008,** *76* (4), 872-877.
33. Wright, L. K.; Zellers, E. T., A nanoparticle-coated chemiresistor array as a microscale gas chromatograph detector for explosive marker compounds: flow rate and temperature effects. *Analyst* **2013,** *138* (22), 6860-6868.
34. Lee, C. Y.; Sharma, R.; Radadia, A. D.; Masel, R. I.; Strano, M. S., On-Chip Micro Gas Chromatograph Enabled by a Noncovalently Functionalized Single-Walled Carbon Nanotube Sensor Array. *Angew. Chem. Int. Ed.* **2008,** *47*, 5018-5021.

35. Kulkarni, G. S.; Reddy, K.; Zhong, Z.; Fan, X., Graphene nanoelectronic heterodyne sensor for rapid and sensitive vapour detection. *Nature Commun.* **2014,** *5*, 4376.
36. Grob, R. L.; Barry, E. F., *Modern practice of gas chromatography*. John Wiley & Sons: 2004.
37. Kulsing, C.; Nolvachai, Y.; Rawson, P.; Evans, D. J.; Marriott, P. J., Continuum in MDGC Technology: From Classical Multidimensional to Comprehensive Two-Dimensional Gas Chromatography. *Anal Chem* **2016,** *88* (7), 3529-3538.
38. Dallüge, J.; Beens, J.; Brinkman, U. A. T., Comprehensive two-dimensional gas chromatography: a powerful and versatile analytical tool. *J. Chromatogr. A* **2003,** *1000* (1–2), 69-108.
39. Marriott, P. J.; Chin, S.-T.; Maikhunthod, B.; Schmarr, H.-G.; Bieri, S., Multidimensional gas chromatography. *TrAC* **2012,** *34*, 1-21.
40. Seeley, J. V.; Seeley, S. K., Multidimensional Gas Chromatography: Fundamental Advances and New Applications. *Anal. Chem.* **2012,** *85* (2), 557-578.
41. Seeley, J. V.; Seeley, S. K., Multidimensional Gas Chromatography: Fundamental Advances and New Applications. *Anal. Chem.* **2013,** *85* (2), 557-578.
42. Chin, S.-T.; Marriott, P. J., Multidimensional gas chromatography beyond simple volatiles separation. *Chem. Comm.* **2014,** *50* (64), 8819-8833.
43. Edwards, M.; Mostafa, A.; Górecki, T., Modulation in comprehensive two-dimensional gas chromatography: 20 years of innovation. *Anal. Bioanal. Chem.* **2011,** *401* (8), 2335-2349.
44. Pursch, M.; Sun, K.; Winniford, B.; Cortes, H.; Weber, A.; McCabe, T.; Luong, J., Modulation techniques and applications in comprehensive two-dimensional gas chromatography (GC×GC). *Anal. Bioanal. Chem.* **2002,** *373* (6), 356-367.
45. Dallüge, J.; Beens, J.; Brinkman, U. A. T., Comprehensive two-dimensional gas chromatography: a powerful and versatile analytical tool. *J. Chromatogr. A* **2003,** *1000*, 69-108.
46. Marriott, P. J.; Kinghorn, R. M., New operational modes for multidimensional and comprehensive gas chromatography by using cryogenic modulation. *Journal of Chromatography A* **2000,** *866* (2), 203-212.
47. Ong, R. C.; Marriott, P. J., A review of basic concepts in comprehensive two-dimensional gas chromatography. *Journal of chromatographic science* **2002,** *40* (5), 276-291.
48. Peter Baugh, J., Advances and Changes in the Techniques of Multi-Dimensional and Comprehensive Chromatography and When Coupled with Mass Spectrometry. *J Anal Bioanal Tech* **2016,** *7* (323), 2.
49. Legrum, C.; Gracia-Moreno, E.; Lopez, R.; Potouridis, T.; Langen, J.; Slabizki, P.; Weiand, J.; Schmarr, H.-G., Quantitative analysis of 3-alkyl-2-methoxypyrazines in German Sauvignon blanc wines by MDGC–MS or MDGC–MS/MS for viticultural and enological studies. *European Food Research and Technology* **2014,** *239* (4), 549-558.
50. Regmi, B. P.; Agah, M., Micro Gas Chromatography: An Overview of Critical Components and Their Integration. *Analytical Chemistry* **2018,** *90* (22), 13133-13150.
51. Jerman, J. H.; Terry, S. C., A miniature gas chromatograph for atmospheric monitoring. *Environ. Int.* **1981,** *5* (2), 77-83.
52. Bond, E. J.; Dumas, T., A portable gas chromatograph for macro- and microdetermination of fumigants in the field. *J. Agric. Food Chem.* **1982,** *30* (5), 986-988.
53. Lorenzelli, L.; Benvenuto, A.; Adami, A.; Guarnieri, V.; Margesin, B.; Mulloni, V.; Vincenzi, D., Development of a gas chromatography silicon-based microsystem in clinical diagnostics. *Biosens. Bioelectron.* **2005,** *20* (10), 1968-1976.

54. Thompson, C. V.; Goedert, M. G., Field-Portable Instrumentation for Gas and Vapor Samples. In *Encyclopedia of Analytical Chemistry*, John Wiley & Sons, Ltd: 2006.
55. Ohira, S.-I.; Toda, K., Micro gas analyzers for environmental and medical applications. *Anal. Chim. Acta.* **2008,** *619* (2), 143-156.
56. Liu, X.; Pawliszyn, J., On-site environmental analysis by membrane extraction with a sorbent interface combined with a portable gas chromatograph system. *Int. J. Environ. Anal. Chem.* **2005,** *85* (15), 1189-1200.
57. Mohsen, Y.; Lahlou, H.; Sanchez, J.-B.; Berger, F.; Bezverkhyy, I.; Weber, G.; Bellat, J.-P., Development of a micro-analytical prototype for selective trace detection of orthonitrotoluene. *Microchem. J.* **2014,** *114*, 48-52.
58. Jian, R.-S.; Wang, T.-Y.; Song, L.-Y.; Kuo, C.-Y.; Tian, W.-C.; Lo, E.-W.; Lu, C.-J., Field investigations and dynamic measurements of process activity induced VOCs inside a semiconductor cleanroom. *Build. Environ.* **2015,** *94*, 287-295.
59. Akbar, M.; Shakeel, H.; Agah, M., GC-on-Chip: Integrated Column and Photo Ionization Detector. *Lab Chip* **2015,** *15*, 1748-1758.
60. Akbar, M.; Restaino, M.; Agah, M., Chip-scale gas chromatography: From injection through detection. *Microsyst. Nanoeng.* **2015,** *1*, 15039.
61. Yutao, Q.; Yogesh, B. G., iGC2 : an architecture for micro gas chromatographs utilizing integrated bi-directional pumps and multi-stage preconcentrators. *J. Micromech. Microeng.* **2014,** *24* (6), 065011.
62. Qin, Y.; Gianchandani, Y. B., iGC1: An Integrated Fluidic System for Gas Chromatography Including Knudsen Pump, Preconcentrator, Column, and Detector Microfabricated by a Three-Mask Process. *J. Microelectromech. Syst.* **2014,** *23* (4), 980-990.
63. Bulbul, A.; Kim, H., A bubble-based microfluidic gas sensor for gas chromatographs. *Lab Chip* **2015,** *15* (1), 94-104.
64. Hsieh, H.-C.; Kim, H., A miniature closed-loop gas chromatography system. *Lab Chip* **2016,** *16* (6), 1002-1012.
65. Jian, R.-S.; Huang, Y.-S.; Lai, S.-L.; Sung, L.-Y.; Lu, C.-J., Compact instrumentation of a μ-GC for real time analysis of sub-ppb VOC mixtures. *Microchem. J.* **2013,** *108*, 161–167.
66. Ali, S.; Ashraf-Khorassani, M.; Taylor, L. T.; Agah, M., MEMS-based semi-packed gas chromatography columns. *Sensors and Actuators B: Chemical* **2009,** *141* (1), 309-315.
67. Sun, J.; Cui, D.; Li, Y.; Zhang, L.; Chen, J.; Li, H.; Chen, X., A high resolution MEMS based gas chromatography column for the analysis of benzene and toluene gaseous mixtures. *Sensors and Actuators B: Chemical* **2009,** *141* (2), 431-435.
68. Agah, M.; Lambertus, G. R.; Sacks, R.; Wise, K., High-speed MEMS-based gas chromatography. *Journal of microelectromechanical systems* **2006,** *15* (5), 1371-1378.
69. Navaei, M.; Mahdavifar, A.; Dimandja, J.-M. D.; McMurray, G.; Hesketh, P. J., All silicon micro-GC column temperature programming using axial heating. *Micromachines* **2015,** *6* (7), 865-878.
70. Li, Y.; Du, X.; Wang, Y.; Tai, H.; Qiu, D.; Lin, Q.; Jiang, Y., Improvement of column efficiency in MEMS-Based gas chromatography column. *RSC Advances* **2014,** *4* (8), 3742-3747.
71. Radadia, A.; Salehi-Khojin, A.; Masel, R.; Shannon, M., The effect of microcolumn geometry on the performance of micro-gas chromatography columns for chip scale gas analyzers. *Sensors and Actuators B: Chemical* **2010,** *150* (1), 456-464.
72. Radadia, A. D.; Morgan, R. D.; Masel, R. I.; Shannon, M. A., Partially Buried Microcolumns for Micro Gas Analyzers. *Analytical Chemistry* **2009,** *81* (9), 3471-3477.

73. Nakai, T.; Nishiyama, S.; Shuzo, M.; Delaunay, J.; Yamada, I., Micro-fabricated semi-packed column for gas chromatography by using functionalized parylene as a stationary phase. *Journal of Micromechanics and Microengineering* **2009,** *19* (6), 065032.
74. MacNaughton, S. I.; Sonkusale, S., Gas Analysis System on Chip With Integrated Diverse Nanomaterial Sensor Array. *IEEE Sensors Journal* **2015,** *15* (6), 3500-3506.
75. Reidy, S.; Lambertus, G.; Reece, J.; Sacks, R., High-performance, static-coated silicon microfabricated columns for gas chromatography. *Analytical Chemistry* **2006,** *78* (8), 2623-2630.
76. Lambertus, G.; Elstro, A.; Sensenig, K.; Potkay, J.; Agah, M.; Scheuering, S.; Wise, K.; Dorman, F.; Sacks, R., Design, Fabrication, and Evaluation of Microfabricated Columns for Gas Chromatography. *Analytical Chemistry* **2004,** *76* (9), 2629-2637.
77. Terry, S. C.; Jerman, J. H.; Angell, J. B., A gas chromatographic air analyzer fabricated on a silicon wafer. *IEEE Transactions on Electron Devices* **1979,** *26* (12), 1880-1886.
78. Narayanan, S.; Alfeeli, B.; Agah, M., A micro gas chromatography chip with an embedded non-cascaded thermal conductivity detector. *Procedia Engineering* **2010,** *5*, 29-32.
79. Narayanan, S.; Agah, M., Fabrication and characterization of a suspended TCD integrated with a gas separation column. *Journal of Microelectromechanical Systems* **2013,** *22* (5), 1166-1173.
80. Deng, C.; Yang, X.; Li, N.; Huang, Y.; Zhang, X., A novel miniaturized flame ionization detector for portable gas chromatography. *Journal of chromatographic science* **2005,** *43* (7), 355-357.
81. Xu, P.; Li, X.; Yu, H.; Xu, T., Advanced nanoporous materials for micro-gravimetric sensing to trace-level bio/chemical molecules. *Sensors* **2014,** *14* (10), 19023-19056.
82. Yeo, L. Y.; Friend, J. R., Ultrafast microfluidics using surface acoustic waves. *Biomicrofluidics* **2009,** *3* (1), 012002.
83. Ballantine Jr, D. S.; Wohltjen, H., Surface acoustic wave devices for chemical analysis. *Analytical Chemistry* **1989,** *61* (11), 704A-715A.
84. Cheng, C.-S.; Chen, Y.-Q.; Lu, C.-J., Organic vapour sensing using localized surface plasmon resonance spectrum of metallic nanoparticles self assemble monolayer. *Talanta* **2007,** *73* (2), 358-365.
85. Chen, Y.-Q.; Lu, C.-J., Surface modification on silver nanoparticles for enhancing vapor selectivity of localized surface plasmon resonance sensors. *Sensors and Actuators B: Chemical* **2009,** *135* (2), 492-498.
86. Kulkarni, G. S.; Reddy, K.; Zhong, Z.; Fan, X., Graphene nanoelectronic heterodyne sensor for rapid and sensitive vapour detection. *Nature communications* **2014,** *5*, 4376.
87. Lee, C. Y.; Sharma, R.; Radadia, A. D.; Masel, R. I.; Strano, M. S., On‐Chip Micro Gas Chromatograph Enabled by a Noncovalently Functionalized Single‐Walled Carbon Nanotube Sensor Array. *Angewandte Chemie International Edition* **2008,** *47* (27), 5018-5021.
88. Steinecker, W. H.; Rowe, M.; Matzger, A.; Zellers, E. In *Chemiresistor array with nanocluster interfaces as a micro-GC detector*, TRANSDUCERS, Solid-State Sensors, Actuators and Microsystems, 12th International Conference on, 2003, IEEE: 2003; pp 1343-1346.
89. Zhong, Q.; Steinecker, W. H.; Zellers, E. T., Characterization of a high-performance portable GC with a chemiresistor array detector. *Analyst* **2009,** *134* (2), 283-293.
90. Kim, S. K.; Chang, H.; Zellers, E. T. In *Prototype micro gas chromatograph for breath biomarkers of respiratory disease*, TRANSDUCERS 2009 - 2009 International Solid-State Sensors, Actuators and Microsystems Conference, 21-25 June 2009; 2009; pp 128-131.

91. Qin, Y.; Gianchandani, Y. B., A fully electronic microfabricated gas chromatograph with complementary capacitive detectors for indoor pollutants. *Microsystems &Amp; Nanoengineering* **2016,** *2*, 15049.
92. Patel, S.; Mlsna, T.; Fruhberger, B.; Klaassen, E.; Cemalovic, S.; Baselt, D., Chemicapacitive microsensors for volatile organic compound detection. *Sensors and Actuators B: Chemical* **2003,** *96* (3), 541-553.
93. Mlsna, T. E.; Cemalovic, S.; Warburton, M.; Hobson, S. T.; Mlsna, D. A.; Patel, S. V., Chemicapacitive microsensors for chemical warfare agent and toxic industrial chemical detection. *Sensors and Actuators B: Chemical* **2006,** *116* (1-2), 192-201.
94. Sun, Y.; Fan, X., Optical ring resonators for biochemical and chemical sensing. *Analytical and bioanalytical chemistry* **2011,** *399* (1), 205-211.
95. Reddy, K.; Guo, Y.; Liu, J.; Lee, W.; Oo, M. K. K.; Fan, X., On-chip Fabry–Pérot interferometric sensors for micro-gas chromatography detection. *Sensors and Actuators B: Chemical* **2011,** *159* (1), 60-65.
96. Scholten, K.; Reddy, K.; Fan, X.; Zellers, E. T., Vapor discrimination by dual-laser reflectance sensing of a single functionalized nanoparticle film. *Analytical Methods* **2013,** *5* (16), 4268-4272.
97. Verner, P., Photoionization detection and its applications in gas chromatography. *J. Chromatogr.* **1984,** *300*, 249-264.
98. Rowe, B. L.; Toccalino, P. L.; Moran, M. J.; Zogorski, J. S.; Price, C. V., Occurrence and potential human-health relevance of volatile organic compounds in drinking water from domestic wells in the United States. *Environmental Health Perspectives* **2007,** *115* (11), 1539.
99. Kampa, M.; Castanas, E., Human health effects of air pollution. *Environ. Pollut.* **2008,** *151* (2), 362-367.
100. Risticevic, S.; Niri, V. H.; Vuckovic, D.; Pawliszyn, J., Recent developments in solid-phase microextraction. *Anal. Bioanal. Chem.* **2009,** *393* (3), 781-795.
101. Penza, M.; Cassano, G., Application of principal component analysis and artificial neural networks to recognize the individual VOCs of methanol/2-propanol in a binary mixture by SAW multi-sensor array. *Sens. Actuators, B* **2003,** *89* (3), 269-284.
102. Si, P.; Mortensen, J.; Komolov, A.; Denborg, J.; Møller, P. J., Polymer coated quartz crystal microbalance sensors for detection of volatile organic compounds in gas mixtures. *Anal. Chim. Acta* **2007,** *597* (2), 223-230.
103. Sundgren, H.; Lundström, I.; Winquist, F.; Lukkari, I.; Carlsson, R.; Wold, S., Evaluation of a multiple gas mixture with a simple MOSFET gas sensor array and pattern recognition. *Sens. Actuators, B* **1990,** *2* (2), 115-123.
104. Feng, L.; Musto, C. J.; Kemling, J. W.; Lim, S. H.; Suslick, K. S., A colorimetric sensor array for identification of toxic gases below permissible exposure limits. *Chem. Commun.* **2010,** *46* (12), 2037-2039.
105. Smith, P. A.; Koch, D.; Hook, G. L.; Erickson, R. P.; Lepage, C. R. J.; Wyatt, H. D.; Betsinger, G.; Eckenrode, B. A., Detection of gas-phase chemical warfare agents using field-portable gas chromatography–mass spectrometry systems: instrument and sampling strategy considerations. *TrAC, Trends Anal. Chem.* **2004,** *23* (4), 296-306.
106. Lee, M.-R.; Chang, C.-M.; Dou, J., Determination of benzene, toluene, ethylbenzene, xylenes in water at sub-ng l^{-1} levels by solid-phase microextraction coupled to cryo-trap gas chromatography–mass spectrometry. *Chemosphere* **2007,** *69* (9), 1381-1387.

107. Mahmoud, M. E.; AlBishri, H. M., Identification of dissolved organic species in non-drinking tap water by solid-phase extraction and gas chromatography–mass spectrometry. *J. Saudi Chem. Soc.* **2010,** *14* (1), 105-115.
108. Zoccolillo, L.; Amendola, L.; Cafaro, C.; Insogna, S., Improved analysis of volatile halogenated hydrocarbons in water by purge-and-trap with gas chromatography and mass spectrometric detection. *J. Chromatogr. A* **2005,** *1077* (2), 181-187.
109. Santos, F.; Galceran, M., Modern developments in gas chromatography–mass spectrometry-based environmental analysis. *J. Chromatogr. A* **2003,** *1000* (1), 125-151.
110. Aragon, P.; Atienza, J.; Climent, M., Analysis of organic compounds in air: a review. *Crit. Rev. Anal. Chem* **2000,** *30* (2-3), 121-151.
111. Dewulf, J.; Van Langenhove, H., Anthropogenic volatile organic compounds in ambient air and natural waters: a review on recent developments of analytical methodology, performance and interpretation of field measurements. *J. Chromatogr. A* **1999,** *843* (1), 163-177.
112. Ji, J.; Deng, C.; Shen, W.; Zhang, X., Field analysis of benzene, toluene, ethylbenzene and xylene in water by portable gas chromatography–microflame ionization detector combined with headspace solid-phase microextraction. *Talanta* **2006,** *69* (4), 894-899.
113. Zhu, H.; Nidetz, R.; Zhou, M.; Lee, J.; Buggaveeti, S.; Kurabayashi, K.; Fan, X., Flow-through microfluidic photoionization detectors for rapid and highly sensitive vapor detection. *Lab Chip* **2015,** *15* (14), 3021-9.
114. Garg, A.; Akbar, M.; Vejerano, E.; Narayanan, S.; Nazhandali, L.; Marr, L. C.; Agah, M., Zebra GC: A mini gas chromatography system for trace-level determination of hazardous air pollutants. *Sens. Actuators, B* **2015,** *212*, 145-154.
115. Antoniou, C. V.; Koukouraki, E. E.; Diamadopoulos, E., Determination of chlorinated volatile organic compounds in water and municipal wastewater using headspace–solid phase microextraction–gas chromatography. *J. Chromatogr. A* **2006,** *1132* (1), 310-314.
116. Techniquea, A. P., METHOD 8260B VOLATILE ORGANIC COMPOUNDS BY GAS CHROMATOGRAPHY/MASS SPECTROMETRY (GC/MS). **1996**.
117. No, C. C., METHOD 5030C PURGE-AND-TRAP FOR AQUEOUS SAMPLES. **2003**.
118. Contreras, J. A.; Murray, J. A.; Tolley, S. E.; Oliphant, J. L.; Tolley, H. D.; Lammert, S. A.; Lee, E. D.; Later, D. W.; Lee, M. L., Hand-portable gas chromatograph-toroidal ion trap mass spectrometer (GC-TMS) for detection of hazardous compounds. *J. Am. Soc. Mass. Spectrom.* **2008,** *19* (10), 1425-1434.
119. Thompson, C. V.; Goedert, M. G., Field‐Portable Instrumentation for Gas and Vapor Samples. *Encycl. Anal. Chem.* **2009**.
120. Staples, E. J.; Matsuda, T.; Viswanathan, S. In *Real time environmental screening of air, water and soil matrices using a novel field portable GC/SAW system*, Environmental Strategies for the 21st Century, Asia Pacific Conference, 1998; pp 8-10.
121. Watson, G. W.; Staples, E. J.; Viswanathan, S., Performance evaluation of a surface acoustic wave analyzer to measure VOCs in air and water. *Environmental progress* **2003,** *22* (3), 215-226.
122. Kim, S. K.; Chang, H.; Zellers, E. T., Microfabricated gas chromatograph for the selective determination of trichloroethylene vapor at sub-parts-per-billion concentrations in complex mixtures. *Anal. Chem.* **2011,** *83* (18), 7198-7206.
123. Haghighi, F.; Talebpour, Z.; Sanati-Nezhad, A., Through the years with on-a-chip gas chromatography: a review. *Lab Chip* **2015,** *15*, 2559-2575.

124. Segal, A.; Górecki, T.; Mussche, P.; Lips, J.; Pawliszyn, J., Development of membrane extraction with a sorbent interface–micro gas chromatography system for field analysis. *J. Chromatogr. A* **2000,** *873* (1), 13-27.
125. Qin, Y.; Gianchandani, Y. B., iGC1: An Integrated Fluidic System for Gas Chromatography Including Knudsen Pump, Preconcentrator, Column, and Detector Microfabricated by a Three-Mask Process. *J. Microelectromech. Syst.* **2014,** *23* (4), 980-990.
126. Akbar, M.; Narayanan, S.; Restaino, M.; Agah, M., A purge and trap integrated microGC platform for chemical identification in aqueous samples. *Analyst* **2014,** *139* (13), 3384-3392.
127. Groves, W.; Grey, A.; O'shaughnessy, P., Surface acoustic wave (SAW) microsensor array for measuring VOCs in drinking water. *J. Environ. Monit.* **2006,** *8* (9), 932-941.
128. Bulbul, A.; Kim, H., A bubble-based microfluidic gas sensor for gas chromatographs. *Lab Chip* **2015,** *15*, 94-104.
129. Zhou, M.; Lee, J.; Zhu, H.; Nidetz, R.; Kurabayashi, K.; Fan, X., A fully automated portable gas chromatography for sensitive and rapid quantification of volatile organic compounds in water. *RSC Adv.* **2016,** *6*.
130. MING, H. T. Novel microextraction techniques for aqueous environmental analysis. 2012.
131. Allonier, A.-S.; Khalanski, M.; Bermond, A.; Camel, V., Determination of trihalomethanes in chlorinated sea water samples using a purge-and-trap system coupled to gas chromatography. *Talanta* **2000,** *51* (3), 467-477.
132. Saridara, C.; Brukh, R.; Mitra, S., Development of continuous on‐line purge and trap analysis. *J. Sep. Sci.* **2006,** *29* (3), 446-452.
133. Menéndez, J. F.; Sánchez, M. F.; Uría, J. S.; Martínez, E. F.; Sanz-Medel, A., Static headspace, solid-phase microextraction and headspace solid-phase microextraction for BTEX determination in aqueous samples by gas chromatography. *Anal. Chim. Acta.* **2000,** *415* (1), 9-20.
134. Sander, R., Compilation of Henry's law constants (version 4.0) for water as solvent. *Atmos. Chem. Phys.* **2015,** *15* (8), 4399-4981.
135. Ehrmann, E.; Dharmasena, H.; Carney, K.; Overton, E., Novel column heater for fast capillary gas chromatography. *J. Chromatogr. Sci.* **1996,** *34* (12), 533-539.
136. Reidy, S.; George, D.; Agah, M.; Sacks, R., Temperature-programmed GC using silicon microfabricated columns with integrated heaters and temperature sensors. *Anal. Chem.* **2007,** *79* (7), 2911-2917.
137. Gvirtzman, H.; Gorelick, S. M., The concept of in-situ vapor stripping for removing VOCs from groundwater. *Transp. Porous Media* **1992,** *8* (1), 71-92.
138. Driss, M.; Bouguerra, M., Analysis of volatile organic compounds in water by purge-and-trap and gas chromatography techniques: operational parameters optimization of the purge step. *Int. J. Environ. Anal. Chem.* **1991,** *45* (3), 193-204.
139. Tian, W.-C.; Pang, S. W.; Lu, C.-J.; Zellers, E. T., Microfabricated preconcentrator-focuser for a microscale gas chromatograph. *J. Microelectromech. Syst.* **2003,** *12* (3), 264-272.
140. Tian, W.-C.; Chan, H. K.; Lu, C.-J.; Pang, S. W.; Zellers, E. T., Multiple-stage microfabricated preconcentrator-focuser for micro gas chromatography system. *J. Microelectromech. Syst.* **2005,** *14* (3), 498-507.
141. Whiting, J. J.; Fix, C. S.; Anderson, J. M.; Staton, A. W.; Manginell, R. P.; Wheeler, D. R.; Myers, E. B.; Roukes, M. L.; Simonson, R. J. In *High-speed two-dimensional gas chromatography using microfabricated GC columns combined with nanoelectromechanical mass*

sensors, TRANSDUCERS 2009 - 2009 International Solid-State Sensors, Actuators and Microsystems Conference, 21-25 June 2009; 2009; pp 1666-1669.
142. Kim, S. J.; Reidy, S. M.; Block, B. P.; Wise, K. D.; Zellers, E. T.; Kurabayashi, K., Microfabricated thermal modulator for comprehensive two-dimensional micro gas chromatography: design, thermal modeling, and preliminary testing. *Lab chip* **2010,** *10* (13), 1647-1654.
143. Serrano, G.; Dibyadeep, P.; Kim, S.-J.; Kurabayashi, K.; Zellers, E. T., Comprehensive Two-Dimensional Gas Chromatographic Separations with a Microfabricated Thermal Modulator. *Anal. Chem.* **2012,** *84* (16), 6973–6980.
144. Kim, S.-J.; Serrano, G.; Wise, K. D.; Kurabayashi, K.; Zellers, E. T., Evaluation of a Microfabricated Thermal Modulator for Comprehensive Two-Dimensional Microscale Gas Chromatography. *Anal. Chem.* **2011,** *83* (14), 5556-5562.
145. Collin, W. R.; Bondy, A.; Paul, D.; Kurabayashi, K.; Zellers, E. T., μGC × μGC: Comprehensive Two-Dimensional Gas Chromatographic Separations with Microfabricated Components. *Anal. Chem.* **2015,** *87*, 1630−1637.
146. Blumberg, L. M., Potentials and Limits of Comprehensive GC X GC. *Anal. Chem.* **2002,** *74*, 503A.
147. Blumberg, L. M.; David, F.; Klee, M. S.; Sandra, P., Comparison of one-dimensional and comprehensive two-dimensional separations by gas chromatography. *J. Chromatogr. A* **2008,** *1188* (2), 2-16.
148. Inc., R. S., *The PID Handbook: Theory and applications of direct reading photoionization detectors (3rd Edn.)*. San Jose, CA, 2013; Vol. 3.
149. Langhorst, M. L., Photoionization Detector Sensitivity of Organic Compounds. *J. Chromatogr. Sci.* **1981,** *19* (2), 98-103.
150. Freedman, A. N., Photoionization detector response. *J. Chromatogr. A* **1982,** *236* (1), 11-15.
151. Drummond, I., On-the-Fly Calibration of Direct Reading Photoionization Detectors. *American Industrial Hygiene Association Journal* **1997,** *58* (11), 820-822.
152. Peng, F. M.; Xie, P. H.; Shi, Y. G.; Wang, J. D.; Liu, W. Q.; Li, H. Y., Photoionization detector for portable rapid GC. *Chromatographia* **2007,** *65* (5-6), 331-336.
153. Davenport, J. N.; Adlard, E. R., Photoionization detectors for gas chromatography. *J. Chromatogr. A* **1984,** *290*, 13-32.
154. Edgett, L. B.; Stotlar, S. C. In *Study Of Possible Solarization - Related Impurities In CaF2 And Other Fluorides*, 1985; pp 134-139.
155. Driscoll, J. N., Evaluation of a new photoionization detector for organic compounds. *J. Chromatogr. A* **1977,** *134* (1), 49-55.
156. Freedman, A. N., The photoionization detector: Theory, performance and application as a low-level monitor of oil vapour. *J. Chromatogr. A* **1980,** *190* (2), 263-273.
157. Blomberg, J.; Schoenmakers, P. J.; Beens, J.; Tijssen, R., Compehensive two-dimensional gas chromatography (GC×GC) and its applicability to the characterization of complex (petrochemical) mixtures. *J. High Resolut. Chromatogr.* **1997,** *20* (10), 539-544.
158. Zeng, Z.-D.; Hugel, H. M.; Marriott, P. J., Simultaneous estimation of retention times of overlapping primary peaks in comprehensive two-dimensional GC. *J Sep. Sci.* **2013,** *36* (17), 2728-2737.

159. Kong, H.; Ye, F.; Lu, X.; Guo, L.; Tian, J.; Xu, G., Deconvolution of overlapped peaks based on the exponentially modified Gaussian model in comprehensive two-dimensional gas chromatography. *J. Chromatogr. A* **2005,** *1086* (1–2), 160-164.
160. Jeansonne, M. S.; Foley, J. P., Review of the Exponentially Modified Gaussian (EMG) Function Since 1983. *J. Chromatogr. Sci.* **1991,** *29* (6), 258-266.
161. Jung, K. H.; Yun, S. J.; Kang, S. H., Characterization of peak shape parameters with normal and derivative chromatograms. *Anal. Chem.* **1984,** *56* (3), 457-462.
162. Kallio, M.; Hyötyläinen, T., Quantitative aspects in comprehensive two-dimensional gas chromatography. *J. Chromatogr. A* **2007,** *1148* (2), 228-235.
163. Siegler, W. C.; Crank, J. A.; Armstrong, D. W.; Synovec, R. E., Increasing selectivity in comprehensive three-dimensional gas chromatography via an ionic liquid stationary phase column in one dimension. *J. Chromatogr. A* **2010,** *1217* (18), 3144-3149.
164. Sinha, A. E.; Prazen, B. J.; Fraga, C. G.; Synovec, R. E., Valve-based comprehensive two-dimensional gas chromatography with time-of-flight mass spectrometric detection: instrumentation and figures-of-merit. *J. Chromatogr. A* **2003,** *1019* (1–2), 79-87.
165. Fitz, B. D.; Wilson, R. B.; Parsons, B. A.; Hoggard, J. C.; Synovec, R. E., Fast, high peak capacity separations in comprehensive two-dimensional gas chromatography with time-of-flight mass spectrometry. *J. Chromatogr. A* **2012,** *1266*, 116-123.
166. Klee, M. S.; Cochran, J.; Merrick, M.; Blumberg, L. M., Evaluation of conditions of comprehensive two-dimensional gas chromatography that yield a near-theoretical maximum in peak capacity gain. *J. Chromatogr. A* **2015,** *1383*, 151-159.
167. Lee, J.; Zhou, M.; Zhu, H.; Nidetz, R.; Kurabayashi, K.; Fan, X., In situ calibration of micro-photoionization detectors in a multi-dimensional micro-gas chromatography system. *Analyst* **2016,** *141* (13), 4100-4107.
168. Rubenfeld, G. D.; Caldwell, E.; Peabody, E.; Weaver, J.; Martin, D. P.; Neff, M.; Stern, E. J.; Hudson, L. D., Incidence and outcomes of acute lung injury. *N. Engl. J. Med.* **2005,** *353* (16), 1685-1693.
169. Zambon M; Vincent J. L, Mortality rates for patients with acute lung injury/ARDS have decreased over time. *Chest* **2008,** *133* (5), 1120-1127.
170. Crader, K. M.; Repine, J. J. D.; Repine, J. E., Breath Biomarkers and the Acute Respiratory Distress Syndrome *J. Pulmonar. Respirat. Med.* **2012,** *2* (1), 111.
171. Herridge, M. S.; Tansey, C. M.; Matte, A.; Tomlinson, G.; Diaz-Granados, N.; Cooper, A.; Guest, C. B.; Mazer, C. D.; Mehta, S.; Stewart, T. E.; Kudlow, P.; Cook, D.; Slutsky, A. S.; Cheung, A. M., Functional disability 5 years after acute respiratory distress syndrome. *N. Engl. J. Med.* **2011,** *364* (14), 1293-1304.
172. Mikkelsen, M. E.; Christie, J. D.; Lanken, P. N.; Biester, R. C.; Thompson, B. T.; Bellamy, S. L.; Localio, A. R.; Demissie, E.; Hopkins, R. O.; Angus, D. C., The adult respiratory distress syndrome cognitive outcomes study: long-term neuropsychological function in survivors of acute lung injury. *Am. J. Respir. Crit. Care Med.* **2012,** *185* (12), 1307-1315.
173. Dasta, J. F.; McLaughlin, T. P.; Mody, S. H.; Piech, C. T., Daily cost of an intensive care unit day: the contribution of mechanical ventilation. *Crt. Care Med.* **2005,** *33*, 1266-1271.
174. Hudson, L. D.; Milberg, J. A.; Anardi, D.; Maunder, R. J., Clinical risks for development of the acute respiratory distress syndrome. *Am. J. Respir. Crit. Care Med.* **1995,** *151* (2 Pt 1), 293-301.
175. Gajic, O.; Dabbagh, O.; Park, P. K.; Adesanya, A.; Chang, S. Y.; Hou, P.; Anderson, H.; Hoth, J. J.; Mikkelsen, M. E.; Gentile, N. T.; Gong, M. N.; Talmor, D.; Bajwa, E.; Watkins, T. R.;

Festic, E.; Yilmaz, M.; Iscimen, R.; Kaufman, D. A.; Esper, A. M.; Sadikot, R.; Douglas, I.; Sevransky, J.; Malinchoc, M., Early Identification of Patients at Risk of Acute Lung Injury. *Am. J. Respir. Crit. Care Med.* **2011,** *183* (4), 462-470.
176. Ranieri, V. M.; Rubenfeld, G. D.; Thompson, B. T.; Ferguson, N. D.; Caldwell, E.; Fan, E.; Camporota, L.; Slutsky, A. S., Acute respiratory distress syndrome: the Berlin Definition. *JAMA* **2012,** *307* (23), 2526-33.
177. Thille, A. W.; Esteban, A.; Fernandez-Segoviano, P.; Rodriguez, J. M.; Aramburu, J. A.; Penuelas, O.; Cortes-Puch, I.; Cardinal-Fernandez, P.; Lorente, J. A.; Frutos-Vivar, F., Comparison of the Berlin definition for acute respiratory distress syndrome with autopsy. *Am. J. Respir. Crit. Care Med.* **2013,** *187* (7), 761-767.
178. Kao, K.-C.; Hu, H.-C.; Chang, C.-H.; Hung, C.-Y.; Chiu, L.-C.; Li, S.-H.; Lin, S.-W.; Chuang, L.-P.; Wang, C.-W.; Li, L.-F.; Chen, N.-H.; Yang, C.-T.; Huang, C.-C.; Tsai, Y.-H., Diffuse alveolar damage associated mortality in selected acute respiratory distress syndrome patients with open lung biopsy. *Crit. Care* **2015,** *19*, 228.
179. Carpenter, C. T.; Price, P. V.; Christman, B. W., Exhaled Breath Condensate Isoprostanes Are Elevated in Patients With Acute Lung Injury or ARDS. *Chest* **1998,** *114* (6), 1653-1659.
180. Rahimpour, E.; Khoubnasabjafari, M.; Jouyban-Gharamaleki, V.; Jouyban, A., Non-volatile compounds in exhaled breath condensate: review of methodological aspects. *Analytical and Bioanalytical Chemistry* **2018,** *410* (25), 6411-6440.
181. McNeil, J. B.; Shaver, C. M.; Kerchberger, V. E.; Russell, D. W.; Grove, B. S.; Warren, M. A.; Wickersham, N. E.; Ware, L. B.; McDonald, W. H.; Bastarache, J. A., Novel Method for Noninvasive Sampling of the Distal Airspace in Acute Respiratory Distress Syndrome. *American journal of respiratory and critical care medicine* **2018,** *197* (8), 1027-1035.
182. Alkhouri, N.; Singh, T.; Alsabbagh, E.; Guirguis, J.; Chami, T.; Hanouneh, I.; Grove, D.; Lopez, R.; Dweik, R., Isoprene in the Exhaled Breath is a Novel Biomarker for Advanced Fibrosis in Patients with Chronic Liver Disease: A Pilot Study. *Clin. Transl. Gastroenterol.* **2015,** *6* (9), 1-7.
183. Miekisch, W.; Schubert, J. K.; Noeldge-Schomburg, G. F. E., Diagnostic potential of breath analysis-focus on volatile organic compounds. *Clin. Chim. Acta* **2004,** *347*, 25–39.
184. Gordon, S. M.; Szidon, J. P.; Krotoszynski, B. K.; Gibbons, R. D.; O'Neill, H. J., Volatile organic compounds in exhaled air from patients with lung cancer. *Clin. Chem.* **1985,** *31* (8), 1278-1282.
185. O'Neill, H. J.; Gordon, S. M.; O'Neill, M. H.; Gibbons, R. D.; Szidon, J. P., A computerized classification technique for screening for the presence of breath biomarkers in lung cancer. *Clin. Chem.* **1988,** *34* (8), 1613-1618.
186. Ware, L. B.; Koyama, T.; Zhao, Z.; Janz, D. R.; Wickersham, N.; Bernard, G. R.; May, A. K.; Calfee, C. S.; Matthay, M. A., Biomarkers of lung epithelial injury and inflammation distinguish severe sepsis patients with acute respiratory distress syndrome. *Crit. Care* **2013,** *17* (5), R253.
187. Bos, L. D. J.; Weda, H.; Wang, Y. Y.; Knobel, H. H.; Nijsen, T. M. E.; Vink, T. J.; Zwinderman, A. H.; Sterk, P. J.; Schultz, M. J., Exhaled breath metabolomics as a noninvasive diagnostic tool for acute respiratory distress syndrome. *Eur. Respir. J.* **2014,** *44* (1), 188-197.
188. Bos, L. D.; Schultz, M. J.; Sterk, P. J., Exhaled breath profiling for diagnosing acute respiratory distress syndrome. *BMC Pulm. Med.* **2014,** *14*, 72.
189. Bos, L. D. J., Diagnosis of acute respiratory distress syndrome by exhaled breath analysis. *Ann. Transl. Med.* **2018,** *6* (2), 33.

190. Saalberg, Y.; Wolff, M., VOC breath biomarkers in lung cancer. *Clinica Chimica Acta* **2016,** *459*, 5-9.
191. Cao, W.; Duan, Y., Current Status of Methods and Techniques for Breath Analysis. *Critical Reviews in Analytical Chemistry* **2007,** *37* (1), 3-13.
192. John V. Seeley; Seeley., S. K., Multidimensional Gas Chromatography: Fundamental Advances and New Applications. *Anal. Chem.* **2012,** *85* (2), 557-578.
193. Jens Dallüge; Jan Beens; Udo A.Th. Brinkman, Comprehensive two-dimensional gas chromatography: a powerful and versatile analytical tool. *J. Chromatogr. A* **2003,** *1000*, 69-108.
194. Ma, H.; Li, X.; Chen, J.; Wang, H.; Cheng, T.; Chen, K.; Xu, S., Analysis of human breath samples of lung cancer patients and healthy controls with solid-phase microextraction (SPME) and flow-modulated comprehensive two-dimensional gas chromatography (GC X GC). *Anal. Methods* **2014,** *6*, 6841-6849.
195. Beccaria, M.; Bobak, C.; Maitshotlo, B.; Mellors, T. R.; Purcaro, G.; Franchina, F. A.; Rees, C. A.; Nasir, M.; Black, A.; Hill, J. E., Exhaled human breath analysis in active pulmonary tuberculosis diagnostics by comprehensive gas chromatography-mass spectrometry and chemometric techniques. *J. Breath Res.* **2019,** *13*, 016005.
196. Phillips, M.; Cataneo, R. N.; Chaturvedi, A.; Kaplan, P. D.; Libardoni, M.; Mundada, M.; Patel, U.; Zhang, X., Detection of an Extended Human Volatome with Comprehensive Two-Dimensional Gas Chromatography Time-of-Flight Mass Spectrometry. *PLOS ONE* **2013,** *8*, e75274.
197. Storer, M.; Curry, K.; Squire, M.; Kingham, S.; Epton, M., Breath testing and personal exposure--SIFT-MS detection of breath acetonitrile for exposure monitoring. *J. Breath Res.* **2015,** *9* (3), 036006.
198. Smith, D.; Spanel, P., SIFT-MS and FA-MS methods for ambient gas phase analysis: developments and applications in the UK. *Analyst* **2015,** *140* (8), 2573-91.
199. Spanel, P.; Smith, D., Progress in SIFT-MS: breath analysis and other applications. *Mass Spectrom Rev* **2011,** *30* (2), 236-67.
200. Cumeras, R.; Figueras, E.; Davis, C. E.; Baumbach, J. I.; Gràciaa, I., Review on Ion Mobility Spectrometry. Part 1: current instrumentation. *Analyst* **2015,** *140*, 1376-1390.
201. Covington, J. A.; van der Schee, M. P.; Edge, A. S.; Boyle, B.; Savage, R. S.; Arasaradnam, R. P., The application of FAIMS gas analysis in medical diagnostics. *Analyst* **2015,** *140* (20), 6775-81.
202. Nakhleh, M. K.; Amal, H.; Jeries, R.; Broza, Y. Y.; Aboud, M.; Gharra, A.; Ivgi, H.; Khatib, S.; Badarneh, S.; Har-Shai, L.; Glass-Marmor, L.; Lejbkowicz, I.; Miller, A.; Badarny, S.; Winer, R.; Finberg, J.; Cohen-Kaminsky, S.; Perros, F.; Montani, D.; Girerd, B.; Garcia, G.; Simonneau, G.; Nakhoul, F.; Baram, S.; Salim, R.; Hakim, M.; Gruber, M.; Ronen, O.; Marshak, T.; Doweck, I.; Nativ, O.; Bahouth, Z.; Shi, D. Y.; Zhang, W.; Hua, Q. L.; Pan, Y. Y.; Tao, L.; Liu, H.; Karban, A.; Koifman, E.; Rainis, T.; Skapars, R.; Sivins, A.; Ancans, G.; Liepniece-Karele, I.; Kikuste, I.; Lasina, I.; Tolmanis, I.; Johnson, D.; Millstone, S. Z.; Fulton, J.; Wells, J. W.; Wilf, L. H.; Humbert, M.; Leja, M.; Peled, N.; Haick, H., Diagnosis and Classification of 17 Diseases from 1404 Subjects via Pattern Analysis of Exhaled Molecules. *ACS Nano* **2017,** *11* (1), 112-125.
203. Nuria Queralto; Anders N Berliner; Brett Goldsmith; Raymond Martino; Paul Rhodes; Sung H Lim, Detecting cancer by breath volatile organic compound analysis: a review of array-based sensors. *J. Breath Res.* **2014,** *8* (2), 027112.

204. Tangerman, A.; Winkel, E. G., The portable gas chromatograph OralChroma™: a method of choice to detect oral and extra-oral halitosis. *Journal of Breath Research* **2008,** *2* (1), 017010-017015.
205. Phillips, M.; Cataneo, R. N.; Saunders, C.; Hope, P.; Schmitt, P.; Wai, J., Volatile biomarkers in the breath of women with breast cancer. *Journal of Breath Research* **2010,** *4* (2), 026003-026011.
206. Phillips, M.; Basa-Dalay, V.; Bothamley, G.; Cataneo, R. N.; Lam, P. K.; Natividad, M. P. R.; Schmitt, P.; Wai, J., Breath biomarkers of active pulmonary tuberculosis. *Tuberculosis* **2010,** *90* (2), 145-151.
207. Moser, B.; Bodrogi, F.; Eibl, G.; Lechner, M.; Rieder, J.; Lirk, P., Mass spectrometric profile of exhaled breath—field study by PTR-MS. *Respiratory Physiology & Neurobiology* **2005,** *145* (2), 295-300.
208. Cai, X.; Chen, L.; Kang, T.; Tang, Y.; Lim, T.; Xu, M.; Hui, H., A Prediction Model with a Combination of Variables for Diagnosis of Lung Cancer. *Medical science monitor : international medical journal of experimental and clinical research* **2017,** *23*, 5620-5629.
209. Lee, J.; Zhou, M.; Zhu, H.; Nidetz, R.; Kurabayashi, K.; Fan, X., Fully Automated Portable Comprehensive 2-Dimensional Gas Chromatography Device. *Anal. Chem.* **2016,** *88*, 10266-10274.
210. Zhu, H.; Nidetz, R.; Zhou, M.; Lee, J.; Buggaveeti, S.; Kurabayashi, K.; Fan, X., Flow-through Microfluidic Photoionization Detectors for Rapid and Highly Sensitive Vapor Detection. *Lab Chip* **2015,** *15*, 3021-3029.
211. Sjoding, M. W.; Hofer, T. P.; Co, I.; Courey, A.; Cooke, C. R.; Iwashyna, T. J., Interobserver Reliability of the Berlin ARDS Definition and Strategies to Improve the Reliability of ARDS Diagnosis. *Chest* **2018,** *153*, 361-367.
212. Andrade, L.; Manolakos, E. S., Signal background estimation and baseline correction algorithms for accurate DNA sequencing. *J. VLSI Sig. Proc. Syst.* **2003,** *35*, 229-243.
213. Zhang, Z. M.; Chen, S.; Liang, Y. Z., Baseline correction using adaptive iteratively reweighted penalized least squares. *Analyst* **2010,** *135*, 1138-1146.
214. Morris, J. S.; Coombes, K. R.; Koomen, J.; Baggerly, K. A.; Kobayashi, R., Feature extraction and quantification for mass spectrometry in biomedical applications using the mean spectrum. *Bioinformatics* **2005,** *21*, 1764-1775.
215. Yasui, Y.; Pepe, M.; Thompson, M. L.; Adam, B. L.; Wright Jr., G. L.; Qu, Y.; Potter, J. D.; Winget, M.; Thornquist, M.; Feng, Z., A data-analytic strategy for protein biomarker discovery: profiling of high-dimensional proteomic data for cancer detection. *Biostatistics* **2003,** *4*, 449-463.
216. Donoho, D. L.; Johnstone, I. M., Adapting to unknown smoothness via wavelet shrinkage. .J. Am. Stat. Assoc**1995,** *90*, 1200-1224.
217. Strang, G.; Nguyen, T., *Wavelets and Filter Banks*. Wellesley-Cambridge Press: Wellesley, MA, 1996.
218. Coombes, K. R.; Tsavachidis, S.; Morris, J. S.; Baggerly, K. A.; Hung, M. C.; Kuerer, H. M., Improved peak detection and quantification of mass spectrometry data acquired from surface-enhanced laser desorption and ionization by denoising spectra with the undecimated discrete wavelet transform. *Proteomics* **2005,** *5*, 4107-4117.
219. Liang, Y. Z.; Xie, P. S.; F. Chau, Chromatographic fingerprinting and related chemometric techniques for quality control of traditional Chinese medicines. *J. Sep. Sci.* **2010,** *33*, 410-421.

220. Tomasi, G.; van den Berg, F.; Andersson, C., Correlation optimized warping and dynamic time warping as preprocessing methods for chromatographic data. *J. Chemom.* **2004,** *18*, 231-241.
221. Smolinska, A.; Hauschild, A. C.; Fijten, R. R. R.; Dallinga, J. W.; Baumbach, J.; van Schooten, F. J., Current breathomics-a review on data pre-processing techniques and machine learning in metabolomics breath analysis. *J. Breath Res.* **2014,** *8*, 027105.
222. Wang, C.; Li, M.; Jiang, H.; Tong, H.; Feng, Y.; Wang, Y.; Pi, X.; Guo, L.; Nie, M.; Feng, H.; Li, E., Comparative Analysis of VOCs in Exhaled Breath of Amyotrophic Lateral Sclerosis and Cervical Spondylotic Myelopathy Patients. *Scientific Reports* **2016,** *6*, 26120.
223. Pereira, J.; Porto-Figueira, P.; Cavaco, C.; Taunk, K.; Rapole, S.; Dhakne, R.; Nagarajaram, H.; Câmara, J. S., Breath Analysis as a Potential and Non-Invasive Frontier in Disease Diagnosis: An Overview. *Metabolites* **2015,** *5* (1), 3-55.
224. Smolinska, A.; Klaassen, E. M. M.; Dallinga, J. W.; van de Kant, K. D. G.; Jobsis, Q.; Moonen, E. J. C.; van Schayck, O. C. P.; Dompeling, E.; van Schooten, F. J., Profiling of Volatile Organic Compounds in Exhaled Breath As a Strategy to Find Early Predictive Signatures of Asthma in Children. *PLOS ONE* **2014,** *9* (4), e95668.
225. Wang, C.; Feng, Y.; Wang, M.; Pi, X.; Tong, H.; Wang, Y.; Zhu, L.; Li, E., Volatile Organic Metabolites Identify Patients with Mesangial Proliferative Glomerulonephritis, IgA Nephropathy and Normal Controls. *Scientific Reports* **2015,** *5*, 14744.
226. Lau, H.-C.; Yu, J.-B.; Lee, H.-W.; Huh, J.-S.; Lim, J.-O., Investigation of Exhaled Breath Samples from Patients with Alzheimer's Disease Using Gas Chromatography-Mass Spectrometry and an Exhaled Breath Sensor System. *Sensors (Basel, Switzerland)* **2017,** *17* (8), 1783.

Chapter 5 Conclusions and Future Directions

5.1 Conclusions

The main topics of this dissertation discussed the design, assembly, characterization, operation and chromatogram reconstruction of 1D & 2D μGC system as well as their applications on water contamination analysis and exhaled breath analysis. This chapter summarizes the aforementioned system performance and application results.

Chapter 1 firstly provided a review of the conventional benchtop GC, including its working principle, performance metrics and critical components. The next section discussed the MDGC, its working principle, the 2D column selection and modulation methods. The last section reviewed the development of μGC components in recent years and then the technical details of the key microfabricated components. As shown in this chapter, μGC (especially multi-dimensional μGC) has undergone significant innovations, and it is critical to improve the separation performance of μGC for handling the complex environmental, agricultural and clinical samples in real world.

Chapter 2 presented the development of our1D μGC system and its application of highly sensitive, rapid, and *in-situ* VOC quantification in water. The results show that the system is able to complete analytical testing in less than 20 minutes with a sub-μg L^{-1} level detection limit. Quantitative comparison with results obtained by analytical lab under standard procedures and benchtop instruments further validated the field-applicability of the portable GC system.

In chapter 3 we developed a new, fully automated, portable 1x4-channel GC x GC device. The highlight of this chapter is the flow routing/modulating from ^{1}D to one of the four ^{2}D subsystem, and the 2D GC reconstruction algorithm. The algorithm utilized not only the four ^{2}D

PIDs signals and also the peak shape information in ^{1}D PID (comprehensive GCxGC only has one ^{2}D signal) hence is more powerful for resolving coeluted ^{1}D peaks. The device is compact (60 cm × 50 cm × 10 cm, and < 5 kg), robust (μTI and μDS), provides rapid analysis (50 VOCs in 14 minutes), and provides excellent peak capacity and peak capacity production without the help of cryogenic modulator (high power consumption). This system can be used for a plethora of field applications, such as *in-situ* continuous environmental monitoring, workplace safety monitoring, industrial in-line monitoring, food and agriculture analysis, and breath analysis.

Chapter 4 focused on exhaled breath analysis and ARDS diagnosis using 1by2 μGC system. It demonstrated the feasibility of using our MDGC for point-of-care clinical application. The high diagnostic accuracy have shown the great potential for early diagnosis and early interventions for ARDS using metabolic study with our high sensitivity and high resolution MDGC system in non-invasive manner.

5.2 System improvement

5.2.1 Chemical detection range

Current system's target analytes are limited by the Krypton UV lamp based PID detector, since chemicals with photon ionization energy near or higher than 10.6eV (such as methane and ethane) are not visible for this PID detector. For getting a broader detection range, more universal detectors (such as HDPID) can be used. In that case, the adsorbents stages in the μPCI and μTI chamber also need to be modified (for example, adding carboxen 1000 for more volatile compounds), so the adsorption chemical range could match the detection chemical range.

5.2.2 Chemical identity

Although the standalone GC could identify compounds by the retention time, it is still desired, under certain application, that the chemical name and structure could be revealed with

high confidence. In these applications, our GC system need to be coupled with a mass spectrum instrument and identify the compounds within samples. If MS instrument is not available, chemical identity can be also be found by performing rigorous retention time matching with preloaded libraries. FTIR, color-metric sensor array or other vapor sensors could also be attached to our system to provide extra information on the compounds identities.

5.2.3 Detection limit (LOD)

Improving the current PIDs' LOD enables the system to detect lower concentrated compounds in sample, or shorten the sampling time for field analysis with the same signal to noise ratio.

5.2.4 Analysis time

Lower detector LOD can shorten the sampling time; higher head pressure can shorten the system cleaning time; Careful optimization on flow rate or column temperature ramping profile could shorten the analyzing time without scarifying the chromatogram resolution.

5.2.5 Robustness

μGCs are mainly developed for field analysis, hence the physical robustness of the μGC systems is also important. External enclosure should be light weighted, and water resistant with customized housing and supporting layer.

5.3 Applications

5.3.1 Exhaled breath analysis

Breath biomarkers have been found for various diseases, such as childhood asthma, acute kidney injury and diabetes. Clinical tests can be conducted on these patients to discover and validate the relevant biomarkers for screening, diagnosis, and monitoring propose.

5.3.2 Other applications

Due to its high sensitivity, portable size and weight, rapid analysis and capability of analyzing complex mixtures, the μGC system could also be used in many other fields, including precision agriculture (such as plant infection detection) and food analysis (such as pesticide residues analysis).